

CERAMIC WAVEGUIDE BANDPASS FILTERS WITH SPURIOUS MODES SUPPRESSION

SHARJEEL AFRIDI



Submitted in accordance with the requirements for
the degree of *Doctor of Philosophy*

The University of Leeds
School of Electronic and Electrical Engineering
DECEMBER 2017

DECLARATION

The candidate confirms that the work submitted is his own, except where work which has formed part of jointly-authored publications has been included. The contribution of the candidate and the other authors to this work has been explicitly indicated below. The candidate confirms the appropriate credit has been given within the thesis where reference has been made to the work of others. It is to assert that the candidate has contributed solely to the technical part of the joint publication under the guidance of his academic supervisors.

Chapter 4 is based on the work from:

Hunter, S. Afridi and M. Sandhu, "Integrated ceramic waveguide filters with improved spurious performance," *2015 European Microwave Conference (EuMC)*, Paris, 2015, pp. 674-677. doi: 10.1109/EuMC.2015.7345853

Prof. Ian Hunter, the supervisor, suggested the study of TEM resonators for improved spurious performance. The postdoc, Dr Muhammad Sandhu and supervisor worked with the student on filter design, analysis of results and paper preparation. The PhD student designs the filter, obtained and analysed the results and wrote a paper.

Chapter 5 is based on the work from:

S. Afridi, M. Sandhu, N. Somjit and I. Hunter, "Monolithic ceramic waveguide filter with wide spurious free bandwidth," *2016 46th European Microwave Conference (EuMC)*, London, 2016, pp. 241-244.

Prof. Ian Hunter, the supervisor, suggested the study of non-uniform width ceramic resonator to improve the out of band performance of ceramic filters. The co-supervisor, Dr Nutapong Somjit, the post doc, Dr Muhammad sandhu and the supervisor worked with the student on filter design, results analysis and preparation of paper. The PhD student developed the design of filter, obtained and analysed the results and wrote a paper.

Chapter 6 is based on the work from:

S. Afridi, M. Sandhu and I. Hunter, "Mixed non-uniform width/evanescent mode ceramic resonator waveguide filter with wide spurious free bandwidth," *2016 IEEE MTT-S International Conference on Numerical Electromagnetic and Multiphysics Modeling and Optimization (NEMO)*, Beijing, 2016, pp. 1-3. doi:10.1109/NEMO.2016.7561667

Prof Ian Hunter, the supervisor, contributed the concept of non-uniform width resonator mixed with TEM resonator to get the improved spurious free region. The post doc, Dr Muhammad Sandhu and supervisor worked with the student on filter design, results analysis and paper preparation. The PhD student design the filter, obtained and analysed the results and wrote a paper.

And:

S. Afridi, M. Sandhu, N. Somjit and I. Hunter, "Monolithic ceramic waveguide filter with wide spurious free bandwidth," *2016 46th European Microwave Conference (EuMC)*, London, 2016, pp. 241-244.

Prof. Ian Hunter, the supervisor, suggested the study of mixed approach of non-uniform width ceramic resonator and TEM resonators for wide spurious free

bandwidth in ceramic filters. The co-supervisor, Dr Nutapong Somjit, the post doc, Dr Muhammad Sandhu and the supervisor worked with the student on filter design, results analysis and preparation of paper. The PhD student developed the design of filter, obtained and analysed the results and wrote a paper.

Chapter 7 is based on the work from:

Hunter, S. Afridi and M. Sandhu, "Integrated ceramic waveguide filters with improved spurious performance," *2015 European Microwave Conference (EuMC)*, Paris, 2015, pp.674-677.doi: 10.1109/EuMC.2015.7345853

Prof. Ian Hunter, the supervisor, suggested the idea of studying stepped impedance resonators for improved spurious performance. The postdoc, Dr Muhammad Sandhu and supervisor worked with the student on filter design, analysis of results and paper preparation. The PhD student designs the filter, obtained and analysed the results and wrote a paper.

This Copy has been supplied on the understanding that it is copyright material and that no quotation from the thesis may be published without proper acknowledgment

© 2017 The University of Leeds and Sharjeel Afridi

This thesis is dedicated to my Mother

ACKNOWLEDGMENT

First and foremost I would like to thank Almighty Allah, for all his blessings. For whatever I achieve in life, it is due to his grace.

Secondly, I am most grateful to my supervisor, Prof Ian Hunter for his continuous guidance during the course of my study in the University of Leeds. It is due to his immense support that I have been successful in completing my thesis. His insights and valuable advices paved the road toward accomplishing the goals of this work. I would also like to thank Dr Nutapong Somjit for his support and guidance in refining and improving my work.

I would like to acknowledge Dr Yameen Sandhu for his continuous support, fruitful discussions and guidance.

I would like to thanks Martin Gostling, Richard Parry, and John Tinker at Radio Design for giving their valuable suggestions and time in fabrication process of filters.

I also acknowledge Mr Graham Brown in the Mechanical workshop for his help in fabrication of filters.

I would like to thank the management of Sukkur IBA University for providing my opportunity to pursue my higher education at University of Leeds.

I would like to thanks Dr Safeer Hyder, Mr Abdullah, Dr Hafiz Gilal, Mr Asif Khan, Mr Saad Luhaib, Mr Mustafa Bakr, Mr Jessada Konpong for their support and company during all these years.

Finally, I would like to express my love and gratefulness to my parents, my wife Maryah and my two princesses Hareem and Umamah for their love, support, patience and understanding during the course of my PhD.

Abstract

An investigation of various ceramic bandpass filters with an improved spurious performance for use in cellular base station filtering applications is presented in this thesis. Monolithic integrated ceramic bandpass filters offer more than 50% size reduction compared to air-filled coaxial resonator filters with the same unloaded Q-factor. However, the stopband performance of these filters is deteriorated by spurious frequencies of the fundamental mode and higher order modes. The probable solution to reducing the effects of these undesired modes is to add a low-pass filter or band-stop filter at the expense of higher in-band losses and bulky volumes. In this work, multiple geometrical design techniques are explored to achieve the optimum out of band performance without any need for a low-pass filter.

The improvement in spurious performance of Chebyshev ceramic bandpass waveguide filters is explored. In particular, its design solution aimed to improve the stopband attenuation for these filters. The design of the Chebyshev monolithic ceramic bandpass filter is reviewed, and some realizations are proposed and compared with the filter.

The sixth order Chebyshev ceramic bandpass filters with posts were designed with improved spurious performance. The input/output couplings are realized through the use of a coaxial cable placed at the center of the external resonator. The inter-resonator couplings are achieved by placing various metal plated through-holes in the broad dimension of a waveguide.

The broad dimension of integrated ceramic waveguide resonators can be utilized as an extra degree of freedom that can be integrated into filter design procedure and a better spurious performance is achieved by mixing resonators of non-uniform widths. Chebyshev ceramic bandpass filters are designed with two and three non-uniform width resonators and significant improvement has been achieved in the stopband performance of the filters.

Other solutions involve the mixing of resonators with posts and non-uniform width resonator. The six order ceramic waveguide bandpass filters are simulated and fabricated in an air filled waveguide with tuning screws. Metal tuning screws are included to overcome mechanical discrepancies and imperfections.

The stepped impedance resonators were previously applied to both planar, coaxial and air-filled rectangular waveguide filters. Here, for the first time, their use has been extended to monolithic integrated ceramic waveguide filters, accomplishing an exceptional spurious free stopband bandwidth for the filters.

Finally, sixth order ceramic loaded waveguide filters were designed and fabricated with ridge and non-uniform width ceramic blocks. Their top and bottom surfaces are metalized through the silver paint with the conductivity of $4 \times 10^7 \text{ s/m}$. Inductive irises are used for inter-resonator coupling where the coaxial probe excites the external resonators of the filter and the excellent stopband attenuation of up to $2.45 * f_o$ is achieved.

CONTENTS

Declaration.....	ii
Acknowledgment.....	vi
Abstract.....	viii
Contents.....	x
List of figures.....	xv
List of table.....	xxiii
Notations.....	xxiv
1 Introduction.....	1
1.1 Background.....	1
1.2 Objective of the Research	8
1.3 Existing Solutions	8
1.4 Thesis Organization.....	9
2 LITERATURE REVIEW.....	12
2.1 Introduction.....	12
2.2 Low-Pass Prototype.....	14
2.3 Transfer Function.....	17
2.3.1 The maximally flat prototype	19
2.3.2 The Chebyshev Prototype	21
2.3.3 Generalised Chebyshev prototype.....	23
2.4 Frequency and Impedance Transformations	24

2.5	Band-pass Transformation.....	26
2.6	Physical Realization of Microwave Filters	29
2.6.1	Coaxial TEM Filters	29
2.6.2	Dielectric Compline Filter	32
2.6.3	Waveguide filters	33
2.6.4	Evanescent Mode Filters	34
2.6.5	Stepped Impedance Resonator Filters	37
2.6.6	Dielectric Waveguide Filters	41
2.6.7	Integrated Ceramic Waveguide Filter	43
2.7	Summary	45
3	Ceramic Waveguide Resonators	47
3.1	Introduction	47
3.2	Rectangular Waveguide Modes.....	49
3.3	Permittivity	57
3.4	Quality Factor	57
3.5	Spurious Performance	61
3.6	Summary	65
4	CERAMIC WAVEGUIDE BANDPASS FILTERS WITH METAL POSTS	66
4.1	Introduction	66
4.2	Filter Specifications.....	67
4.3	Ceramic Waveguide Resonator	68

4.4	Steps for Ceramic Chebyshev Waveguide Filter Design	71
4.5	Results.....	77
4.6	Inter resonator coupling.....	80
4.7	Input/output Coupling.....	87
4.8	Ceramic bandpass Waveguide Filters with posts	89
4.8.1	Ceramic Resonator with Post	89
4.8.2	Ceramic bandpass waveguide filter with two Posts	92
4.8.3	Ceramic bandpass waveguide filter with all posts having same height	94
4.9	High-Frequency Structure Simulator (HFSS).....	97
4.10	Summary	101
5 CERAMIC BANDPASS WAVEGUIDE FILTERS WITH NON-UNIFORM WIDTH RESONATORS.....		102
5.1	Introduction	102
5.2	Ceramic Waveguide Filter with Two Non-Uniform Width Resonators 105	
5.3	Ceramic Waveguide Filter with Three Non-Uniform Width Resonators	109
5.4	Summary	113
6 CERAMIC BANDPASS WAVEGUIDE FILTERS WITH METAL POSTS AND NON-UNIFORM WIDTH RESONATORS		115
6.1	Introduction	115

6.2	Ceramic bandpass waveguide filter with all posts having different post height	116
6.3	Ceramic non-Uniform width filter with metal posts	120
6.4	Ceramic non-uniform width filter with two metal posts	124
6.4.1	Fabrication Details	128
6.4.2	Filter Tuning.....	129
6.5	Summary	132
7 CERAMIC WAVEGUIDE FILTERS WITH STEPPED IMPEDANCE RESONATORS AND CERAMIC LOADED RESONATORS.....		134
7.1	Introduction	134
7.2	Ceramic Bandpass Filter with Stepped Impedance Resonator...	135
7.3	Ceramic Bandpass Filter with Ceramic Loaded Resonators.....	140
7.3.1	Fabrication Details	149
7.4	Summary	157
8 CONCLUSIONS AND FUTURE WORK.....		158
8.1	Introduction	158
8.2	Future work.....	160
References		163
Publications.....		Error! Bookmark not defined.

List of Figures

Figure 1.1: Block diagram of the RF front end of a cellular base station[1].....	2
Figure 1.2: Types of filter characteristics [2].....	2
Figure 1.3 Waveguide bandpass filter (i) Top view (ii) Side view[1]	6
Figure 2.1: Low-Pass Prototype for an all –pole transfer function.....	15
Figure 2.2: Impedance inverter terminated with a load	16
Figure 2.3: General Nth Degree inverter coupled a low-pass prototype with (a) inductors, and (b) capacitors	17
Figure 2.4: Butterworth low-pass response	19
Figure 2.5: Chebyshev low-pass response.....	23
Figure 2.6: Generalised Chebyshev low-pass filter response	24
Figure 2.7: Low-pass to Band-pass transformation	27
Figure 2.8: Prototype filter transformations[22].....	28
Figure 2.9: Coaxial TEM filters; (i) Interdigital (ii) combline	30
Figure 2.10: TEM coaxial resonator; (i) top view (ii) side view.....	31
Figure 2.11: Dielectric combline resonator; (i) top view (ii) side view ..	33
Figure 2.12: Comparison of different resonant structures.....	37

Figure 2.13: (a) Uniform impedance resonator (b) Quarter wavelength stepped impedance resonator (c) Half wavelength stepped impedance resonator	38
Figure 2.14: Dielectric resonator with puck inside	43
Figure 2.15: Integrated Dielectric Waveguide Resonator	44
Figure 3.1: Ceramic Filled waveguide Resonator	48
Figure 3.2: E-field and H-field pattern of rectangular waveguide resonator[22]	50
Figure 3.3: Electric field distribution in ceramic waveguide resonator for a TE_{101} mode (from HFSS) (i) Vector form (ii) magnitude form	54
Figure 3.4: Electric field distribution of ceramic waveguide resonator for a TE_{102} mode (from HFSS) (i) vector form (ii) magnitude form	55
Figure 3.5: Electric field distribution of ceramic waveguide resonator for a TE_{011} mode (from HFSS) (i) vector form (ii) magnitude form	55
Figure 3.6: Electric field distribution of ceramic waveguide resonator for a TE_{201} mode (from HFSS) (i) vector form (ii) magnitude form	56
Figure 3.7: Electric field distribution of ceramic waveguide resonator for a TE_{111} mode (from HFSS) (i) vector form (ii) magnitude form	56
Figure 3.8: The $TE_{01\delta}$ resonant peak and associated parameters [52].	60
Figure 3.9: Mode chart for a rectangular waveguide resonator [2]	62
Figure 3.10: comparison of Q-factor, first spurious signal and post height in an integrated TEM ceramic waveguide resonator.....	64

Figure 4.1: Equivalent final circuit for six order ceramic bandpass waveguide filter.....	76
Figure 4.2: Simulated passband response of ceramic waveguide filter	78
Figure 4.3: passband insertion loss of ceramic waveguide filter	79
Figure 4.4: The full band response of ceramic waveguide filter	79
Figure 4.5: Normalized Susceptance of posts in a waveguide will change both this pictures later with good [65]	80
Figure 4.6: Shunt inductive through-holes in ceramic waveguide; (i) Top view (ii) Side view (iii) equivalent circuit.....	81
Figure 4.7: Iris embedded shunt inductive section of a waveguide	83
Figure 4.8: Ceramic waveguide resonator with metal post; (i) Top view (ii) 3D view (iii) equivalent circuit	90
Figure 4.9: Electric field distribution of the ceramic waveguide resonator with a post for TEM₀₀ mode (from HFSS) (i) Vector and (ii) Magnitude form	91
Figure 4.10: Ceramic bandpass waveguide filter with two posts one at each end (i) Top view (ii) Side view (iii) 3D view	93
Figure 4.11: Simulated pass band response of ceramic bandpass waveguide filter with two posts.....	93
Figure 4.12: Full band spurious performance of Ceramic bandpass waveguide filter with two posts.....	94
Figure 4.13: Physical layout of a ceramic bandpass filter with all posts having same height (i) Top view (ii) Side view (iii) 3D view	95

Figure 4.14: Simulated pass band response of a ceramic bandpass waveguide filter with all posts having same height.....	95
Figure 4.15: Full band simulated response of a ceramic bandpass waveguide filter with all posts having same height.....	96
Figure 4.16: Compariosn of spurious performance of test filter with ceramic bandpass waveguide filters having posts	97
Figure 4.17: Mesh with tetrahedral elements to approximate the shape and 3D object	98
Figure 4.18: Finite element method analysis of integrated dielectric resonators; (a) mesh with 0.6λ (b) mesh with 0.2λ	100
Figure 5.1: Non-Uniform width resonators (i) Top view (ii) 3D view	104
Figure 5.2: Ceramic waveguide filter with non-uniform width resonators (i) Top view (ii) Side view (iii) 3D view	106
Figure 5.3: Simulated pass band response of ceramic waveguide filter with two non-uniform width resonators.....	107
Figure 5.4: Broad band simulated response of ceramic waveguide filter with two non-uniform width resonators.....	107
Figure 5.5: Physical layout of 7-pole ceramic waveguide filter with two non-uniform width resonators (i) Top view (ii) Side view (iii) 3D view	108
Figure 5.6: Broad band simulated response of 7-pole ceramic waveguide filter with two non-uniform width resonators.....	109

Figure 5.7: physical layout of three different width ceramic waveguide resonators (i) Top view (ii) 3D view	110
Figure 5.8: Physical layout of ceramic waveguide filter with three non-uniform width resonators (i) Top view (ii) Side view (iii) 3D view	111
Figure 5.9: Simulated pass band response of ceramic waveguide filter with three non-uniform width resonators	111
Figure 5.10: Simulated broad band response of ceramic waveguide filter with three non-uniform width resonators	112
Figure 5.11: Comparison of spurious performance of both six order ceramic non-uniform width resonator filters with test filter	113
Figure 6.1: Three resonators with different post heights (i) Top view (ii) 3D view	116
Figure 6.2: Physical layout of a filter with all posts resonators having different posts heights (i) Top view (ii) Side view (iii) 3D view	118
Figure 6.3: Simulated (HFSS) Pass band response of a ceramic waveguide filter with all posts having different height.....	119
Figure 6.4: Full band simulated (HFSS) response of a ceramic waveguide filter with all posts having different height.....	119
Figure 6.5: Two non-uniform width resonators posts having equal height (i) Top view (ii) 3D view.....	121
Figure 6.6: Physical layout of ceramic bandpass filter of non-uniform width resonators having posts of equal height (i) Top view (ii) Side view (iii) 3D view	122

Figure 6.7: Simulated (HFSS) pass band response of ceramic bandpass filter of non-uniform width resonator having posts of equal height	123
Figure 6.8: Simulated (HFSS) Broadband response of ceramic bandpass filter of non-uniform width resonator having posts of equal height	123
Figure 6.9: Structural layout of TEM and non-uniform width resonators (i) Top view (ii) 3D view	125
Figure 6.10: Simulated design of ceramic waveguide filter with two posts and non-uniform width resonators (i) Top view (ii) Side view (iii) 3D view	125
Figure 6.11: Simulated pass band response of ceramic TEM and non-uniform width filter	126
Figure 6.12: Simulated Broadband response of ceramic TEM and non-uniform width filter	126
Figure 6.13: Simulated pass band response of air filled TEM and non-uniform width filter	127
Figure 6.14: Broadband simulated response of air filled TEM and non-uniform width filter	127
Figure 6.15: Comparison of broadband response of all simulated ceramic filters with test filter	128
Figure 6.16: Fabricated silver plated air filled TEM and non-uniform width filter with tuning screws	129

Figure 6.17: Resonator with tuning Screw (i) Top view (ii) Side view [68]	130
.....	
Figure 6.18: Comparison of simulated and measured passband response of air-filled waveguide filter having two metal posts and non-uniform width resonators.....	131
Figure 6.19: Detailed comparison of simulated and measured passband response of air-filled waveguide filter having two metal posts and non-uniform width resonators.....	131
Figure 6.20: Comparison of simulated and measured broadband response of air-filled waveguide filter with post and non-uniform width resonators.....	132
Figure 7.1: Stepped impedance resonator (i) 3D view (ii) Top view	137
Figure 7.2: Ceramic Stepped impedance resonator filter (i) Top view (ii) Side view (iii) 3D view.....	138
Figure 7.3: Simulated pass band response of a ceramic stepped impedance resonator filter.....	139
Figure 7.4: Simulated Broadband response of a ceramic stepped impedance resonator filter.....	140
Figure 7.5: ceramic loaded resonator with centralized ceramic block (i) Side view (ii) Top view.....	141
Figure 7.6: structural layout of ceramic loaded resonators with ceramic TEM and non-uniform width blocks (i) Top view (ii) 3D view.....	143

Figure 7.7: Structural layout of ceramic loaded filter with ceramic TEM and non-uniform width blocks (i) Top view (ii) Side View (iii) 3D view	144
Figure 7.8: Structural layout of a ceramic loaded resonators with ceramic ridge and non-uniform width blocks (i) Top view (ii) 3D view	145
Figure 7.9: Structural layout of a ceramic loaded filter with ceramic ridge and non-uniform width blocks (i) Top view (ii) Side view (iii) 3D view	146
Figure 7.10: Resonators with non-uniform width and TEM Ceramic Blocks (i) Top view (ii) Side View	147
Figure 7.11: Simulated Passband response for a ceramic loaded filter with ridge and non-uniform width ceramic blocks	148
Figure 7.12: Simulated broadband response of a ceramic loaded filter with ridge and non-uniform width ceramic blocks	148
Figure 7.13: Comparison broad band response of Test filter with ceramic stepped impedance filter and ceramic loaded filter	149
Figure 7.14: grooves on thin metal copper sheet	151
Figure 7.15: Soldering of Ceramic blocks with copper sheet from bottom.....	152
Figure 7.16: The aluminium side walls with the inductive irises without soldering.....	152
Figure 7.17: Fabricated filter with tuning screws.....	153

Figure 7.18: Clamping of a filter	153
Figure 7.19: Pass band response of simulated and fabricated filter ...	154
Figure 7.20: Broad band response of simulated and fabricated filter .	154
Figure 7.21: Ceramic top and bottom soldered with the cavity	155
Figure 7.22: fabricated filter with copper plated aluminium cavity	155
Figure 7.23: Passband response of simulated and fabricated filter	156
Figure 7.24: Broadband response of simulated and fabricated filter ..	156
Figure 8.1: 3rd order generalised chebyshev ceramic loaded filter with ridge and non- ridge ceramic block (i) Side view (ii) Top view	162
Figure 8.2: Broadband response of 3rd order generalised chebyshev ceramic loaded filter with ridge and non-ridge ceramic blocks ..	162

LIST OF TABLES

Table 2-1 Commonly Used Dielectric Materials.....	44
Table 4-1 Specifications for ceramic waveguide filter (provided by radio design).....	67
Table 4-2 Eigen mode data (HFSS) for the ceramic waveguide resonator	71
Table 4-3 Simulated Design filter dimensions for fabrication.....	77
Table 4-4 Eigen mode data (HFSS) for ceramic resonator with post	91
Table 5-1 Dimensions and Eigen mode data for two non-uniform width resonators	105
Table 6-1 Details of Quality factor, post heights and volume of resonators	117
Table 6-2 details of Q factor, post height and volume of two non-uniform width resonators	122
Table 7-1 Different Resonator impedance Dimensions-ratios for Improved Stop band[37].....	135
Table 7-2 Frequencies and Q factor of Stepped impedance resonator	137
Table 7-3 Mode chart for ceramic loaded resonator	141
Table 7-4 Details of height and Q factor for dielectric loaded resonator	142
Table 7-5 Comparison of Ceramic TEM resonator and Ceramic Ridge resonator	145
Table 7-6 details of ceramic loaded resonators with ridge and non-uniform width ceramic blocks	147

Notations

$ABCD$	Transmission parameters
ω	Angular frequency
g_o	Low pass prototype values
Z_o	Characteristic impedance
z_{in}	Input impedance
z_{load}	Load impedance
ε	Ripple constant
S_{21}	Transmission coefficient
IL	Insertion loss
dB	Decibel
$f_n(\omega)$	Filtering function
S_{11}	Reflection coefficient
L_r	Return loss
L_A	Stop band attenuation
ω_c	Cutoff frequency
N	Degree or order of filter
S	Stop band to pass band ratio
ω_s	Stop band frequency
ω_p	Passband frequency
T_N	Nth order chebyshev polynomial
$K_{r,r+1}$	Coupling coefficient between resonator r and r+1
PLR	Power loss ratio
FBW	Fractional bandwidth
ω_o	Center frequency
PEC	Perfect electrical conductor
ε_r	Relative permittivity
θ	Electrical length
θ_T	Total electrical length

β	Propagation constant
β_p	Phase constant
K	Impedance ratio
f_o	Fundamental frequency
a_r	Resonator width
b_r	Resonator height
l_r	Resonator length
l	Half wave variation of electric field along width of waveguide resonator
m	Half wave variation of electric field along height of waveguide resonator
n	Half wave variation of electric field along length of waveguide resonator
ϵ_o	Absolute permittivity
μ_r	Relative permeability
$\tan\delta$	Dielectric loss tangent
E_y	E-field component in y direction
E_x	E-field component in x direction
H_x	H-field component in x-direction
H_y	H-field component in y-direction
λ_d	Dielectric wavelength
λ_o	Free space wavelength
Q	Quality factor
Q_u	Unloaded quality factor
Δf	Half power bandwidth
$\frac{1}{Q_d}$	Dielectric loss
$\frac{1}{Q_c}$	Conduction loss
$\frac{1}{Q_r}$	Radiation loss
$\frac{1}{Q_{ext}}$	External loss
B	Susceptance
φ	Phase length

σ	Conductivity
P_h	Post height
P_r	Post radius
Z_{coax}	Impedance of coaxial cable
Z_{wave}	Impedance of rectangular waveguide
Z_{TE}	Impedance of rectangular waveguide in TE mode
c	Speed of light
λ_g	Guide wavelength
K_e	External coupling coefficient
f_c	Cut-off frequency
Ω	Normalized cut-off frequency of lowpass prototype
T	Transfer matrix
A_T	A parameter of transfer matrix
B_T	B parameter of transfer matrix
C_T	C parameter of transfer matrix
D_T	D parameter of transfer matrix
Z_1	Impedance of first section
Z_2	Impedance of second section
CL	Ceramic length
CW	Ceramic width
CH	Ceramic height

1 Introduction

1.1 Background

Microwave filters are a fundamental part of many communication systems. Satellite, navigation, radar, remote sensing and cellular base stations all utilize their property of selective frequency transmission which allows energy to pass through their passbands and blocks or attenuates energy in their stop bands. The frequency requirement for such applications range from 100 MHz to 100 GHz and, in order for their usage to be feasible must have low cost, small size and efficient devices like filters and antennas to operate at the front end of these systems. The cellular base station employs these filters to provide attenuation for both transmitters and receivers. The block diagram of the RF front end of the cellular base station is given below in figure 1.1. The microwave filters are two-port networks and can be categorized as having low pass, band pass, high pass and band stop attenuation characteristics, depending on the specific requirements of the filters, as shown in figure 1.2.

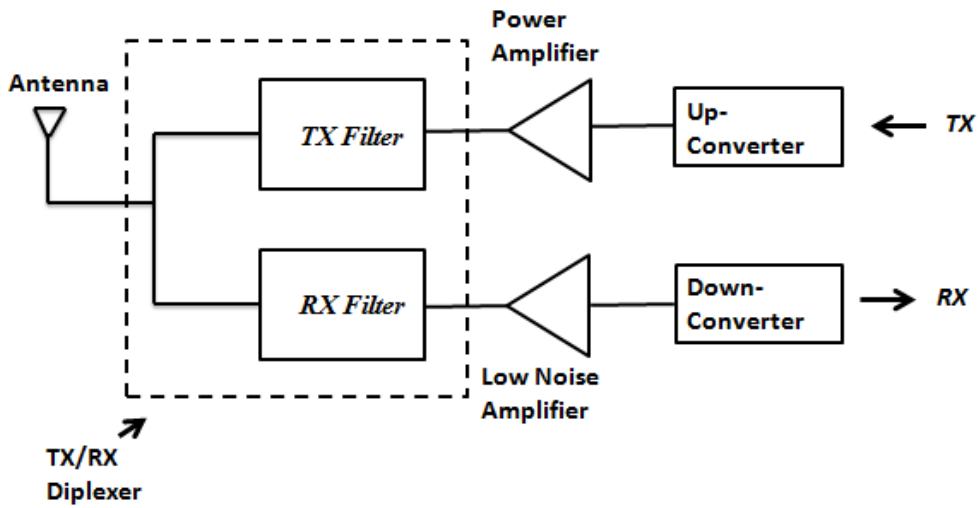


Figure 1.1: Block diagram of the RF front end of a cellular base station[1].

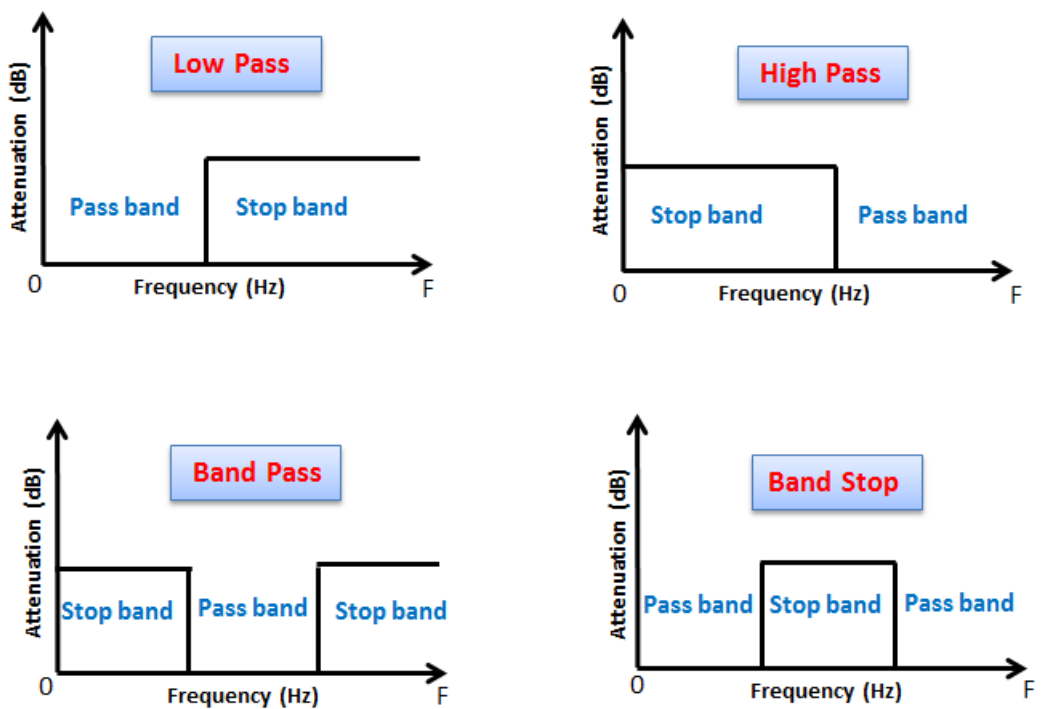


Figure 1.2: Types of filter characteristics [2]

In communication systems, microwave filters are required to exhibit excellent electrical and mechanical performance. The electrical performance of filters is driven by low insertion loss, good return loss, small group delay and good selectivity and the guard band must be small in order to efficiently utilize the available bandwidth. The mechanical aspect of filters requires that they have a small volume, low mass and excellent temperature stability. The ideal filter exhibits flat passband response, infinite attenuation in stop band and linear group delay, which is very impractical. Thus, practical filters deviate in relation to the typical response, depending on the design and material properties used for filter realization. The performance of a filter is critically affected by the material impairment in the form of energy dissipation, especially in those with a narrow bandwidth.

Today, microwave filters have a wide range of applications in the field of communication; however the initial motivation for designing devices at microwave frequencies was for military purposes. In the late 19th century, Maxwell and Faraday gave experimental verification of electromagnetic theory, which suddenly started to attract the attention of engineers and physicists in the field of electromagnetics. Heaviside introduced the basis for transmission line theory and also developed the concept of metallic conductors, which act to guide electromagnetic waves [3]. He convinced himself that a guided wave requires at least “two leads as a pair of parallel wires; or if but one be used, there is earth, or something equivalent, to make another” [3]. After some time, J. Larmor and Lord Rayleigh investigated resonant structure theory and confirmed the possibility of electromagnetic waves in the hollow cavity. The fundamentals of Microwave filter theory were established before World War II; major

applications were implemented using image parameters during World War II in the United States between 1941 and 1945. Previously, in 1937, W.P Mason and R.A Sykes published various papers in which they used ABCD parameters and derived the attenuation functions and image phase and impedance of filter sections. The MIT radiation laboratory and Harvard Radio Research Laboratory focused their research on waveguide filters, low pass, high pass, band pass filters for ECM (Electronic countermeasure) applications and narrowband tunable coaxial filters for search receivers. K. Kuroda introduces a set of transformations which is used to enable the elements of characteristic impedance equal to the generator or load to be introduced into a network to physically move apart stubs. This transformation was first published in a Japanese thesis in 1955 and later in English by Ozaki and Ishii 1958 [4]. Fano and Lawson initially introduced a direct coupled cavity filter based on a low pass prototype, in which they make the argument that the simple resonant cavity does not have proper out of band rejection for a given minimum stopband insertion loss. This led to the investigation into the use of a chain cavity of directly coupled resonators, which also showed that narrowband microwave filters consisting of chained cavities with a single frequency could be derived from lumped element filters. The implementation of this was very tedious in an era without any computers because of the challenging synthesis technique [4] [5]. The classical paper of Cohn in 1957 on directly coupled microwave filters paved the way for subsequent work on microwave filters, which extends the applicability of Lawson and Fano's work [6]. The paper describes easy to use formulas for Butterworth and Chebyshev response filter designs in comparison to Darlington's precedent work. He also puts forward the idea of impedance

inverters by way of inter-cavity coupling which was later extended by Levy [6] [7]. A parallel-coupled filter was also introduced by Cohn in 1958 which established the foundation for combline and interdigital filters [8]. George Matthaei introduced the design procedure for lumped element interdigital bandpass filters and also published a paper on the theory and realization of combline bandpass filters in 1962 and 1963 respectively [9] [10]. Around the same time, a waveguide filter with axially spaced screws, exhibiting the bandpass characteristics below the cut off frequency was also introduced, termed 'evanescent mode filters'. The similarities in response and construction arguably make it a waveguide coupled version of a combline filter [11].

Since then, significant progress has been made on filter design methods and techniques to meet the stringent electrical and mechanical specifications and to obtain a drastic reduction in both costs and development time. Hence, the area of microwave filters, especially in satellite and cellular communication, has achieved significant improvements in performance, in areas such as good selectivity, better stopband attenuation, reduced volume, etc. The rectangular waveguide filter consist of a uniform section of a rectangular guide separated with inductive discontinuities (post) placed across the broad walls of the guide at approximately half-guide wavelength intervals shown in figure 1.3.

The selectivity increases as the number of resonant sections of the filter increases, but with higher insertion loss and increase in volume, so the transmission zeros have been introduced. Multi-mode filters are also used to reduce the weight and size of the filters by exploiting the two degenerate modes (i.e., modes with different field patterns but with same resonant frequency). The

multi band filters can be used to support different bands or different standards by the same wireless communication system, such as mobile base station. A dual-band filter can be used to support 900 MHz or 1800 MHz band on same base station or can be used to support different standards like GSM-CDMA. Better spurious performance is needed to improve out of band rejection performance as neighboring modes act as spurious modes and interfere with filter performance.

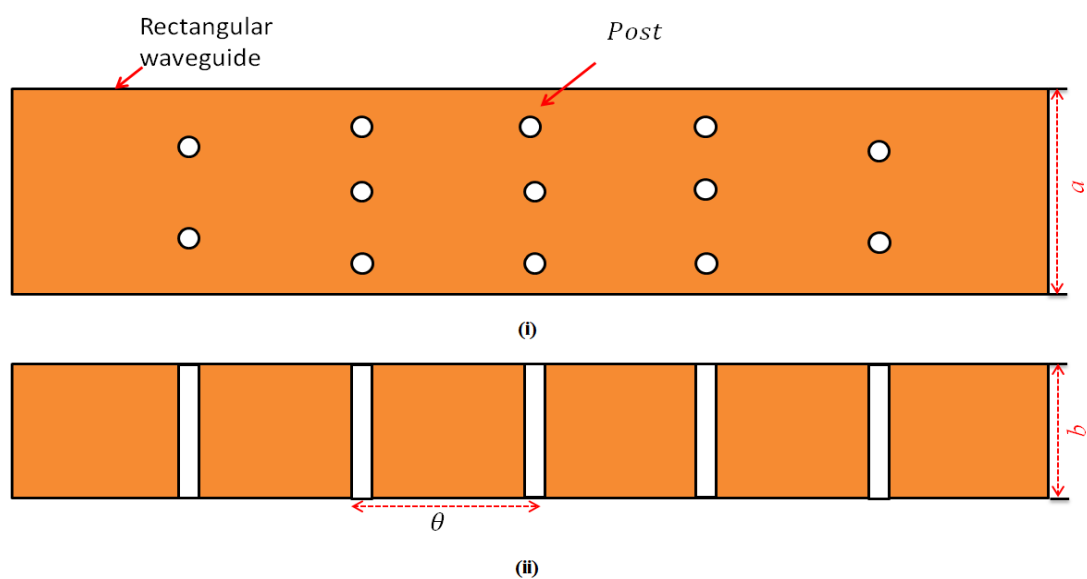


Figure 1.3 Waveguide bandpass filter (i) Top view (ii) Side view[1]

However, significant demand in cellular communication for low loss, small size, high Q with good out of band rejection filters still remains. TEM filters fulfill the need for high Q and good spurious performance but with greater physical size, whereas dielectric filters provide a good size reduction with good Q values and hence becomes a good alternative for coaxial cavity filters. Waveguide filters have an advantage for their multiple modes with greater power handling and low loss compared to coaxial or microstrip filters. The distinct disadvantage

comes with their bigger size and spurious modes. The filter out of band attenuation is required to meet higher demand in today's arena. Therefore, a number of approaches have been proposed to improve the out of band performance of the filters. Details of these approaches are given in the next sections. The dielectric waveguide resonator filters showed very good Q factor, small size and excellent spurious performance, where the combination of waveguide dielectric resonators with TEM dielectric resonators can be used to improve the stop band attenuation of a filter. Microwave circuits are modelled through inherent electromagnetic solvers on established numerical methods for solving Maxwell's equations. Computer-aided design (CAD) for circuit theory received recognition in the late 1970's with the wide availability of mainframe computers. Field solvers became commercially available in the late 1990's with the use of UNIX based computers or personal computers [12].

Full-wave electromagnetic (EM) analysis has become an important part of microwave filter design and been used from past decade. It allows design engineers to obtain accurate responses of EM structures and also consider higher order effects for complex three-dimensional discontinuities, unwanted coupling, radiation and interaction of components with the layout. There are couple of EM simulation software programmes available in the market, such as HFSS from Ansys, CST Microwave Studios from Computer Simulation Technology and Momentum from Agilent. These programmes help designers to solve any high-frequency EM analysis problem, design and optimize any complex microwave structure and provide reliable and nearly accurate results in the time and frequency domains.

1.2 Objective of the Research

Recent developments in modern communication systems require base station filters with excellent in band and out of band performance. Ceramic filled and ceramic loaded rectangular waveguide filters proved to be a good choice as they are easy to manufacture, have a high Q factor and are small in volume, but the mode chart of these filters are crowded with unwanted modes in close proximity of the fundamental mode. The use of a low pass filter in cascade fashion with band pass filters has been a useful option to suppress the unwanted modes near the pass band. However, the stringent requirement of size and cost allow us to integrate a low pass and band pass filtering behaviour in one device which can lead to significant size and cost reduction. Therefore, the aim of this research is to design a ceramic filled and ceramic loaded rectangular waveguide filter which possesses a low pass filtering function i.e. an improved out of band performance along with the required in band performance.

1.3 Existing Solutions

A number of solutions have been proposed to improve the out of band performance of rectangular waveguide filters. In 1964, H. J. Riblet [13] proposed the use of waveguide resonators with different sections. If the lengths of the resonator have been suitably chosen, their fundamental frequency will remain the same, while spurious resonances will spread over a wider frequency range and hence their level will be kept lower compared to standard waveguide filters. This is because of the fact that the different width cavities have different cut off frequencies and if the interest is in the harmonic resonances of the

fundamental mode and the TE_{102} mode, then it is necessary to have resonators with different widths instead of changing both width and height [13]. The same principle has been proposed by Balasubramanian [14] and Morelli [15], where a procedure has been proposed to design a 10 GHz inductive iris filter with different resonators widths. The effectiveness of the idea has been demonstrated and the stop band has been extended by the use of sections with different widths. Morelli also proposed the use of stepped impedance resonators in waveguide filters, where more freedom is available to control the spurious resonances of the waveguide filter by changing the impedance of a resonator [16]. The use of capacitive posts in the waveguide also decreases the resonant frequency of the resonator below the cut-off, as well as the Q factor and the size of resonator. This makes it possible to improve the spurious performance of a filter albeit with degradation of the Q factor [17]. A different solution has also been proposed by Budimir [18], where the metal inserts between adjacent coupling septa are narrower than the height of the waveguide, forming a ridge waveguide resonator.

1.4 Thesis Organization

The present chapter gives an insight into microwave filters used in RF front end. Application of microwave filters is explained here in detail. Objective of the research with existing solutions are defined in this first chapter.

Chapter 2 reviews microwave filter design and a commonly used approximation for filter transfer functions with insertion loss method is explained in detail. Various physical realizations of microwave filter types are also reviewed in this section.

Chapter 3 explains integrated ceramic resonator designs. Resonator mode details with Q factor and spurious performance are also discussed, and HFSS is also reviewed in this section.

A novel filter design for six order monolithic ceramic chebyshev waveguide filter with posts is presented in Chapter 4. The monolithic integrated ceramic waveguide filter is designed with metal coated through-holes for inter-resonator coupling. Input/output coupling is realized by the use of a coaxial probe in the centre of the first and last resonator. A step by step design procedure of ceramic waveguide filter is explained. Simulated results of six degree Chebyshev filter is presented and compared with test filter of the same specifications.

A new design for monolithic ceramic chebyshev waveguide filters with non-uniform width ceramic resonators presented in Chapter 5. The filter design used metal coated through-holes for internal coupling and a coaxial probe for external coupling. Filters with two non-uniform width and three non-uniform width monolithic ceramic resonators are designed. The results are presented and compared with the test filter.

In Chapter 6, three new filters designs were presented with posts and non-uniform width monolithic ceramic waveguide resonators. The filters used the same technique for inter-resonator coupling and external coupling. One six order filter with posts and non-uniform width resonators is fabricated in air filled configuration and results are presented and explained. The simulated and measured results are then compared and discussed.

Chapter 7 presents the new design of a six order filter with a monolithic ceramic stepped impedance resonator and ceramic loaded resonators. The ceramic stepped impedance resonator filter is designed with metal coated through-holes and a coaxial probe for internal and external coupling. The simulated result is presented and discussed. The ceramic loaded filter is designed with ridge and non-uniform width ceramic blocks to improve the out of band performance of the filter. The filter is realized with an inductive iris for inter-resonator coupling and it uses the coaxial probe for input/output coupling. The six order filter is fabricated and results are compared and presented in detail in this chapter.

Chapter 8 summarises the basic aspect of this thesis. Suggested avenues for the possible extension of present work are also included in this chapter.

2

LITERATURE REVIEW

2.1 Introduction

In communication networks, filter networks are required to control the frequency response of a system by allowing or attenuating the signals in specified frequency bands. Ideally, the filter should provide a zero insertion loss and constant group delay over the passband and infinite attenuation everywhere else. Depending on the nature of the stopband and the passband, filters can be classified into these four types: low-pass, high-pass, band-pass and band-stop. According to their operating mechanism, filters can also be categorized as reflective, absorptive and lossy filters. In the filter design process, the proper transfer function of a low-pass prototype is approximated and then changed to the desired configuration, like band-pass, high-pass or band-stop. After the synthesis, the filter can be physically realized as a microstrip, strip line or waveguide cavity structure. The design procedure is followed by the filter specification, outlining the required transfer function, center frequency, bandwidth, degree of filter and return loss and, if required, the location of the transmission zeros to form the ideal characteristics of filter polynomials. The first recursive technique to calculate the polynomials for symmetrical and asymmetrical performance was introduced in [19]. These polynomials may then be converted into a prototype network, either by using lumped element network

synthesis methods or by using the coupling matrix approaches [19-21]. There are two well-known lumped element methods for filter design. The first is the image parameter method based on the properties of the transmission line and the second is the insertion loss method is also known as a polynomial method. "An image parameter method consists of a cascade of simple two port filter sections to provide the desired cut-off frequencies and attenuation characteristics, but not allow the specification of a frequency range over the complete range" [22]. It may have a good filter response but have no control to improve the design of the filter. The insertion loss method begins by obtaining the complete specifications of a filter and allows a systematic way to control the passband and stopband characteristics, whilst also offering a way to generate a required frequency response. The frequency response of a filter can depend on various parameters like insertion loss in the passband, the selectivity of a filter, bandwidth, return loss, centre frequency, out of band rejection and Q-factor to meet the desired specifications. The Q (quality) factor indicates the energy loss within a resonator, and hence defines the selectivity and insertion loss of the filter. The order of the filter also determines the selectivity, the more resonators, the better the selectivity, albeit at the expense of higher insertion loss.

The presence of higher order modes in close proximity of fundamental mode determines the spurious performance of a filter. In microwave bandpass filters these spurious modes deteriorates the stop band performance of a filter which may cause the interference in the passband.

The physical implementation of more complex transfer functions is made easier by using the coupling matrix method of filter design. The optimised dimension of

the filter may then be realized by the use of EM simulation tools. Tuning methods are also used to reduce the discrepancies between simulated and fabricated filter results by considering the manufacturing limitations. This chapter focuses on basic principles of the filter design procedure and reviews different kinds of microwave filters.

2.2 Low-Pass Prototype

The low-pass prototype is defined as a two port lumped element operating in a 1Ω system with an angular frequency of 1 rad/s, i.e. $\omega = 1$. The design of microwave filters begins with the synthesis of this low-pass prototype network. The total number of reactive elements in the filter determine the order of the filter; and, the selectivity of the filter is directly proportional to the order of filter. Unfortunately, the ideal low-pass filter is impossible to realize physically; therefore, there are several functions that can be used to approximate the ideal low-pass response which are physically realizable. The most common choices of such approximations functions are given in the next section. The low-pass filter can be formed with a ladder-type network with shunt capacitors interconnected with series inductors, as shown in figure 2.1 for a network of degree N.

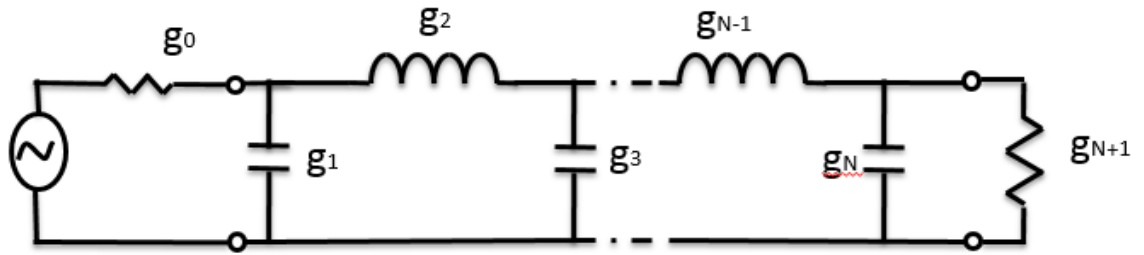


Figure 2.1: Low-Pass Prototype for an all –pole transfer function

$$g_0 = \begin{cases} R_o & \text{if } g_1 \text{ is a shunt capacitor} \\ G_o & \text{if } g_1 \text{ is a series inductor} \end{cases}$$

$$g_{N+1} = \begin{cases} R_L & \text{if } g_N \text{ is a shunt capacitor} \\ G_L & \text{if } g_N \text{ is a series inductor} \end{cases}$$

This series parallel ladder network is also known as Cauer’s network because of Wilhelm Cauer’s pioneering work in the field of network synthesis. g_r ($r = 0,1,2,\dots, N+1$) will be the element’s values and g_1, g_2, \dots, g_N would be the inductor and capacitor values accordingly. The values R_o and R_L are the generator and load impedances respectively.

The ladder network can also be realized by the use of impedance or admittance inverters, which are lossless and frequency independent two port networks, shown in figure 2.2, and can also be defined by the below matrix [1].

$$[T] = \begin{bmatrix} 0 & jK \\ j/K & 0 \end{bmatrix} \quad \text{Eq 2.1}$$

Where 'K' is the characteristic impedance and admittance of an inverter and can be written as

$$Z_{in} = \frac{K^2}{Z_{load}} \quad \text{Eq 2.2}$$

Where Z_{in} and Z_{load} is the input and output impedance of inverter.

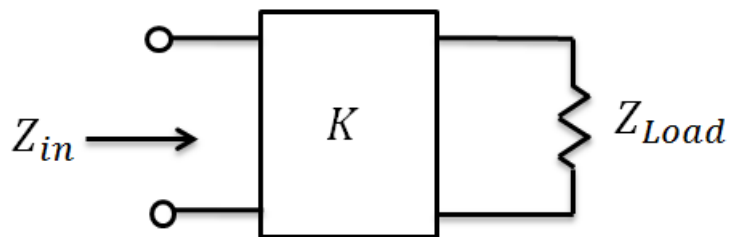


Figure 2.2: Impedance inverter terminated with a load

The low-pass prototype can be designed with inverters coupled with series inductors or shunt capacitors as shown in figure 2.3. These inverters used to transform between shunt connected and series connected elements. Thus, a parallel LC resonator can be transformed into series LC resonator and vice versa.

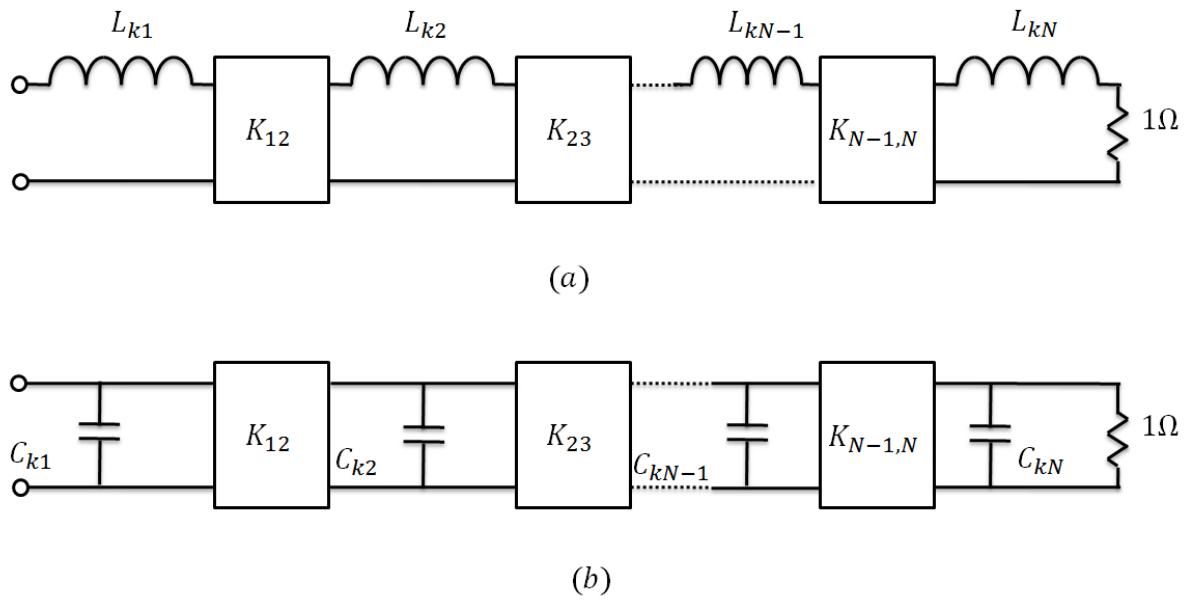


Figure 2.3: General Nth Degree inverter coupled a low-pass prototype with (a) inductors, and (b) capacitors

2.3 Transfer Function

A two port linear time variant low pass filter network transfer function can be represented as

$$|S_{21}(\omega)| = \frac{1}{1 + \varepsilon^2 F_n^2(\omega)} \quad \text{Eq 2.3}$$

Where ε is the ripple constant, ω is the angular frequency and $F_n(\omega)$ is the filtering function. It is approximated by several transfer functions, depending upon the ripple behaviour in the passband and stopband. The transfer function insertion loss is expressed as

$$IL (dB) = 10 \log \frac{1}{|S_{21}(j\omega)|} dB \quad \text{Eq 2.4}$$

The input reflection coefficient and power can be related and defined through unitary conditions as

$$|S_{11}(j\omega)|^2 + |S_{21}(j\omega)|^2 = 1 \quad (\text{Loss less network}) \quad \text{Eq 2.5}$$

It also gives

$$L_r(\omega) = 10 \log[1 - |S_{21}(j\omega)|^2] dB \quad \text{Eq 2.6}$$

Return loss is the measurement of attenuation of a reflected signal, and a perfectly matched filter would have infinite return loss. Thus it can be defined as

[1]

$$L_r(\omega) = -20 \log |S_{11}(j\omega)| dB \quad \text{Eq 2.7}$$

2.3.1 The maximally flat prototype

It is the simplest approximation to an ideal low-pass filter prototype as it has a flat response in the passband [1]. Figure 2.4 shows the response of the Butterworth low-pass filter.

$$|S_{21}(j\omega)|^2 = \frac{1}{1 + \omega^{2N}} \quad \text{Eq 2.8}$$

The insertion loss (IL) becomes

$$IL(\omega) = 20 \log(1 + \omega^{2N}) \text{dB} \quad \text{Eq 2.9}$$

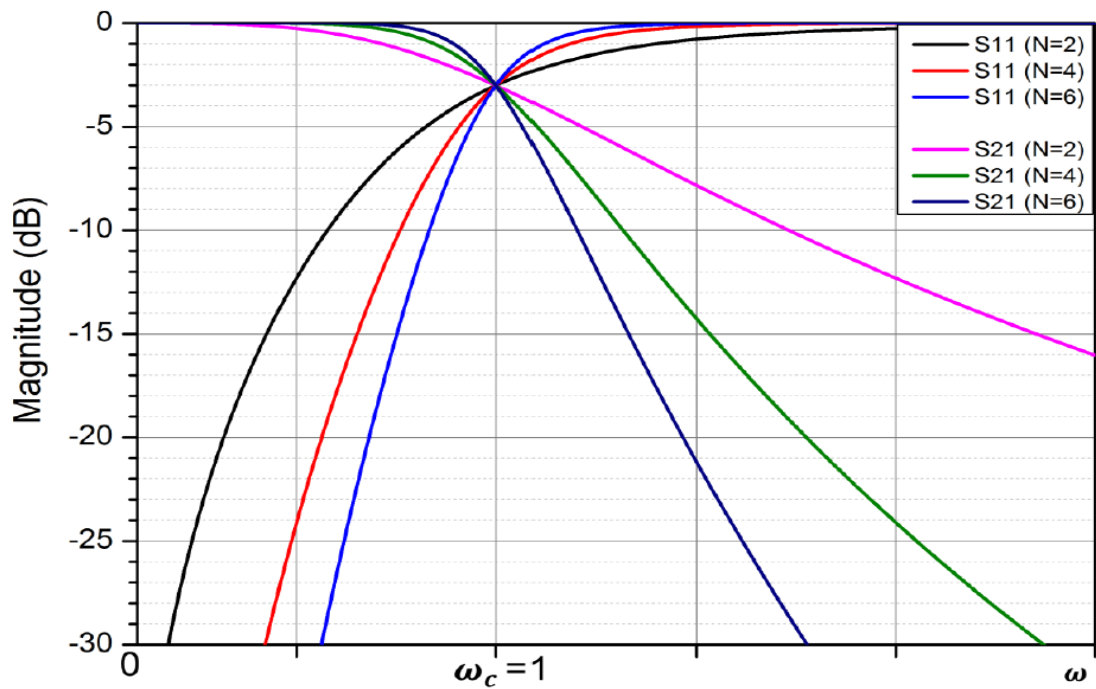


Figure 2.4: Butterworth low-pass response

This filter shows the 3 dB frequency response at $\Omega = \frac{\omega}{\omega_c} = 1$. The name maximally flat indicates that the filter represents the optimum value of insertion loss at the passband, which has no ripples and a smooth transfer function with a slow cut off. All the N transmission zeros lie at $\omega = \infty$ and the filter becomes more and more selective as we increase the degree N, as shown in fig 1.3. To meet the specific attenuation level, the order of the filter can be calculated as:

$$N \geq \frac{L_A + L_R}{20 \log(S)} \quad \text{Eq 2.10}$$

Where

$$S = \frac{\omega_s}{\omega_p} \geq 1 \quad \text{Eq 2.11}$$

Here L_R and L_A are the return loss and insertion loss of a filter and ω_s and ω_p represents the stopband and passband frequencies. For the maximally flat inverter coupled low-pass prototype, explicit formulas have been developed for the element values, shown in figure 1.1. The element values g_r are given by

$$g_r = \sin \left[\frac{(2r-1)\pi}{2N} \right] \quad r = 1, 2, \dots, N \quad \text{Eq 2.12}$$

Where

$$g_r = \begin{cases} L_{kr} & (r \text{ odd}) \\ C_{kr} & (r \text{ even}) \end{cases} \quad \text{Eq 2.13}$$

And $g_0 = g_{N+1} = 1$

2.3.2 The Chebyshev Prototype

The Chebyshev Prototype has a better roll off than the Butterworth, but introduces some ripples between two values in the passband up to its cut-off frequency, i.e., $\omega = 1$ which then rolls off quickly in the stopband. Therefore, better selectivity can be achieved between the passband and the stopband with the Chebyshev prototype [1, 2].

$$|S_{21}(j\omega)|^2 = \frac{1}{1 + \varepsilon^2 T_N^2(\omega)} \quad \text{Eq 2.14}$$

Where ' ε ' is the ripple level in passband and can be described as:

$$\varepsilon = \left(10^{\frac{L_R}{10}} - 1\right)^2 \quad \text{Eq 2.15}$$

$T_n(\omega)$ is the Nth order Chebyshev polynomial and can be defined as:

$$T_n(\omega) = \cos[N \cos^{-1}(\omega)] \quad \text{Eq 2.16}$$

Insertion loss can also be calculated as:

$$IL = 10 \log[1 + \varepsilon^2 T_N^2(\omega)] \quad \text{Eq 2.17}$$

And

$$IL = 10 \log[1 + \varepsilon^2] \quad \text{Eq 2.18}$$

The degree of Chebyshev filter can be calculated as:

$$N \geq \frac{L_A + L_R + 6}{20 \log \left[S + (S^2 - 1)^{\frac{1}{2}} \right]} \quad \text{Eq 2.19}$$

Where L_A and L_R are the stopband attenuation and passband return loss. 'S' shows the ratio between the stopband and passband frequencies. In figure 2.5, the response of the Chebyshev prototype is shown. To calculate the element values of the Nth order, the Chebyshev prototype with impedance inverter is defined as

$$K_{r,r+1} = \frac{\left[\eta^2 + \sin^2 \left(\frac{\pi r}{N} \right) \right]^{\frac{1}{2}}}{\eta} \quad r = 1, 2, \dots, N - 1 \quad \text{Eq 2.20}$$

And

$$L_{kr} = \frac{2}{\eta} \sin \left[\frac{(2r - 1)\pi}{2N} \right] \quad r = 1, 2, \dots, N \quad \text{Eq 2.21}$$

Where η is expressed as

$$\eta = \sinh \left[\frac{1}{N} \sinh^{-1} \left(\frac{1}{\varepsilon} \right) \right] \quad \text{Eq 2.22}$$

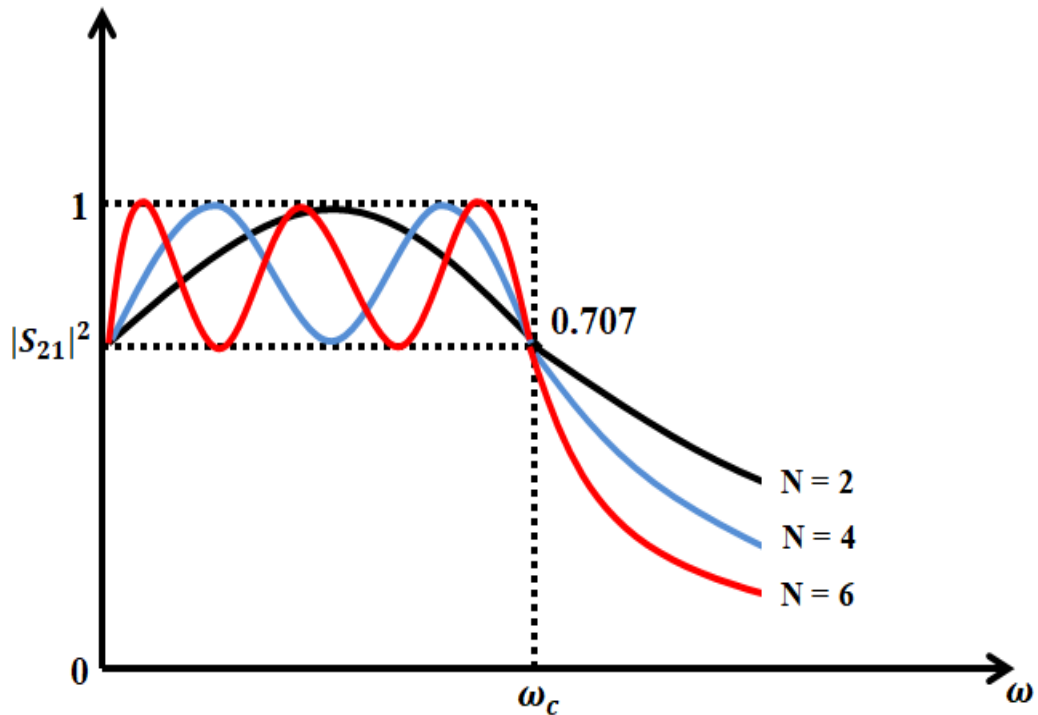


Figure 2.5: Chebyshev low-pass response

2.3.3 Generalised Chebyshev prototype

This type of approximation has a passband with the equiripple response and placed transmission zeros arbitrarily outside the passband. The symmetric and asymmetric response can be achieved by placing attenuation poles at any finite frequency value. The generalized Chebyshev approximation can be classified as [1]:

$$|S_{21}(j\omega)|^2 = \frac{1}{1 + \varepsilon^2 F_n^2(\omega)} \quad \text{Eq 2.23}$$

with $-1 < F_N(\omega) < +1$ for $-1 < \omega < +1$

moreover, $F_N(\omega_r) = \infty$ $r = 1, 2, \dots, N$

where ' ω_r ' is the r^{th} attenuation pole frequency. It makes possible a sharp cut off between the passband and the stopband. It can be produced by different methods defined by different authors in [23, 24]. The *extracted pole technique* and *cross coupling* are famous techniques used to produce arbitrary transmission zeros. A novel technique with different waveguide topologies and design to produce an arbitrary placed transmission zeros is also discussed in [25]. Figure 2.6 shows the filter response of a generalized Chebyshev prototype.

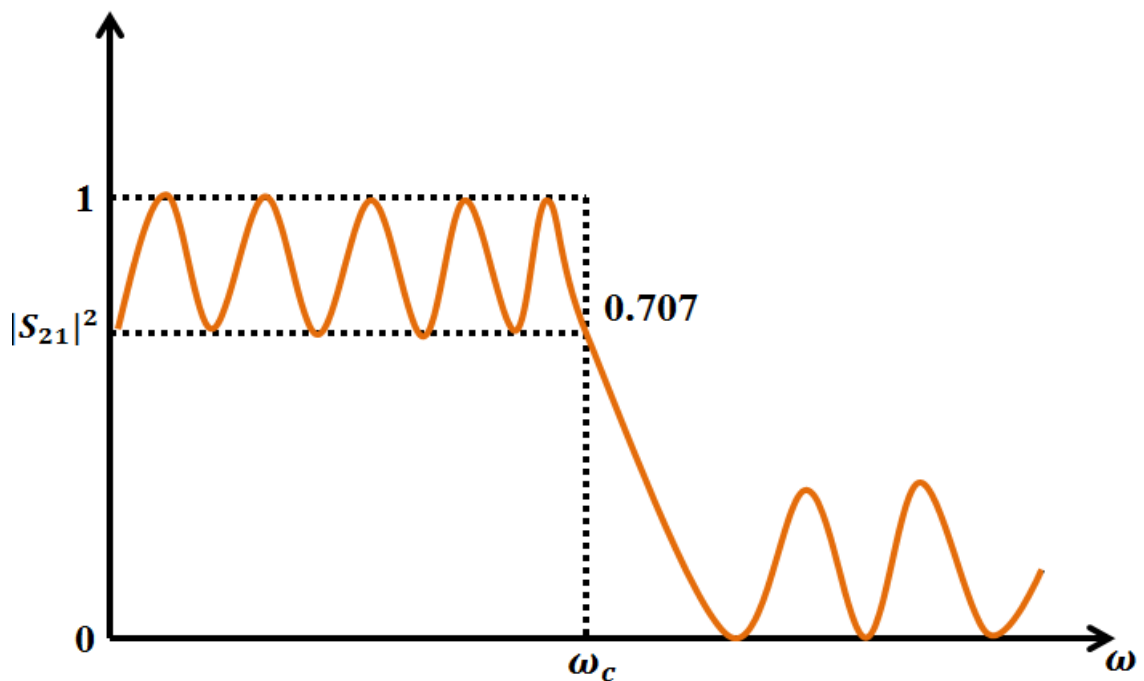


Figure 2.6: Generalised Chebyshev low-pass filter response

2.4 Frequency and Impedance Transformations

A normalized prototype filter has been shown in figure 1.1 which illustrates that normalized designs have a source and load impedance of 1ohm and cut off

frequency equal to 1. A low-pass design needs to be scaled from a source resistance of 1 to R_o and cut-off frequency of 1 to ω_c and then converted into high-pass, band-pass and band-stop filter characteristics, depending on system requirements. If we let the primes denote frequency and impedance scaled quantities, the new filter components can be obtained by following relations [22].

$$L' = R_o L_k \quad \text{Eq 2.24}$$

$$C' = \frac{C_k}{R_o} \quad \text{Eq 2.25}$$

$$R'_s = R_o \quad \text{Eq 2.26}$$

$$R'_L = R_o R_L \quad \text{Eq 2.27}$$

where R_L , L and C are the original prototype components and ' ω ' in the low-pass prototype can be changed from unity to $\frac{\omega}{\omega_c}$. Therefore, the power loss ratio of the filter will be

$$PLR'(\omega) = PLR\left(\frac{\omega}{\omega_c}\right) \quad \text{Eq 2.28}$$

where ' ω_c ' is the cut-off frequency of the filter. The new filter element values with frequency and impedance transformation can be determined by using the following expressions [22]:

$$L'_K = \frac{R_o L_k}{\omega_c} \quad \text{Eq 2.29}$$

$$C'_K = \frac{C_k}{R_o \omega_c} \quad \text{Eq 2.30}$$

Transformation and element normalization significantly reduced the efforts involved in filter synthesis. They also enable band-pass, band-stop or high-pass filter synthesis with an arbitrary frequency bandwidth and source impedance from a low-pass prototype with unity source impedance and unity cut-off frequency [26].

2.5 Band-pass Transformation

A low-pass prototype design can also be transformed to have a band-pass response. If ω_1 and ω_2 represent the edges of the passband, then the band-pass filter response can be obtained by following expressions [22]:

$$\omega \leftarrow \frac{\omega_o}{\omega_2 - \omega_1} \left(\frac{\omega}{\omega_o} - \frac{\omega_o}{\omega} \right) = \frac{1}{FBW} \left(\frac{\omega}{\omega_o} - \frac{\omega_o}{\omega} \right) \quad \text{Eq 2.31}$$

Where

$$FBW = \frac{\omega_2 - \omega_1}{\omega_o} \quad \text{Eq 2.32}$$

and

$$\omega_o = (\omega_1\omega_2)^{\frac{1}{2}} \quad \text{Eq 2.33}$$

Where FBW and ω_o represent the passband fractional bandwidth and centre frequency. The transformation of equation 2.30 maps the response of the low-pass filter to a band-pass response, shown in figure 2.7.

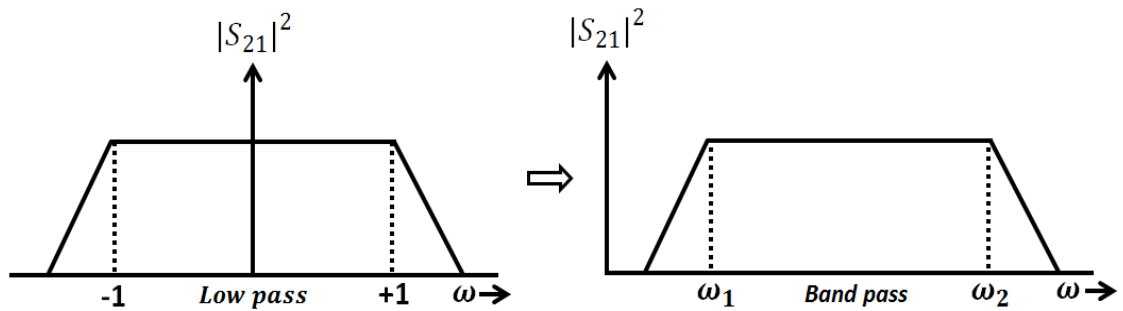


Figure 2.7: Low-pass to Band-pass transformation

For a band-pass transformation, a series inductor is transformed to a series LC circuit with impedance and frequency scaled values as

$$L'_K = \frac{L_k}{\omega_o FBW} \quad \text{Eq 2.34}$$

$$C'_k = \frac{FBW}{\omega_o L_k} \quad \text{Eq 2.35}$$

Moreover, a shunt capacitor is transformed to a shunt LC circuit with impedance and frequency scaled values as

$$L'_K = \frac{FBW}{\omega_o C_k} \quad \text{Eq 2.36}$$

$$C'_K = \frac{C_k}{\omega_o FBW} \quad \text{Eq 2.37}$$

This synthesis method provides excellent results for moderate and narrow bandwidths (upto 20% normalized bandwidth in some cases) and is therefore adequate for a variety of microwave band-pass filter applications. Though, direct applications of exact network synthesis techniques to the design of microwave filters is possible in very few cases because of the physical constraints imposed by the physical structures the makeup the filters [27].

The band-pass transformation of inductor and capacitor is given in figure 2.8.

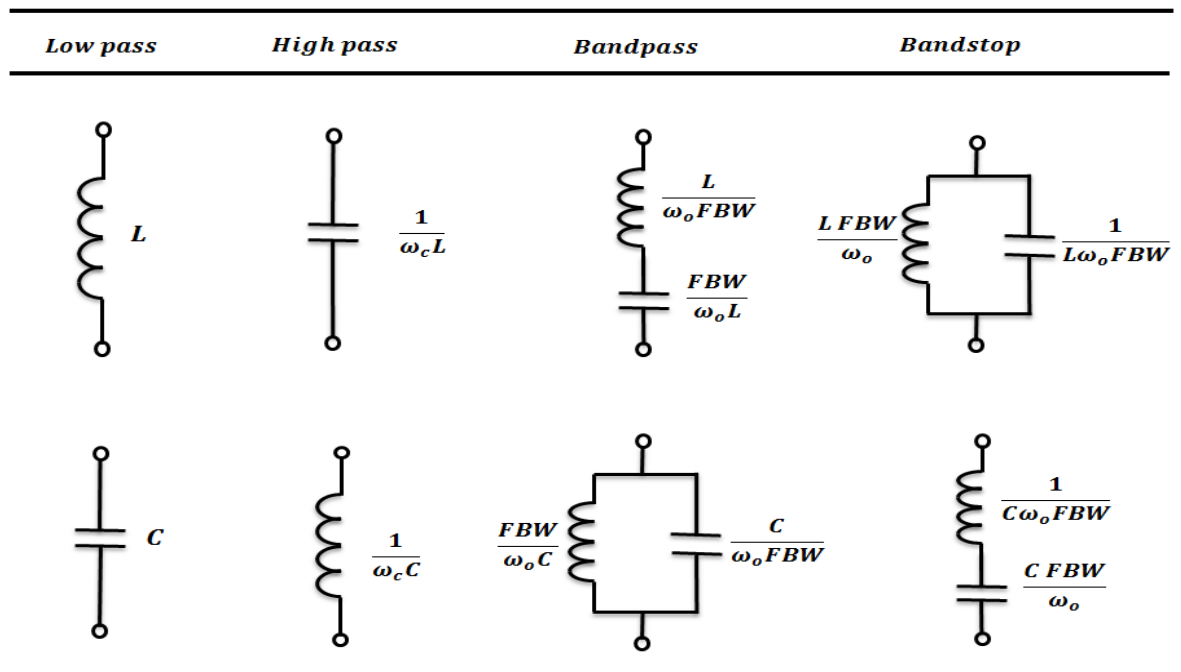


Figure 2.8: Prototype filter transformations[22]

2.6 Physical Realization of Microwave Filters

The physical realization of microwave filters in any technology depends on many factors. These factors include frequency range, passband insertion loss, Q-factor, physical size, power handling capability, cost, selectivity and the temperature drift of a filter. The extensive consideration of the entirety of these factors is especially needed before choosing any technology for the microwave filter.

Today's wireless communication systems have very stringent in-band and out-of-band requirements. Conventional cellular base stations use air-filled coaxial and waveguide filters. The air-filled coaxial filter is low-cost, has good spurious performance and wide tuning range but is very bulky and has a low Q-factor. To improve low Q-factor, the high dielectric rod is introduced by replacing the inner metal rod which makes the Q-factor of the resonator approximately double, but has worse spurious performance and is not suited for future miniaturized devices due to their higher volume [28]. Air-filled waveguide filters also suffer from their big size but offer simple design structure, and very high Q-factor values make it suitable for low loss devices. A brief explanation of different kinds of coaxial and waveguide filters used in cellular base stations is given in the following subsections.

2.6.1 Coaxial TEM Filters

A cavity filter with a metallic center conductor has broad applications in satellite and mobile communications because of their low cost, wide spurious free stopband and greater tuning range [28]. Coaxial cavity TEM filters are typically

inter-digital or combline in structure. The interdigital filters are usually required when wider bandwidths are needed. They are somewhat similar to combline filters but have inverted resonators, where combline resonator filters can be used with a bandwidth of 1-50% and are widely employed in mobile base stations [21]. The structure for the combline and interdigital filter are given in figures 2.9.

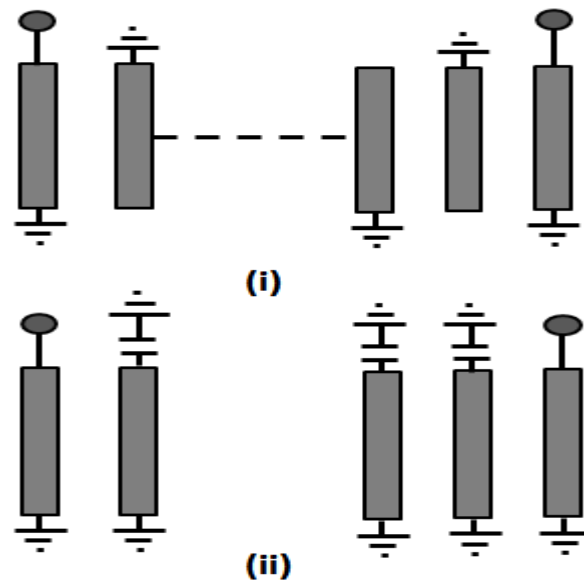


Figure 2.9: Coaxial TEM filters; (i) Interdigital (ii) combline

The combline resonator has a metallic rod in its center which is grounded from one end and open at another end. The first combline was introduced by G. L. Matthaei in 1963 [29]. Combline resonators have an inner conductor equal or less than a quarter of a wavelength. The gap between the resonator and the ground spacing can be realized as capacitance while the other end of the resonator is short-circuited with ground spacing. This configuration also showed in figure 2.10.

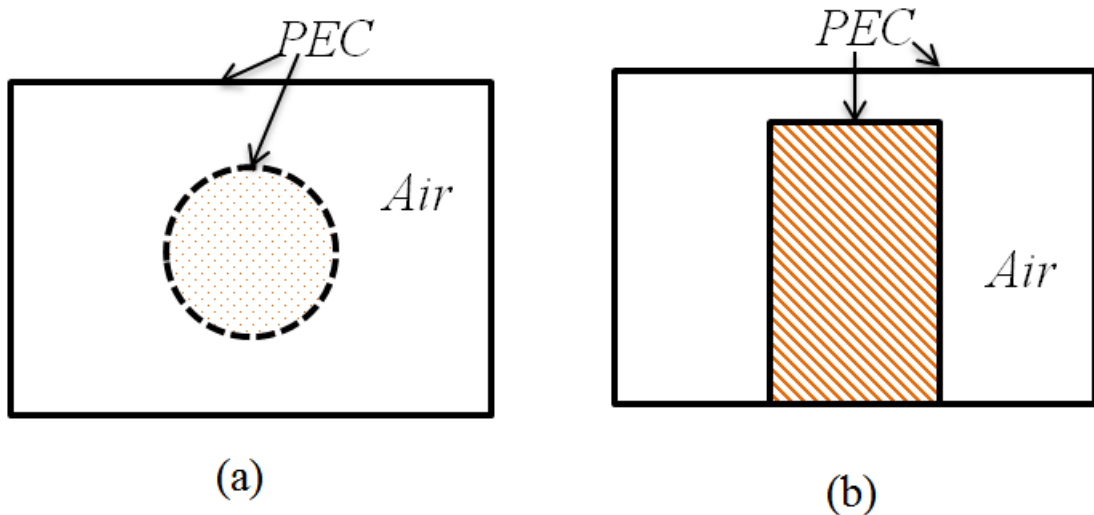


Figure 2.10: TEM coaxial resonator; (i) top view (ii) side view

The low Q-factor of metallic combline resonator is due to the conductor loss dissipated on the inner conductor of the resonator. This Q-factor can be increased by replacing the central metal rod with a high dielectric material or by applying different techniques like round base and periodic disks inner conductor [30, 31]. The combline structure can also be viewed as TEM a transmission line which increases the selectivity on the high side of the passband when the length of the resonators increased. The cross-sectional structure of the combline filter has inner conductors of different shapes; circular, rectangular and square. The outer conductor is also circular, square or rectangular. The characteristic impedance of these coaxial resonators is a function of their cross-sectional dimension of line and dielectric constants between the conductors [1]. These combline filters also act differently when their ground plane spacing become appreciable relative to the wavelength and the waveguide modes become dominant in coupling the structure; the filter will no longer have a TEM structure and this kind of filter is usually termed as Evanescent-mode

waveguide filter. It is used widely in wireless base stations and has good unloaded Q and excellent rejection with better symmetry in comparison to combline with small ground plane spacing. The major drawback lies in the asymmetry of the coaxial combline filter insertion loss, which is weaker on the low side of the response for broad bandwidths. It also makes it difficult to introduce the transmission zero on the low side due to dispersion effect for broad bandwidths [32].

2.6.2 Dielectric Combline Filter

As the conventional coaxial combline filters have shown high losses, these losses can be reduced by replacing the center conductor with a high permittivity dielectric rod. This dielectric combline filter amalgamates the merits of the dielectric and combline filter by offering high Q-factor, wide spurious performance and simple structure. The continuous magnetic field at the dielectric boundary eliminates the current on the dielectric rod, thus resulting in a higher unloaded Q-factor [33]. However, unfortunately, there is no optimum value of inner and outer conductor radius ratio for the dielectric combline filter, which gives a maximum unloaded Q-factor [28]. The dielectric material is not a conductor but an insulator, but not all insulators are dielectric. They have the property of becoming polarized and conducting very little electricity, but is a very strong candidate of electric field [34]. For the same size, the dielectric combline filter loss is reduced to half when compared to a coaxial combline filter. Rod diameter length and proximity determine the resonant frequency, Q-factor and spurious free bandwidth of the resonator, although the resonant frequency and unloaded Q-factor of the resonator is inversely proportional to the dielectric rod

radius and length. The fundamental mode is quite sensitive to rod length whereas the spurious modes are very sensitive to rod diameter. So, for better spurious performance, the resonators with a height and diameter ratio of 1 or greater are preferred [28]. A graphical representation of a dielectric combline filter is shown in figure 2.11.

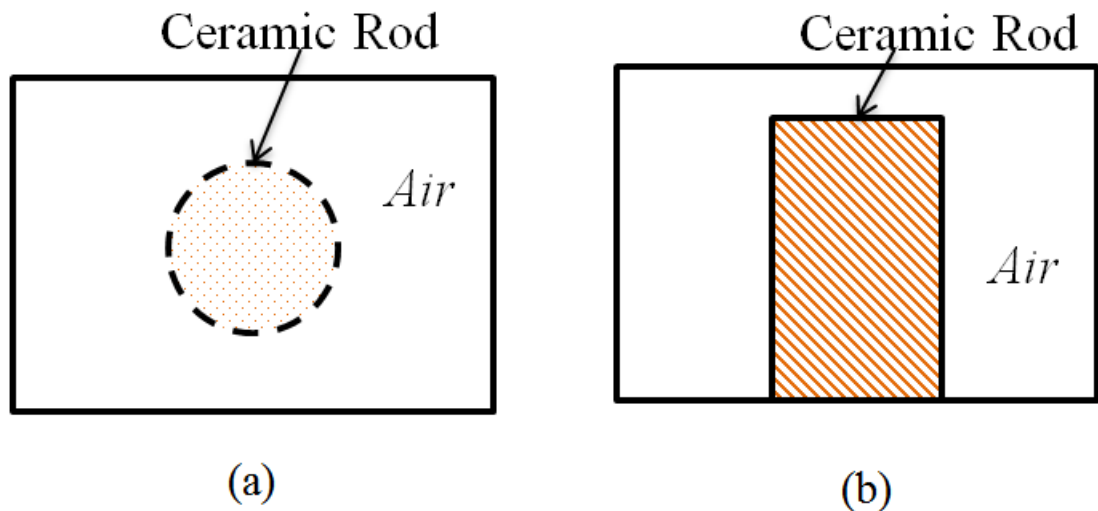


Figure 2.11: Dielectric combline resonator; (i) top view (ii) side view

2.6.3 Waveguide filters

Waveguides can be used to guide electromagnetic energy from one point to another. The most common types of waveguides are rectangular and circular waveguides. The waveguide's structure is short circuited from both ends, forming a closed box or cavity called resonator, which has the function of confining electromagnetic energy. Waveguide resonators have the capability to store both electric and magnetic energy which dissipates power in their walls or in the material which fills the cavity. They have been used for high power and high Q-factor applications. They support infinite numbers of TE_{mn} , TM_{mn} and

hybrid modes, where TEM mode does not exist in it because it is a single conductor. Here 'm' shows the half wave variations in the 'x' direction and 'n' shows the half wave variations in the 'y' direction. TE_{10} is the fundamental mode of the rectangular waveguide, whereas circular waveguides support TE_{11} or TM_{11} as their fundamental modes [1, 22]. Coupling between resonators can be achieved through inductive or capacitive windows or by an inductive post in the resonator common wall. The disadvantage of these kind of filters are their larger volume which can also be reduced through dual mode resonators. Their stopband performance also suffers with close proximity to higher order modes and re-resonances of fundamental mode.

2.6.4 Evanescent Mode Filters

Seymour B. Cohn (1965) published a paper which states the reasons for his continuing attraction to microwave filters [35]. He also elaborates in another paper that when we blindly accepted the scientific rules, laws, theorems and common knowledge, it will lead us to making errors and will become a mental obstacle that prevents us from making new discoveries. The Evanescent-mode waveguide is a good example of these barriers. Early work done on waveguides concluded that below the cut-off conditions in the waveguide, wave propagation could not exist. For this reason, the waves below the cut-off region could be called 'evanescent,' which usually fades quickly. However, this conclusion is only true for the conditions when the waveguide is infinitely long or could be terminated in matched impedance. Waveguides are designed in such a way that its fundamental mode will operate above the cut-off frequency of the waveguide. As the cut-off frequency is inversely proportional to the size of the

waveguide, some restrictions apply to the reduction of size for a given frequency of interest. We can further reduce the size of the waveguide if there is no constraint for the fundamental mode to propagate above the cut-off frequency of the waveguide. Filters which operate in this region are called evanescent-mode waveguide filters [36]. It is shown by P Jerry that evanescent mode filters with given Chebyshev functions can be realized.

The initial appearances of evanescent modes were usually seen as 'ghost modes' which sometimes made results in a breakdown in waveguides carrying high power. They are called 'evanescent' because they have a real propagation constant and imaginary wave impedance. Lebedev and Guttsait first discovered the resonant behavior of evanescent modes provided the necessary, terminating conditions [21]. They suggested that these simple resonators can be used for wideband applications. If a waveguide provided with a long a wide screw, placed in the middle of the cavity, it has a large capacitance. This capacitance can be combined with a waveguide below cut-off frequency (evanescent mode). This cavity will then have an inductive reactance that resonates with the capacitance from the screw. It is also possible to use ridge waveguides to introduce the distributed capacitance instead of posts or screws [37].

Evanescent mode filters use scattering waves created from discontinuities in waveguides to form inductively coupled high Q filters. The filter design approach which considers the cut-off waveguide modes is termed the evanescent mode design technique [38]. This technique uses circuit elements which represent the frequency variations of below cut-off waveguide modes. In evanescent mode

filter design, a major assumption has been made that the TE_{01} is the only mode existing in the guide. If the rectangular waveguide with the conventional aspect ratio is excited in a pure evanescent mode TE_{10} , all the other modes in the guide will have very high attenuation constants. For this reason, if there is a moderate distance from the obstacle, the field will have a virtually pure evanescent TE_{10} mode [39]. Evanescent mode filters have the advantage of having a small volume and lighter weight in comparison to traditional waveguide filters. They can be used to couple directly with a coaxial line or above cut off propagating waveguide. They are usually likely to be used at low frequencies, where waveguide size is a major obstacle to design a filter, but a different filter is being designed for higher frequencies as well [40]. A band stop filter using short circuited cylindrical waveguide cavities is reported here, where it shows that evanescent mode structure is smaller than the conventional cylindrical cavity structure operating above the cut off frequency without sacrificing performance [41]. The major drawback for this filter is their lower Q-factor. The Q-factor will be higher for large filters but the width of the filter should not be close to the cut-off [21]. If a waveguide cavity is provided with a short trim screw at the centre, where the electric field is strongest, It will act as a tuning screw. If the same screw is long and wide, the resonator will then have an inductive reactance that resonates with the high capacitance of the screw. Eventually the waveguide resonator works below the cut-off frequency and is called an evanescent mode resonator. The waveguide resonant structure comparison with the tuning screw, evanescent mode screw and combline resonator discussed above is shown in figure 2.12 [37].

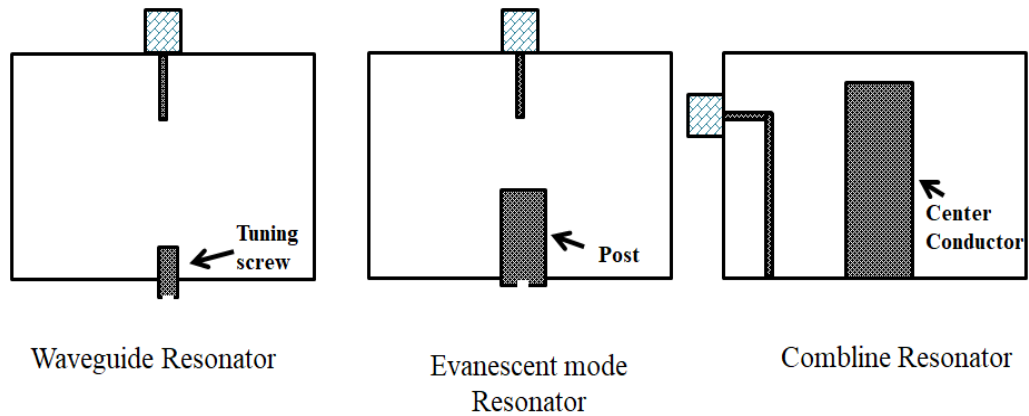
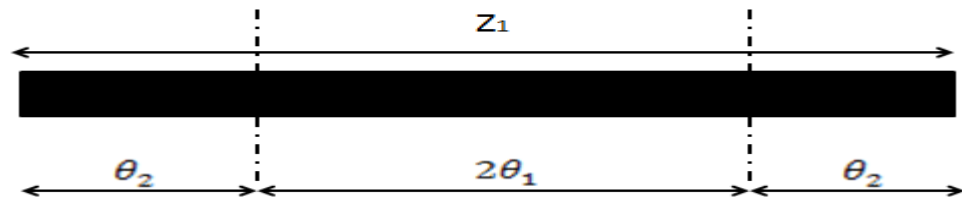


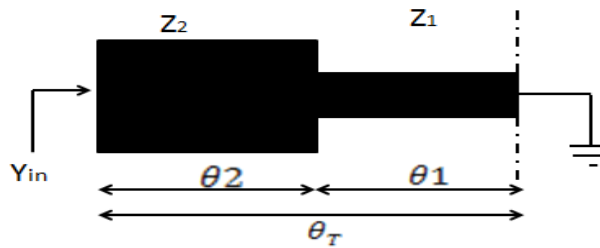
Figure 2.12: Comparison of different resonant structures

2.6.5 Stepped Impedance Resonator Filters

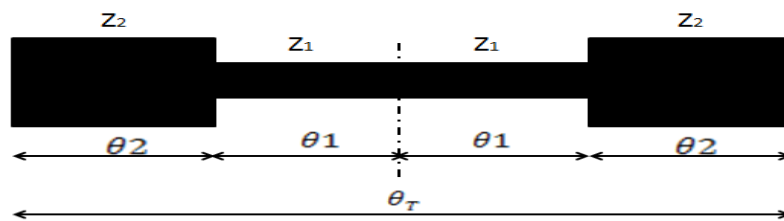
Stepped impedance resonators (SIRs) are formed by cascading two sections of different characteristic impedance. With the use of shorter physical length, the electrical resonance can also be achieved. The coaxial band-pass filter was the first reported application of SIR [42]. It is designed to be a compact band-pass filter without degrading the Q-factor, which is a problem in conventional comblines resonator filters. Nowadays, SIRs are extensively used where we need to control the first spurious response of the filter. If a transmission line has a uniform characteristic impedance with an electrical length of π radian, this kind of transmission line resonator is known as uniform impedance resonator (UIR). A UIR and SIR in coaxial form with quarter wave length and half wavelength is given in the figure 2.13 [43].



(a)



(b)



(c)

Figure 2.13: (a) Uniform impedance resonator (b) Quarter wavelength stepped impedance resonator (c) Half wavelength stepped impedance resonator

A stepped impedance resonator is a TEM or Quasi TEM transmission line, having two or more transmission lines with different characteristic impedance. Conventional wavelength resonators have continuous distributed capacitance and inductance. At the ground end, the capacitance has a minimum effect and, at the open end, the inductance has a minimum effect. The distributed capacitance and inductance is increased by increasing the impedance of the

transmission line, which certainly decreases the resonant frequency as they have the inverse relationship between them. The two most popular SIR configurations are short-circuited quarter wavelength resonators and open circuited half wavelength resonators, as shown in figure 2.13. It is shown that a quarter wavelength resonator has short ended characteristic impedance Z_1 and electrical length θ_1 connected to an open end transmission line with a characteristic impedance of Z_2 and θ_2 . This will be the fundamental structure of SIRs, and half wavelength resonators consist of two quarter wavelength sections connected to each other with short circuited ends by replacing the ground for this connection. The resonant condition of stepped impedance resonators may be given as [42]:

$$\frac{Z_2}{Z_1} = \tan \beta_1 l_1 \cdot \tan \beta_2 l_2 \equiv K \text{ (Impedance Ratio)} \quad \text{Eq 2.38}$$

When the medium is uniform (air)

$$\beta_{p1} = \beta_{p2} = \beta_p \quad \text{Eq 2.39}$$

Where β_p is a phase constant. From equation 2.38

$$K = \frac{\tan \theta_1 \cdot (\tan \theta_T - \tan \theta_1)}{1 + \tan \theta_T \cdot \tan \theta_1} \quad \text{Eq 2.40}$$

Where 'θ' is the electrical length, so

$$\theta_T = \theta_1 + \theta_2 \quad \text{Eq 2.41}$$

Therefore θ_T is minimum when

$$\theta_1 = \theta_2 = \tan^{-1}\sqrt{K} \quad \text{Eq 2.42}$$

We get the minimum electrical length when $K \leq 1$, and it is not practical to design a resonator with $K > 1$, because of its greater length.

$$\theta_{T,min} = \tan^{-1}\left(\frac{2\sqrt{K}}{1-K}\right) \quad \text{Eq 2.43}$$

In a dielectric filled stepped impedance resonator

$$\beta_2 = \sqrt{\epsilon_r}\beta_1, \quad \text{Eq 2.44}$$

Where ϵ_r is relative dielectric constant.

The total resonator length becomes a minimum when l_1 is:

$$\frac{l_1}{l_0} = \frac{2}{\pi} \sin^{-1}\left(\frac{K(1-\sqrt{\epsilon_r}K)}{\sqrt{\epsilon_r}-1}\right) \text{ when } 0 < \sqrt{\epsilon_r}K < 1 \quad \text{Eq 2.45}$$

And

$$\frac{l_1}{l_0} = 0, \text{ when } \sqrt{\epsilon_r} K \geq 1 \quad \text{Eq 2.46}$$

Where l_0 is the length of a quarter wavelength uniform line resonator without dielectric material.

In SIRs, the resonator length can be controlled by using the impedance ratio 'K,' which is not the case in UIRs. It makes possible to design SIRs shorter than UIRs of the same resonant frequency. SIRs are used to design band-pass filters to control the first spurious signal in the stopband region. Stepped impedance resonators are used to design filters with wide spurious free stopbands, as well as dual band-pass filters [15, 16, 44].

2.6.6 Dielectric Waveguide Filters

The idea of dielectric was introduced decades before, where it was shown that dielectric objects could perform like metallic cavities and can have the advantage of being small in size and having temperature stability [45]. After that, Seymour B. Cohn introduced the dielectric resonator filter with $\epsilon_r = 100$ and loss tangent $\delta = 0.0001$ having $Q = 10,000$, with some mathematical description of resonant frequencies and coupling of dielectric resonators. Dielectric resonators can be designed by a ceramic puck being placed inside the conducting cavity with or without low dielectric support. The dielectric supports are used to reduce the cavity losses and provide high thermal conductivity. At resonance, most of the electric and magnetic energy is stored within the resonator. The field outside the ceramic puck vanishes rapidly as it goes away from the puck. The conductive cavity encloses the radiation inside

the cavity. The dielectric resonator supports infinite number of modes, and can also be used to design the multimode structure. The resonance of dielectric material depends upon the permittivity, diameter and shape of the resonator. In the mid-1960's, Cohn presented the mathematical explanation of resonant frequencies, coupling and field distribution of dielectric resonator for band-pass filters. The author suggests different structures and properties of dielectric resonators, and gives the formulas for adjacent resonators of a dielectric puck placed inside the metallic conducting box [46]. A dielectric band-pass filter was also proposed with $TE_{01\delta}$ mode dielectric resonator placed coaxially in circular waveguide [47]. It is also mentioned that dielectric resonators provide great physical size reduction, as compared to others with similar Q, but the temperature sensitivity issue of material was present at that time causing unwanted frequency shifts in microwave systems. In 1970's, the temperature stable and low loss barium tetratitanate ceramics were introduced [48, 49], which led to the first realisation of microwave components, but these materials were in very short supply and not available for commercial purposes. The first commercial dielectric was provided by a company named Murata manufacturing, which offered (Z_r, S_a) TiO_4 ceramics with variable temperature coefficients from +10 and -12 ppm/ $^{\circ}C$. It was from this point onwards that dielectric resonators were widely used in microwave filters. A design analysis and procedure of dielectric loaded resonator filters and generalized Chebyshev dielectric loaded filters were also discussed here [50, 51] The Dielectric puck enclosed in a box is shown in figure 2.14.

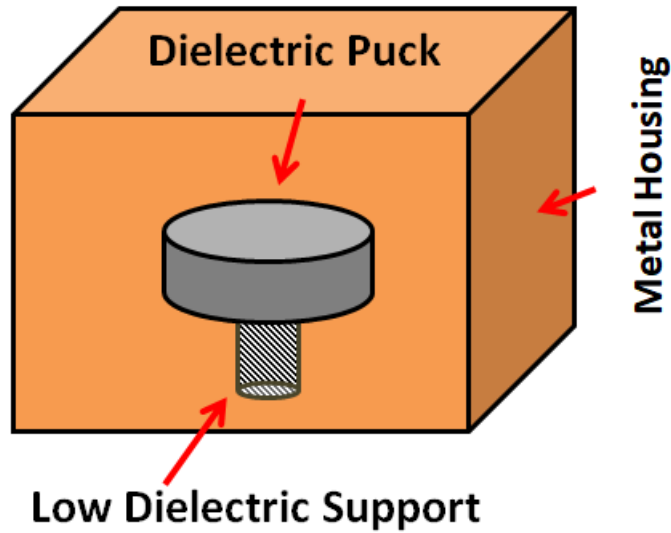


Figure 2.14: Dielectric resonator with puck inside

2.6.7 Integrated Ceramic Waveguide Filter

The dielectric waveguide resonator can also be made by truncating a mono block dielectric material at half of the guide wavelength, making it short circuit at both ends. The Q-Factor and volume of dielectric waveguide resonator reduce by the factor $1/\sqrt{\epsilon_r}$ in comparison with air filled waveguide resonators [52-54].

The resonant frequency of fundamental TE mode can be calculated as [2]:

$$F_0 = \left(\frac{1}{2\sqrt{\epsilon_0 \epsilon_r \mu_r}} \right) \sqrt{\left[\left(\frac{l}{a_r} \right)^2 + \left(\frac{m}{b_r} \right)^2 + \left(\frac{n}{l_r} \right)^2 \right]} \quad \text{Eq 2.47}$$

Where 'l', 'm' and 'n' shows the half wave variation of the electric field along the width, height, and length of resonators. The structural layout of integrated ceramic resonator is depicted in figure 2.15.

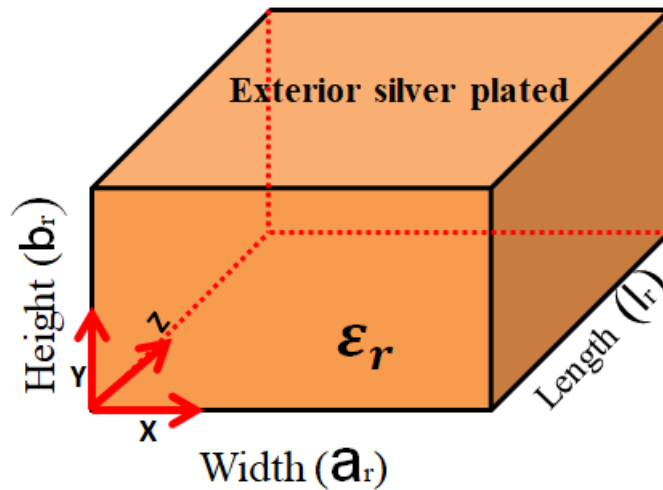


Figure 2.15: Integrated Dielectric Waveguide Resonator

Fiedziusko et al. present detailed description of dielectric material properties, a dielectric waveguide, components, available dielectric materials and their power handling capabilities [55]. Some common dielectric materials used in microwave devices are given in table 2.1.

Table 2-1 Commonly Used Dielectric Materials

Material	Permittivity	Q Values	Frequency (in GHz)	τ_f ($ppm/^{\circ}c$)
MgTiO₃-CaTiO₃	21	8000	7	0
Ba(Mg,Ta)O₃	25	16000	10	3
Ba(Mg,Ta)O₃	25	35000	10	4
Ba(Sn,Mg,Ta)O₃	25	20000	10	0
Ba(Mg,Ta)O₃- Ba(Zn,Ta)O₃	27	15000	10	0

Ba(Zn,Nb)O₃- Ba(Zn,Ta)O₃	30	14000	12	0
Ba(Zr,Zn,Ta)O₃	30	10000	10	0
(Ca,Sr,Ba)ZrO₃	30	4000	11	5
BaO-TiO₂-WO₃	37	8800	6	2
(Zr,Sn)TiO₄	38	7000	7	0
Ba₂Ti₉O₂₀	40	8000	4	2
Sr(Zn,Nb)O₃-SrTiO₃	43	5000	5	±5
BaO-Sm₂O₃-5TiO₂	77	4000	2	15
BaO-PbO-Nd₂O₃-TiO₂	90	5000	1	0

A detailed explanation of single mode ceramic TE₀₁ mode filters and half wave TM₀₁ mode ceramic filters with simple layout and design is given in [56], where the author also discusses the variety of cross coupling schemes for implementing symmetric and asymmetric transmission zeros for a PCS wireless base station.

2.7 Summary

A review of well-known design procedures for microwave band-pass filter design has been presented. Knowing the approximation of ideal low-pass characteristics, a low-pass prototype filter is synthesised using ladder network. Transformations are applied in order to realize the band-pass prototype, which is then simplified by using impedance inverters. The distributed element band-pass prototype is then implemented in commonly adopted technologies depending on its requirements. A few of the commonly used filter technologies

have been described in this chapter. In the next chapter, the focus will be put on ceramic waveguide filters.

3 Ceramic Waveguide Resonators

3.1 Introduction

A rectangular waveguide is a hollow/dielectric filled structure used as a conduit for transferring electromagnetic energy from one point to another. These waveguide filters are widely used due to their high power handling capabilities and high Q-factors, which are important for communication systems such as satellite communication, mobile base stations and radar. Nowadays, most researchers are focused on waveguide miniaturization as conventional waveguide filters are large in volume and hence increase the space required for the wireless system, as well as the cost.

A waveguide resonator is a half guide wavelength section of a waveguide with both ends short circuited. Rectangular and cylindrical shape resonators are most commonly used. At resonance, electric and magnetic fields are equal to each other and provide maximum energy storage by resonator fields. An air filled waveguide resonator can provide a high Q-factor of up to 50,000 with very high power handling [57], but a ceramic filled resonator can provide a great miniaturization though the material has a property of reducing the Q-factor, wavelength and velocity of electromagnetic waves by a factor of $\frac{1}{\sqrt{\epsilon_r}}$ as compared to air filled waveguide [43]. Resonator bandwidth is inversely proportional to the Q-factor. Thus, for narrow bandwidths, the high Q resonator

will be used [58]. A ceramic filled resonator can be made by truncating the piece of ceramic material at half guide wavelength with metallized walls around it. Figure 3.1 shows a ceramic filled rectangular waveguide resonator. The resonant frequency of fundamental TE_{101} mode of a half wavelength ceramic waveguide resonator can be calculated from equation 2.47 [22]. Where 'm', 'n' and 'l' represents the half sinusoidal waveform along the width (a_r), height (b_r) and length (l_r) of resonator respectively, and, for fundamental TE_{101} mode, the half wave varies in the x-direction and z-directions with no variation in the y-direction. It is also evident that the resonant frequency is dependent on the width and length of the resonator regardless of the height. The height usually contributes when the Q-factor and higher order modes are taken into an account. The increase in height increases the Q-factor but also allows the spurious modes to come closer to the fundamental mode. Therefore, rectangular waveguide resonator height is often set to half of its broad dimension, which is a trade-off between good spurious performance and a good Q-factor.

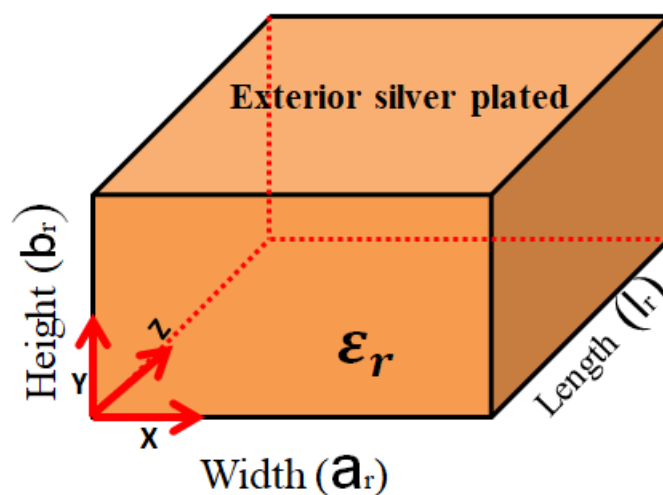


Figure 3.1: Ceramic Filled waveguide Resonator

3.2 Rectangular Waveguide Modes

For a rectangular waveguide resonator, any possible distribution of electric and magnetic fields is called modes. These modes can be categorized into two major groups; transverse electric (TE) and transverse magnetic (TM) modes. In a TE mode of propagation, the electric field is perpendicular to the direction of propagation while the magnetic field is in the direction of propagation. In a TM mode of propagation, the magnetic field is at a right-angle to the direction of propagation and the electric field is in the direction of propagation. The Transverse electromagnetic (TEM) mode is not able to propagate into the waveguide because it is a single conductor transmission line. The most common mode is the TE_{101} mode called the dominant or fundamental mode [22]. Figure 2.15 showed the mode chart of cut-off frequencies of rectangular waveguide modes with an side ratio of $a = 2b$. The lowest frequency that a waveguide will handle is the cut-off frequency, that depends on the cross dimension of a waveguide. The larger the size of the waveguide, the lower the cut-off frequency of the waveguide. Modes with same cut-off frequency, but with different field distributions are called degenerate modes. In most of the applications, waveguide operating frequency and dimensions are chosen so that the only the dominant mode TE_{101} will be propagated, or we make sure that only the single mode is propagated in the waveguide, so we used the waveguide with an aspect ratio of $b/a = 0.5$. The cut-off frequency is normally 30% lower than the operating frequency for such waveguide, to minimize the effect of dispersion caused by different group velocities for different frequency components and to reduce signal distortion caused by a higher mode's

propagation [59]. Figure 3.2 shows the electric field and magnetic field distribution of a rectangular waveguide resonator.

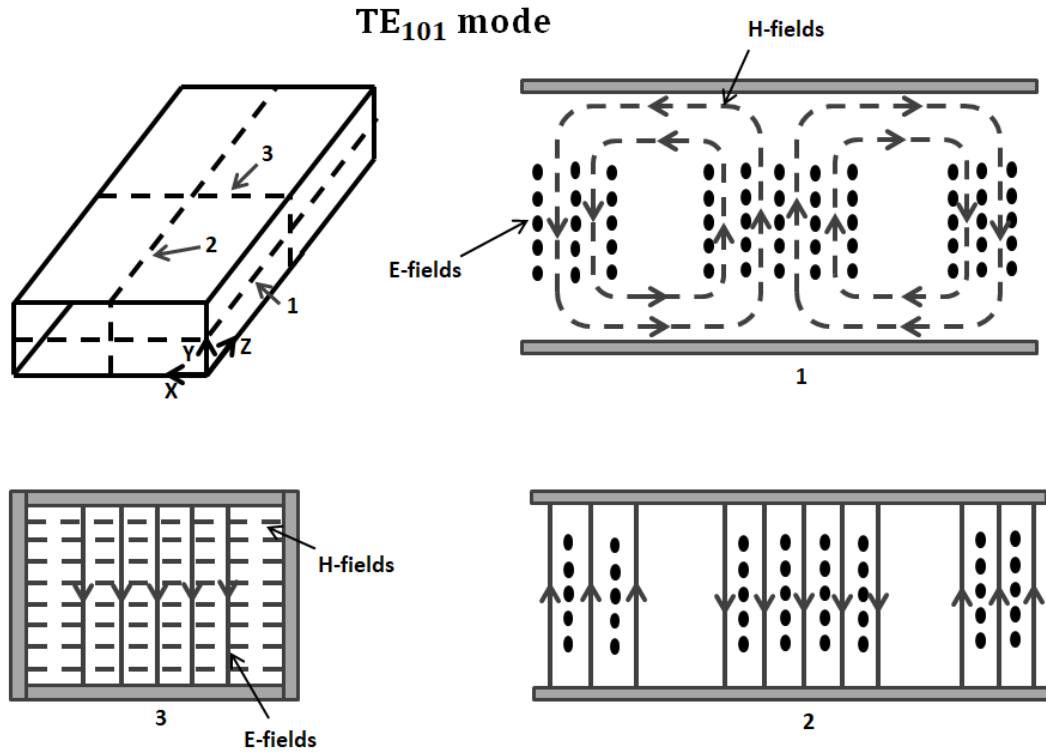


Figure 3.2: E-field and H-field pattern of rectangular waveguide resonator[22]

The field components for fundamental TE_{101} mode in rectangular waveguide for Height < Width < Length are [60]

$$E_y = -2 \frac{A\omega\mu a_r}{\pi} \sin\left(\frac{\pi}{a_r}x\right) \sin\left(\frac{\pi}{l_r}z\right) \quad \text{Eq 3.1}$$

$$H_x = j \frac{Aa_r}{l_r} \sin\left(\frac{\pi}{a_r}x\right) \cos\left(\frac{\pi}{l_r}z\right) \quad \text{Eq 3.2}$$

$$H_z = -j2A \cos\left(\frac{\pi}{a_r}x\right) \sin\left(\frac{\pi}{l_r}z\right) \quad \text{Eq 3.3}$$

$$E_x = E_z = H_y = 0 \quad \text{Eq 3.4}$$

The fundamental frequency of TE₁₀₁ cavity can be calculated from equation 3.1, and the cut-off frequency of this mode can be calculated as [1]

$$\omega_c = \frac{1}{\sqrt{\mu\epsilon}} \sqrt{\left(\frac{m\pi}{a_r}\right)^2 + \left(\frac{n\pi}{b_r}\right)^2} \quad \text{Eq 3.5}$$

For the aspect ratio of $a_r = 2b_r$ in free space, ω_c , is given as

$$\omega_c = \frac{c\pi}{a_r} (m^2 + 4n^2)^{\frac{1}{2}} \quad \text{Eq 3.6}$$

Relative cut-off frequencies of waveguide with an aspect ratio of 1 and 0.5 are also shown in figure 3.3 [59]. The characteristic impedance of TE₁₀₁ mode of rectangular waveguide can be defined as the ratio of the transverse E and H fields [1], i.e.

$$Z_{TE} = \frac{E_y}{H_x} = \frac{\omega\mu}{\beta} \quad \text{Eq 3.7}$$

And the propagation constant (β) can be calculated as

$$\beta = \left[\omega^2 \mu \varepsilon - \left(\frac{\pi}{a} \right)^2 \right]^{\frac{1}{2}} \quad \text{Eq 3.8}$$

Since $\frac{\pi}{a} = \frac{\omega_c}{v}$, therefore

$$\beta = \frac{\omega}{v} \left[1 - \left(\frac{\omega}{\omega_c} \right)^2 \right]^{\frac{1}{2}} \quad \text{Eq 3.9}$$

The guide wavelength (λ_g) is related to propagation constant by

$$\lambda_g = \frac{2\pi}{\beta} \quad \text{Eq 3.10}$$

The guide wavelength is defined as the distance travelled by a wave in a phase shift of 2π radians, and is measured in the direction of propagation, as given by

$$\lambda_g = \frac{2\pi}{\beta} = \frac{\lambda_0}{\sqrt{1 - \left(\frac{\lambda_0}{\lambda_c} \right)^2}} = \frac{\lambda_0}{\sqrt{1 - \left(\frac{\omega_c}{\omega} \right)^2}} \quad \text{Eq 3.11}$$

Where λ_0 is the free space wavelength, and we can compute the group velocity (v_g) from

$$v_g = \frac{d\omega}{d\beta} = v \left[1 - \left(\frac{\omega_c}{\omega} \right)^2 \right]^{\frac{1}{2}} \quad \text{Eq 3.12}$$

Here we see as β tends to zero, λ_g tends to infinity, ' ω ' approaches ' ω_c ' and v_g approaches zero, it will cause phase distortion as the signal frequency is too close to the cut-off frequency[1]. For the electric field to be zero at $z = 0$ and $z = l$ to form a TE_{101} rectangular cavity resonator, ' l ' must be half guide wavelength. Therefore

$$l = \frac{\lambda_g}{2} = \frac{\lambda_0}{2 \left[1 - \left(\frac{\omega_c}{\omega} \right)^2 \right]^{\frac{1}{2}}} \quad \text{Eq 3.13}$$

$$l = \frac{\lambda_0}{2 \left[1 - \left(\frac{\lambda_0}{2a} \right)^2 \right]^{1/2}} \quad \text{Eq 3.14}$$

The resonant frequency of a rectangular waveguide cavity resonator can be approximated as

$$f_0 = \frac{c}{\lambda_0} = \frac{c(a^2 + l^2)^{1/2}}{2al} \quad \text{Eq 3.15}$$

The resonant TE_{101} mode is independent of b as there is no field variation in the y direction. Figure 3.3 show the electric field and magnetic field distribution of a TE_{101} mode, where the electric field makes a half wave variation in width and

length of a ceramic resonator and no field variation occur along the height of the resonator. It also shows that the maximum electric field occurs at the centre region where the magnetic field is minimum and maximum magnetic field strength is present near the side walls of the resonator where the electric field is minimum. For the next TE_{102} mode, the electric field makes two half wave variations along the length of ceramic waveguide resonator, as shown in figure 3.4. The other resonator modes are shown in figure 3.5, 3.6 and 3.7.

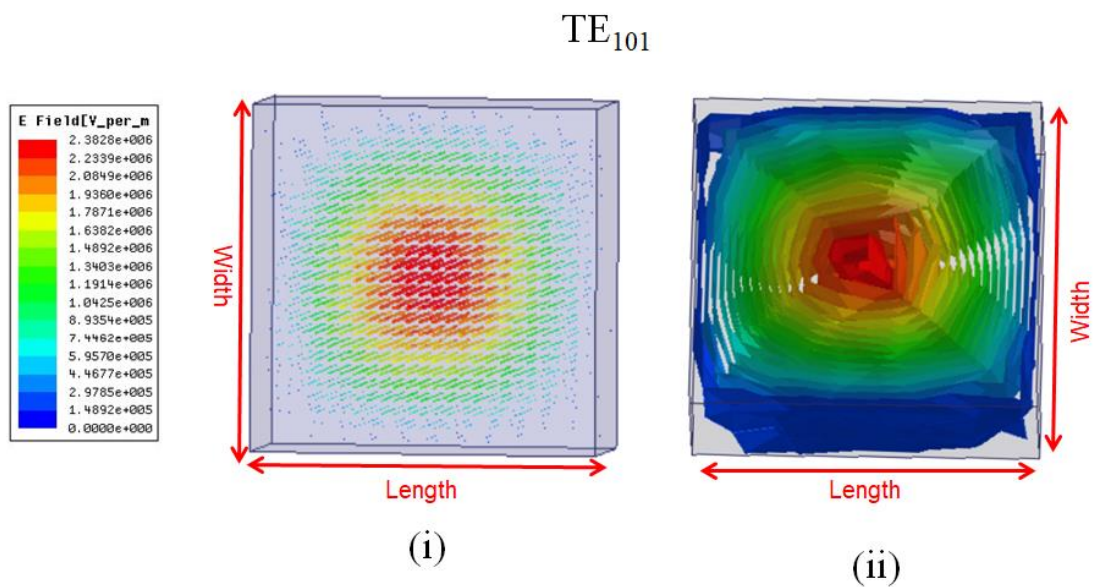


Figure 3.3: Electric field distribution in ceramic waveguide resonator for a TE_{101} mode (from HFSS) (i) Vector form (ii) magnitude form

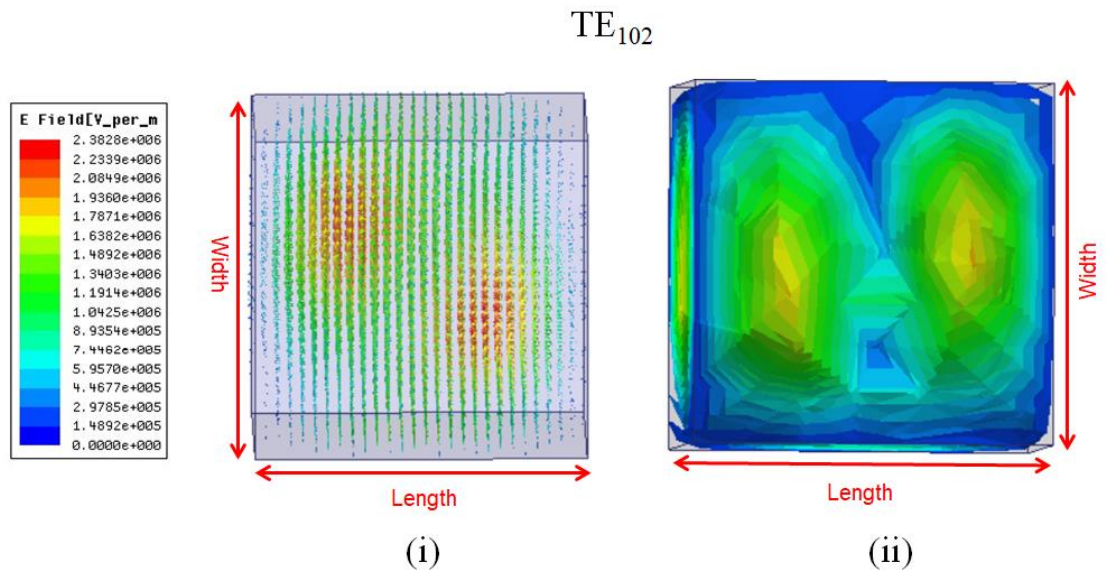


Figure 3.4: Electric field distribution of ceramic waveguide resonator for a TE_{102} mode (from HFSS) (i) vector form (ii) magnitude form

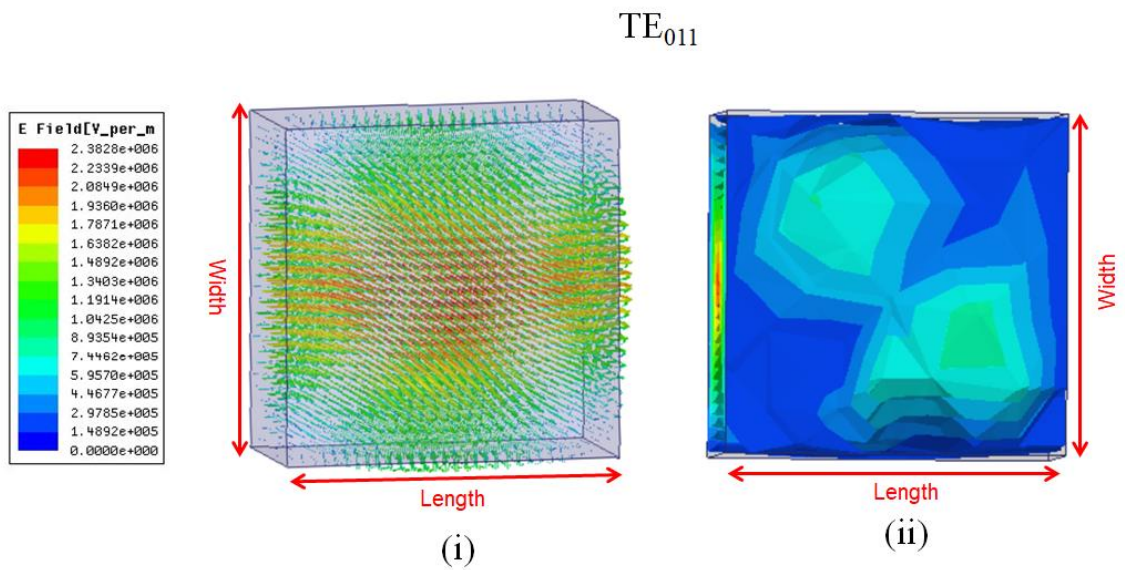


Figure 3.5: Electric field distribution of ceramic waveguide resonator for a TE_{011} mode (from HFSS) (i) vector form (ii) magnitude form

TE_{201}

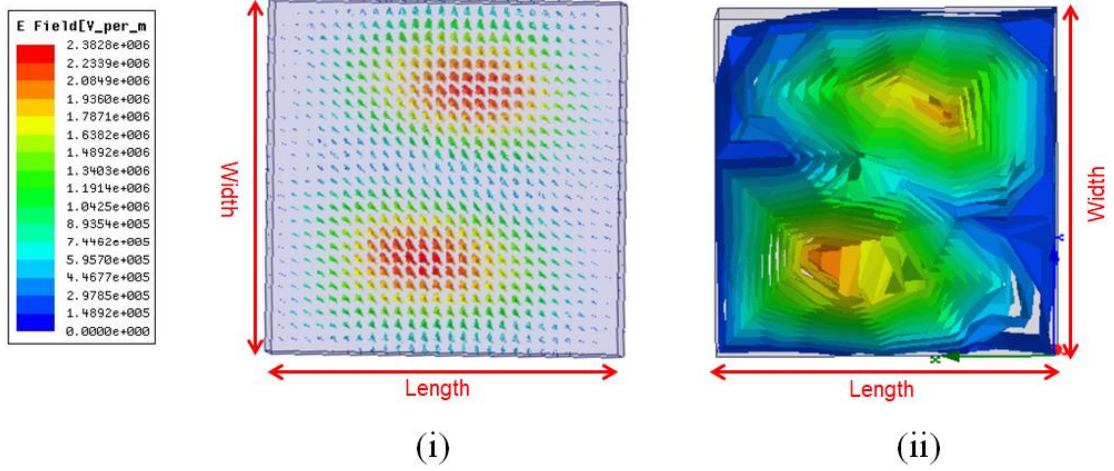


Figure 3.6: Electric field distribution of ceramic waveguide resonator for a TE_{201} mode (from HFSS) (i) vector form (ii) magnitude form

TE_{111}

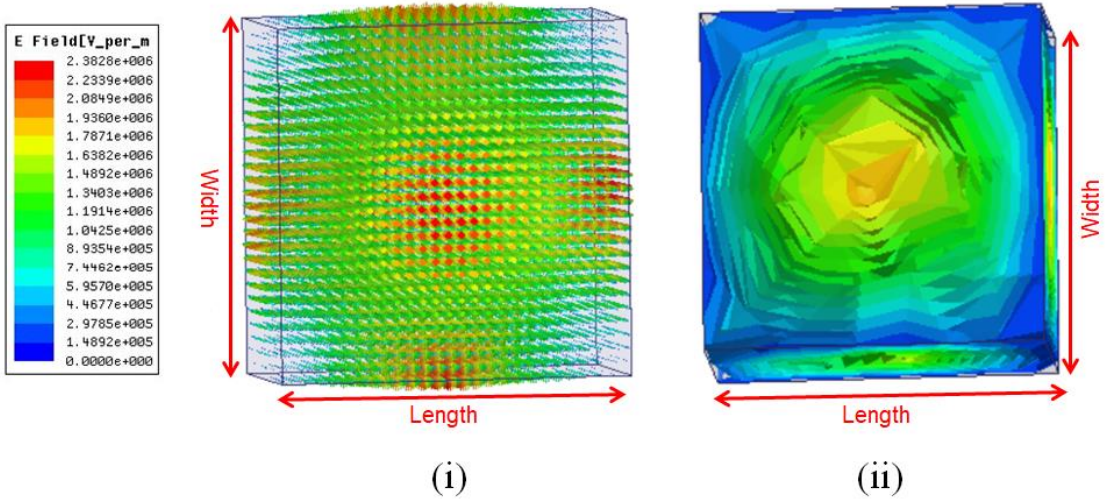


Figure 3.7: Electric field distribution of ceramic waveguide resonator for a TE_{111} mode (from HFSS) (i) vector form (ii) magnitude form

3.3 Permittivity

The permittivity of a material defines its capability to store energy when external potential is applied across it or how much a medium can polarize in response of an electric field. This property determines the relative speed that an electromagnetic signal can travel in that material. A high permittivity material will slow down the microwave entering a dielectric material by a factor equal to the square root of permittivity. The high permittivity also offers circuit miniaturization due to the wavelength which is inversely proportional to the square root of material permittivity as given in this equation:

$$\lambda_d = \frac{\lambda_0}{\sqrt{\epsilon_r}} \quad \text{Eq 3.16}$$

Where λ_d , λ_0 and ϵ_r represents the dielectric wavelength, free space wavelength and permittivity of dielectric medium [52].

3.4 Quality Factor

Quality factor (Q-factor) is defined as the measure of power loss in microwave systems. The insertion loss, selectivity and bandwidth are affected by Q-factor. It is also called a reciprocal of the dielectric loss tangent ($\tan \delta$) of the material, which denotes quantitative dissipation of electrical energy due to different physical processes, such as dielectric relaxation, electrical conduction, dielectric resonance and loss from non-linear processes [52]. This quantity should be carefully distinguished from Q-factor of the resonator which is defined as:

$$Q = 2\pi \frac{\text{maximum energy stored per cycle}}{\text{average energy dissipated per cycle}} \quad \text{Eq 3.17}$$

Q-factor is a dimensionless quantity and has an inverse relationship with bandwidth and insertion loss of the resonator [58]. For the microwave resonators, losses can be of four types [58]:

- I. Conduction
- II. Dielectric
- III. Radiation
- IV. external

The unloaded Q-factor Q_u can be related to $\tan \delta$ and other Q-factors by

$$Q_u = \frac{1}{\tan \delta} \quad \text{Eq 3.18}$$

And

$$\frac{1}{Q_u} = \frac{1}{Q_d} + \frac{1}{Q_c} + \frac{1}{Q_r} \quad \text{Eq 3.19}$$

Where $1/Q_d$, $1/Q_c$ and $1/Q_r$ represent dielectric loss, loss due to conductivity of metallic plates and radiation losses of resonator. The loss tangent of a dielectric material is also defined by

$$\tan \delta = \frac{\sigma}{\omega \varepsilon_0 \varepsilon_r} \quad \text{Eq 3.20}$$

Where $\varepsilon_0 \varepsilon_r$ is the dielectric constant, ω is the radian frequency and σ is the conductivity of the medium [61]. Some resonant cavities are perfectly shielded, so there are no radiation losses but the metal housing of the shielded cavity of the resonator plays an important role in circuit performance, such as insertion loss, spurious mode suppression and temperature stability. The external losses are introduced by the use of external coupling into the circuit, so the total and loaded Q-factor is defined as

$$\frac{1}{Q_L} = \frac{1}{Q_d} + \frac{1}{Q_c} + \frac{1}{Q_r} + \frac{1}{Q_{ext}} \quad \text{Eq 3.21}$$

Q_L can be calculated experimentally by the shape of a resonance peak as shown in figure 3.8, and can also be measured by resonant frequency f and half power bandwidth Δf of a TE₀₁₁ mode resonance.

$$Q_L = \frac{f}{\Delta f} \quad \text{Eq 3.22}$$

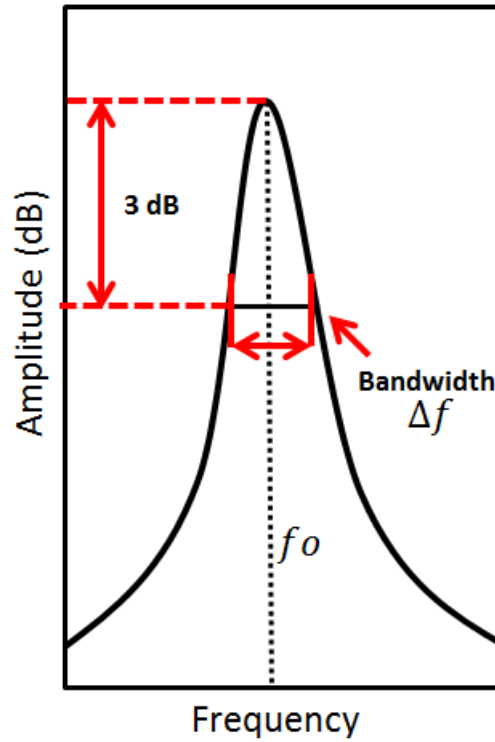


Figure 3.8: The $TE_{01\delta}$ resonant peak and associated parameters [52]

The inverse relationship of Q-factor with bandwidth shows the higher the Q-factor, the narrower the bandwidth. In Chebyshev prototypes, the unloaded Q-factor with N^{th} degree band-pass filter of centre frequency, f_o , and bandwidth Δf , would be calculated as

$$Q_u = \frac{4.343 f_o}{\Delta f I_L} \sum_{r=1}^N g_r \quad \text{Eq 3.23}$$

Where I_L is the midband insertion loss and g_r is r^{th} element value of low-pass prototype.

3.5 Spurious Performance

The presence of higher order modes in proximity to a fundamental mode determines the spurious performance of the filter. These modes, when excited, perturb the response of the filter [58]. The waveguide resonators have an infinite number of modes with their resonant frequencies. It is useful to estimate these modes to gain insight into the spurious performance of a filter. The easiest way to predict these higher order modes is to use a mode chart given in figure 3.9.

This chart gives you the method to estimate the resonant frequencies of a rectangular waveguide resonator with an aspect ratio of $b=2a$, where a , b , and l are measured in inches and frequency in GHz [1]. The aspect ratio (width to height) of a dielectric resonator must be chosen properly to keep the spurious modes' resonances outside the operating band in order to avoid interference [58]. In a microwave band-pass filter, it is obvious that spurious modes are also coupled through the filter with the fundamental mode, which deteriorates the out of band performance of the filter. To avoid these unwanted signals, a number of methods and techniques will be used in the band-pass filter design. The most common is to use a low-pass filter with the cascade fashion with band-pass to remove the unwanted spurious signals.

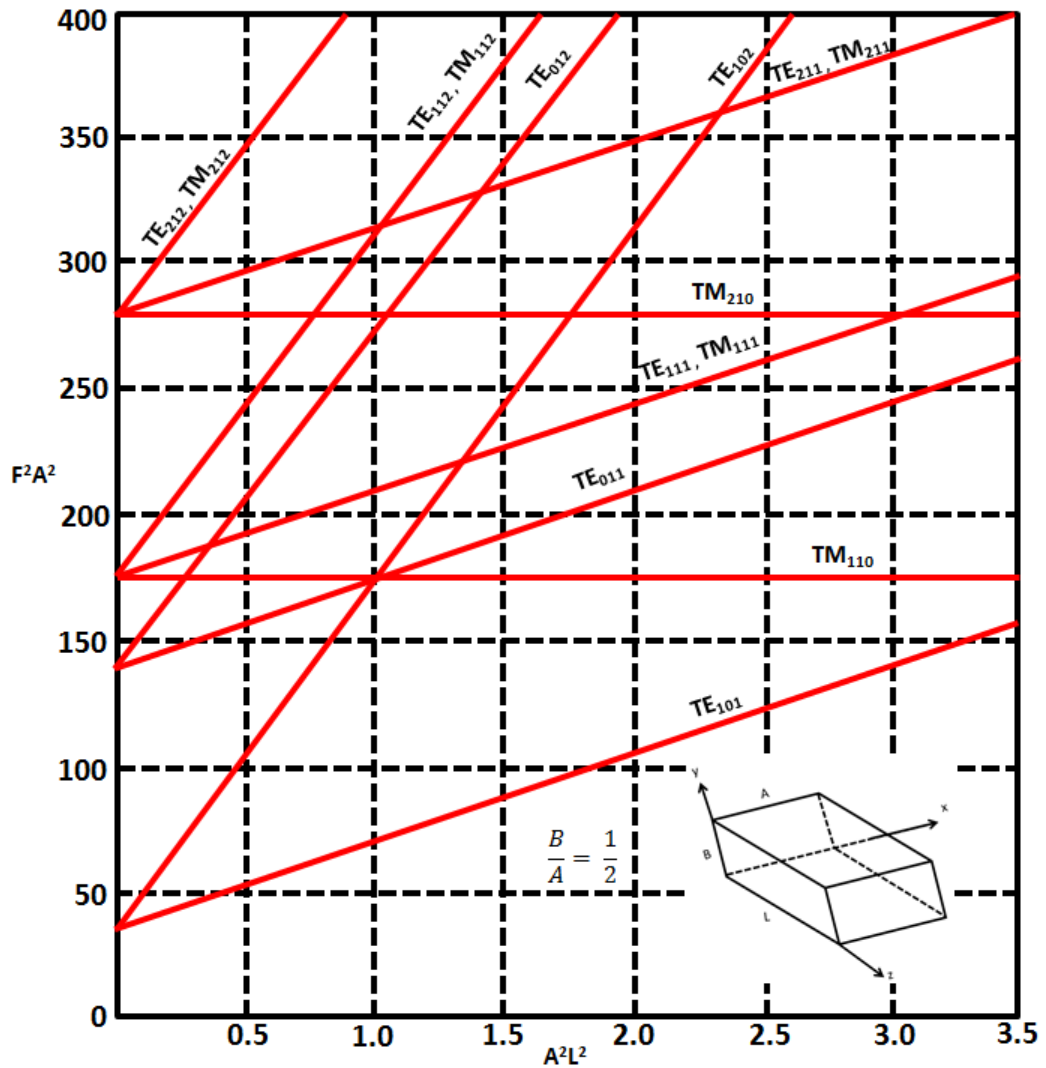


Figure 3.9: Mode chart for a rectangular waveguide resonator [2]

The low-pass filter has a very wide passband and a wide stopband, which attenuates potentially interfering spurious signals at specific frequency ranges away from the filter passband. The low-pass coaxial filter, corrugated filters and waffle iron filter are some examples of low-pass filters. The other method is to introduce or integrate the low-pass filtering behaviour in band-pass filters which can lead to significant size and cost reduction. A number of solutions have been proposed to improve the stopband performance of rectangular waveguide

filters. In 1964, Riblet proposed the idea of using different width resonators to suppress the parasitic passbands. It is shown that if the resonators dimensions are chosen suitably, then their fundamental signal would have the same frequency, but their harmonic signals will occur at different frequencies so that their effect will be spread over a wide frequency range [61]. In [15], different width resonators were used to suppress the stopband's spurious modes. The introduction of capacitive posts at the centre of the resonators also increases the separation between the fundamental and first spurious modes. The fundamental frequency is kept the same by changing the length of the resonators. The capacitive post in a rectangular waveguide resonator shifts down the resonant frequency of resonator below cut-off and makes the waveguide resonator an evanescent mode waveguide resonator. The increase in post height further shifts the frequency and Q-factor down, but increases the separation between the fundamental and first harmonic. To increase the resonant frequency, the size of the resonator needs to be decreased. Thus a miniaturized size is achieved with improved spurious performance [62]. The same concept can be applied in monolithic integrated ceramic waveguide resonators by the introduction of a metal coated blind hole [63]. The relationship between fundamental frequency, the first spurious signal and Q-factor is also illustrated in figure 3.10. The diameter of the post is fixed to 2 mm and the change in post heights offers different values of Q-factor and first spurious signal of the resonator.

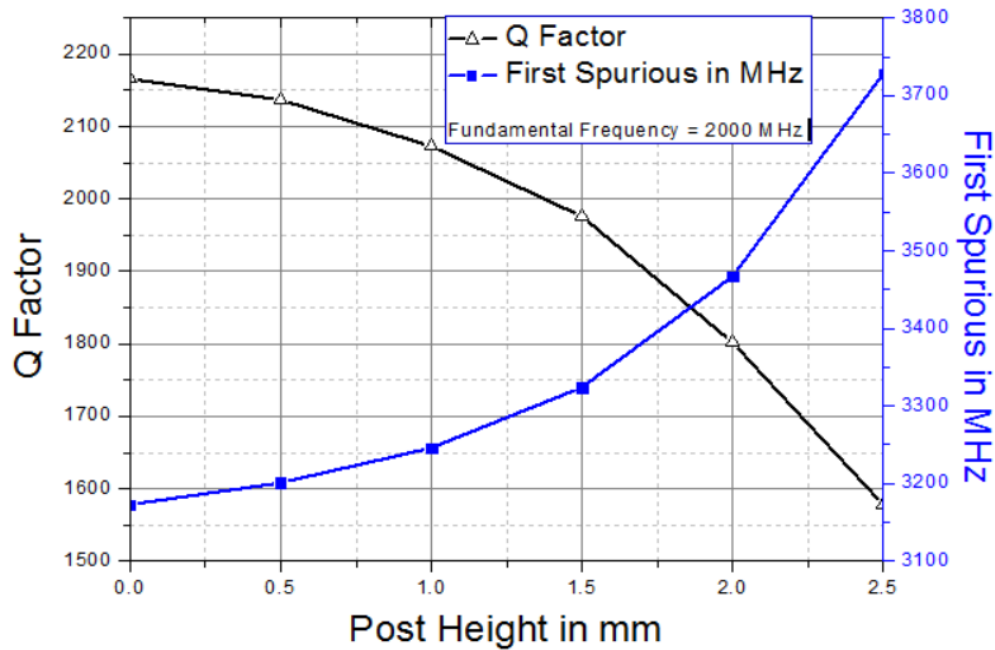


Figure 3.10: comparison of Q-factor, first spurious signal and post height in an integrated TEM ceramic waveguide resonator

The best possible value that can be chosen is with the highest Q-factor and spurious performance as there is a trade-off between both. There have been other practical approaches for improving the stopband performance of waveguide filters by using stepped impedance resonators (SIR) and ridge waveguide resonators [16, 18]. The SIR shows very improved spurious performance with reduced volume but at the expense of lower Q-factor. The dielectric resonator filters exhibit the worst spurious performance, but by employing different techniques like mixed dielectric-coaxial resonators or cascading coaxial filter with dielectric filters improves the spurious performance of these filters, but with a large volume and increased insertion loss [21].

3.6 Summary

The details of a ceramic waveguide resonator are presented in this chapter. This ceramic resonator offers considerable size reduction in comparison of air filled coaxial resonators while maintaining the same performance. The Q-factor and spurious performance of the resonator is briefly reviewed.

4 CERAMIC WAVEGUIDE BANDPASS FILTERS WITH METAL POSTS

4.1 Introduction

High-performance microwave filters with low loss, high selectivity, small size and good out of band performance are always a favoured candidate for wireless and satellite communication systems. Dielectric TEM filters offer excellent spurious performance but are high volume; whereas ceramic filled waveguide filters provide 50% size reduction but have a crowded mode chart in the proximity of the passband [28, 54]. Many contributions have been made to improve the stopband performance of waveguide filters.

In this chapter, a six order monolithic ceramic chebyshev test filter is designed with the specifications given by the company radio design. A dielectric permittivity of 43 is used to design test filter. After words two six order monolithic ceramic waveguide resonator filters of same permittivity with posts are designed and presented. Both designs are presented to show the improvement in spurious performance in comparison of a test filter. The ceramic waveguide resonators and ceramic waveguide resonators with capacitively loaded post provide a good way of dealing with the spurious problem as well as maintaining proper miniaturization. The volume of ceramic waveguide resonators reduce by a factor of $\frac{1}{\sqrt{\epsilon_r}}$ when compared to the air filled waveguide

resonator [43, 64]. Two different six order Chebyshev ceramic waveguide filters are designed using ceramic resonators with posts. These ceramic filters used 50 Ω coaxial probes for input/output coupling placed at the centre of broad wall of the first and last resonators of the filters. The inter-resonator coupling is realized by a metal coated through-hole placed at the broad wall and it controls the coupling obtained by the coupling coefficient of the lumped element equivalent filter. The input/output coupling can be adjusted by using the probe position for a shorted back end and adjusting its depth inside the ceramic cavity. All simulated design results are in good agreement with the theoretical concepts.

4.2 Filter Specifications

A ceramic band pass filter is designed with ceramic resonators using Chebyshev transfer function approximation:

$$|S_{21}(j\omega)|^2 = \frac{1}{1 + \varepsilon^2 T_n^2(\omega)} \quad \text{Eq 4.1}$$

The required filter specification for the filter design is as follows:

Table 4-1 Specifications for ceramic waveguide filter (provided by radio design)

Parameters Name	Parameters Value
Center frequency (f_o)	1842.5 MHz
Bandwidth (Bw)	75 MHz
StopBand Rejection	> 50 dB at f < 1750 MHz > 50 dB at f < 1930 MHz

Passband Insertion loss (I_L)	> 0.7 dB
Passband return loss (R_L)	> 20 dB
System impedance (Z_o)	50 Ω

4.3 Ceramic Waveguide Resonator

The silver coated half guide wavelength long ceramic resonator is composed of zirconium-titanate ($Pb[Zr_x Ti_{1-x}]O_3$) with a permittivity of 43 and dielectric loss tangent of 0.000036. The conductivity of the silver coating has the value around 4.4e7 Siemens/meter. Equation 3.1 is used to calculate the dimensions of the ceramic waveguide resonator which is based on the fundamental mode (TE_{101}) of the ceramic waveguide resonator [2]. The resonators dimensions are calculated as a width (a) = 17.55 mm, when put the $f_o = 1842.5$ MHz and $\epsilon_r = 43$ with the aspect ratio of $a = 2b$.

$$\text{Width } (a_r) = \text{Length } (l_r) = 2 * \text{Height } (b_r) = 17.55 \text{ mm}$$

The effective wavelength of a ceramic resonator at a permittivity of 43 can be calculated as:

$$\lambda_d = \frac{\lambda_0}{\sqrt{\epsilon_r}} \quad \text{Eq 4.2}$$

Where

$$\lambda_o = \frac{c}{f} \quad \text{Eq 4.3}$$

$$\lambda_o = \frac{300000000}{1842.5 \text{ MHz}} = 162.866 \text{ mm}$$

$$\lambda_d = \frac{162.866}{\sqrt{43}}$$

$$\lambda_d = 24.836 \text{ mm}$$

The cut-off wavelength of a resonator can be calculated as [1]:

$$\lambda_c = 2a_r = 35.1 \text{ mm} \quad \text{Eq 4.4}$$

Moreover, the cut-off frequency of a ceramic waveguide resonator, when its broad dimensions equals to a_r can be calculated as [1]:

$$\omega_c = \frac{\pi v}{a_r} = \frac{\pi}{a_r \sqrt{\mu_o \epsilon_o \epsilon_r}} \quad \text{Eq 4.5}$$

$$= 8.189303568$$

Therefore,

$$f_c = \frac{\omega_c}{2\pi} \quad \text{Eq 4.6}$$

$$= 1.3034 \text{ GHz}$$

The Q-factor of the ceramic resonator for TE₁₀₁ mode can be calculated from the relation below [59]:

$$Q_u = \frac{1}{\sqrt{\epsilon_r} \delta} \frac{\lambda a_r b_r l_r}{2} \frac{\left(\frac{1}{a_r^2} + \frac{1}{l_r^2}\right)^{\frac{3}{2}}}{\frac{l}{a_r^2} (a_r + 2b_r) + \frac{a_r}{l_r^2} (l_r + 2b_r)} \quad \text{Eq 4.7}$$

Putting $a_r = l_r$ and $b_r = \frac{a_r}{2}$, we get

$$Q_u = \frac{0.17677 \lambda}{\sqrt{\epsilon_r} \delta} \quad \text{Eq 4.8}$$

With silver coating of $5.8 \times 10^7 \Omega^{-1}m^{-1}$ [1]

$$\frac{\lambda}{\delta} = \frac{1.479 \times 10^5}{\sqrt{f_{GHz}}} \quad \text{Eq 4.9}$$

The unloaded Q-factor of a ceramic resonator is calculated as 2937. However, by including the dielectric loss tangent value of a ceramic material, we get

$$\begin{aligned} Q_{total} &= \left(\frac{1}{Q_u} - \frac{1}{Q_L} \right)^{-1} \quad \text{Eq 4.10} \\ &= 2628 \end{aligned}$$

The simulated Q-factor value given by HFSS was 2248, which is due to the practical value of the silver coating ($4.4 \times 10^7 \Omega^{-1}m^{-1}$) used to simulate the ceramic waveguide resonator. The Eigen mode data of ceramic waveguide resonator is given in table 4.1, which shows the fundamental frequency, Q-factor and spurious resonances of the resonator.

Table 4-2 Eigen mode data (HFSS) for the ceramic waveguide resonator

Mode #	Frequency (MHz)	Mode	Q-Factor
1	1842.00	TE ₁₀₁	2248
2	2912.01	TE ₁₀₂	2608
3	2912.50	TE ₀₁₁	2438
4	2914.85	TE ₂₀₁	2595
5	2931.76	TM ₀₁₁	2740
6	3219.49	TE ₁₁₁ /TM ₁₁₁	1974

4.4 Steps for Ceramic Chebyshev Waveguide Filter Design

The following steps were used to design the integrated ceramic Chebyshev filter.

Firstly, the implementation needs to calculate the required dimension for the resonator.

The resonator dimensions were calculated earlier as 17.55 x 17.55 x 8.775 (mm),

which resonates at a frequency of 1842.5 MHz. The effective wavelength of a

resonator in a ceramic material can be calculated as [1]:

$$\lambda_d = \frac{\lambda_o}{\sqrt{\epsilon_r}} \quad \text{Eq 4.11}$$

Where

$$\lambda_o = \frac{c}{f} \quad \text{Eq 4.12}$$

$$\lambda_d = \frac{0.1628}{\sqrt{43}} = 0.02482 = 24.82 \text{ mm}$$

The lower and upper guide wavelength with a center frequency of 1842.5 MHz of the band pass filter can be calculated as [1]:

$$\lambda_{gor} = \frac{\lambda_{dor}}{[1 - (\frac{\omega_c}{\omega_{or}})^2]^{1/2}} \quad \text{Eq 4.13}$$

Where

$$\lambda_{dor} = \frac{\lambda_{o-or}}{\sqrt{\epsilon_r}} \quad \text{Eq 4.14}$$

This gives

$$\lambda_{d01} = 25.289 \text{ mm}$$

$$\lambda_{d02} = 24.334 \text{ mm}$$

Where λ_{d01} and λ_{d02} are the effective wavelengths of upper and lower band edges in ceramic material with a dielectric constant of 43. Now, by putting both these values in equation 4.55 above, we get

$$\lambda_{g01} = 36.544 \text{ mm}$$

$$\lambda_{g02} = 33.757 \text{ mm}$$

λ_{g01} and λ_{g02} are the free space wavelengths of the lower and upper pass band edges. Now, to calculate the effective guide wavelength of a resonator we have, [1]

$$\lambda_{go} = \frac{\lambda_{go1} + \lambda_{go2}}{2} + \frac{1}{\pi} \left[\frac{\lambda_{go1} \cos\left(\frac{\pi \lambda_{go2}}{2 \lambda_{go1}}\right) + \lambda_{go2} \cos\left(\frac{\pi \lambda_{go1}}{2 \lambda_{go2}}\right)}{\sin\left(\frac{\pi \lambda_{go2}}{2 \lambda_{go1}}\right) + \sin\left(\frac{\pi \lambda_{go1}}{2 \lambda_{go2}}\right)} \right] \quad \text{Eq 4.15}$$

$$\lambda_{go} = 35.150 \text{ mm}$$

The term α is defined as

$$\alpha = \left[\frac{\lambda_{go1}}{\lambda_{go}} \sin\left(\frac{\pi \lambda_{go}}{\lambda_{go1}}\right) \right]^{-1} \quad \text{Eq 4.16}$$

$$\alpha = 8.042$$

The impedance inverter in a cascaded unit element circuit is equivalent to the discontinuity in a waveguide. Therefore, it can be approximated with a unit element circuit for the waveguide filter. The response of the Chebyshev bandpass filter is given as [1]:

$$|S_{21}(j\omega)|^2 = \frac{1}{1 + \varepsilon^2 T_N^2 \left[\alpha \left(\frac{\lambda_g}{\lambda_{go}} \right) \sin\left(\frac{\pi \lambda_{go}}{\lambda_g}\right) \right]} \quad \text{Eq 4.17}$$

The degree of a filter which can be determined by the insertion loss function of Chebyshev waveguide filter is

$$L = 10 \log \left\{ 1 + \varepsilon^2 T_N^2 \left[\alpha \frac{\lambda_g}{\lambda_{go}} \sin\left(\pi \frac{\lambda_{go}}{\lambda_g}\right) \right] \right\} \quad \text{Eq 4.18}$$

The element's value (normalized to 1Ω) of each resonator can be calculated as [1]

$$Z_r = \frac{2\alpha}{\eta} \sin \left[\frac{(2r-1)\pi}{2N} \right] - \frac{1}{4\alpha\eta} \left\{ \frac{\eta^2 + \sin^2 \left(\frac{r\pi}{N} \right)}{\sin \left[\frac{(2r+1)\pi}{2N} \right]} + \frac{\eta^2 + \sin^2 \left[\frac{(r-1)\pi}{N} \right]}{\sin \left[\frac{(2r-3)\pi}{2N} \right]} \right\}$$

Eq 4.19

Where

$$\eta = \sinh \left[\frac{1}{N} \sinh^{-1} \left(\frac{1}{\varepsilon} \right) \right] \quad \text{Eq 4.20}$$

$$\eta = 0.52$$

Gives,

$$Z_0 = Z_7 = 1$$

$$Z_1 = Z_6 = 8.0222$$

$$Z_2 = Z_5 = 21.687$$

$$Z_3 = Z_4 = 29.685$$

The inter-resonator coupling values for a Chebyshev filter can be calculated as

$$K_{r,r+1} = \frac{\left[\eta^2 + \sin^2 \left(\frac{r\pi}{N} \right) \right]^{\frac{1}{2}}}{\eta} \quad \text{Eq 4.21}$$

This gives

$$K_{i_1} = K_{6_0} = 1$$

$$K_{12} = K_{56} = 1.38$$

$$K_{23} = K_{45} = 1.942$$

$$K_{34} = 2.167$$

The susceptance of the inductive metal plated holes between the ceramic waveguide resonators can be determined as

$$B_{r,r+1} = \frac{(Z_r Z_{r+1})^{\frac{1}{2}}}{K_{r,r+1}} - \frac{K_{r,r+1}}{(Z_r Z_{r+1})^{1/2}} \quad \text{Eq 4.22}$$

This gives,

$$B_{i_1} = B_{6_o} = 2.47$$

$$B_{12} = B_{56} = 9.452$$

$$B_{23} = B_{45} = 12.988$$

$$B_{34} = 13.625$$

The phase lengths of a guide between the metal plated holes in a ceramic waveguide can be calculated by subtracting the negative lengths of a guide from a half wavelength, giving [1]

$$\varphi_r = \pi - \frac{1}{2} \left[\cot^{-1} \left(\frac{B_{r-1,r}}{2} \right) + \cot^{-1} \left(\frac{B_{r,r+1}}{2} \right) \right] \quad \text{Eq 4.23}$$

which gives,

$$\varphi_1 = \varphi_6 = 2.697$$

$$\varphi_2 = \varphi_5 = 2.959$$

$$\varphi_3 = \varphi_4 = 2.992$$

These phase lengths are in radians, but the physical lengths of resonators between the posts' centers can be determined as

$$l_r = \frac{\varphi_r \lambda_{g0}}{\pi} \quad \text{Eq 4.24}$$

which gives,

$$l_1 = l_6 = 15.088 \text{ mm}$$

$$l_2 = l_5 = 16.554 \text{ mm}$$

$$l_3 = l_4 = 16.738 \text{ mm}$$

The transmission line model of Chebyshev bandpass waveguide filter is shown in figure 4.1:

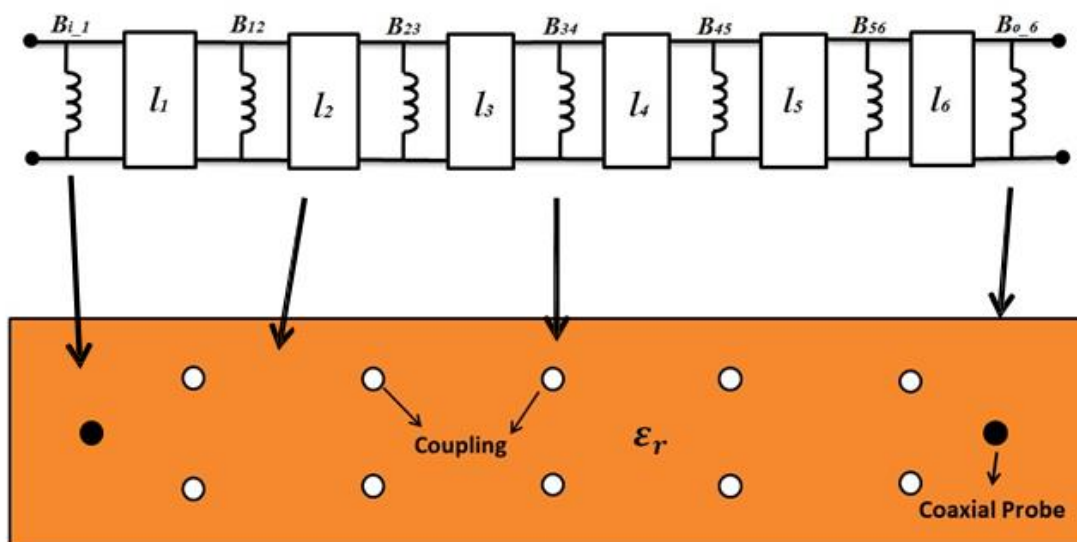


Figure 4.1: Equivalent final circuit for six order ceramic bandpass waveguide filter

4.5 Results

A ceramic Chebyshev waveguide filter is designed and simulated. This filter will be referred to as the **test filter**, and its in-band and out of band performance will be used as a reference, which the proposed design techniques described in this and the next chapters which aimed to improve the out of band performance will be compared to. Figure 4.2 shows the simulated passband of Chebyshev filter which is in good agreement with the theory. Figure 4.3 and 4.4 shows more comprehensive insertion loss and out of band response of the test filter. The other filter realizations focused on improving the out of band performance of this ceramic Chebyshev waveguide filter without compromising the performance of the filter and the use of a low pass filter. Table 4-2 summarizes the simulated filter dimension of the ceramic filter.

Table 4-3 Simulated Design filter dimensions for fabrication

Dimension	Variable	Value
Width of waveguide	a	17.55 mm
Height of Waveguide	b	8.8 mm
Length of resonator 1 and 6	$l_1 = l_6$	16.31 mm
Length of resonator 2 and 5	$l_2 = l_5$	17.12 mm
Length of resonator 3 and 4	$l_3 = l_4$	17.325 mm
Input/output cable diameter	d_{input}	2 mm
Input/output cable depth inside	h_{input}	3.83 mm
Input/output cable length from shorter back end	$l_{shorted}$	8.775 mm

Through hole distance from side walls for K_{12} and K_{56}	S_1	4.88 mm
Through hole distance from side walls for K_{23} and K_{45}	S_2	5.26 mm
Through hole distance from side walls for K_{34}	S_3	5.33 mm
Radius of through holes	H_r	0.86 mm

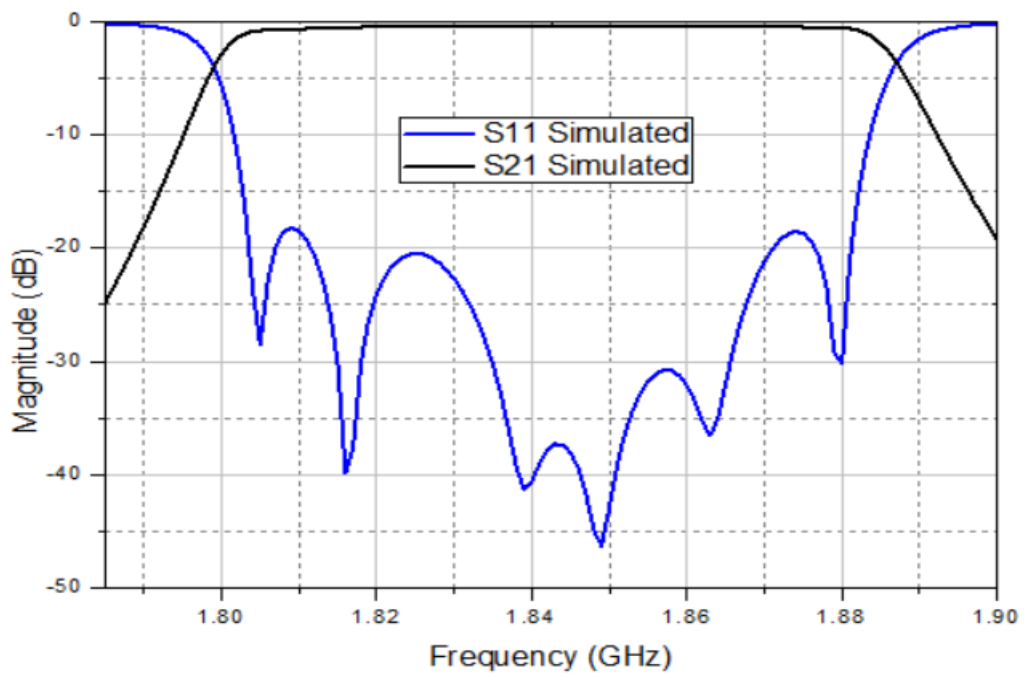


Figure 4.2: Simulated passband response of ceramic waveguide filter

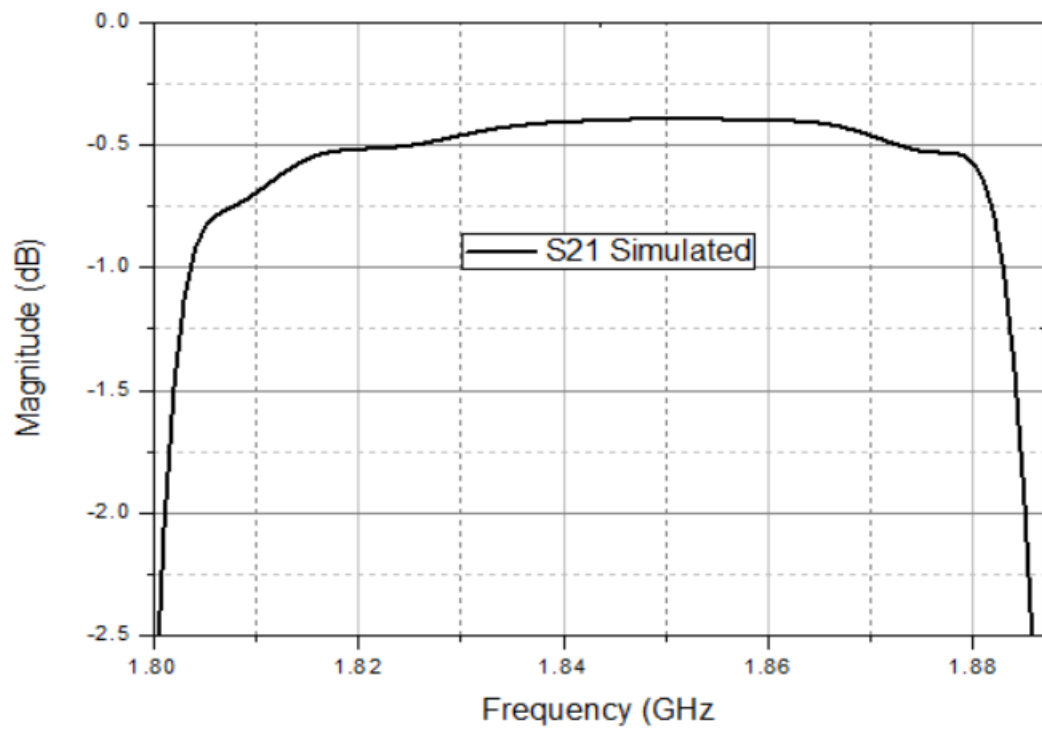


Figure 4.3: passband insertion loss of ceramic waveguide filter

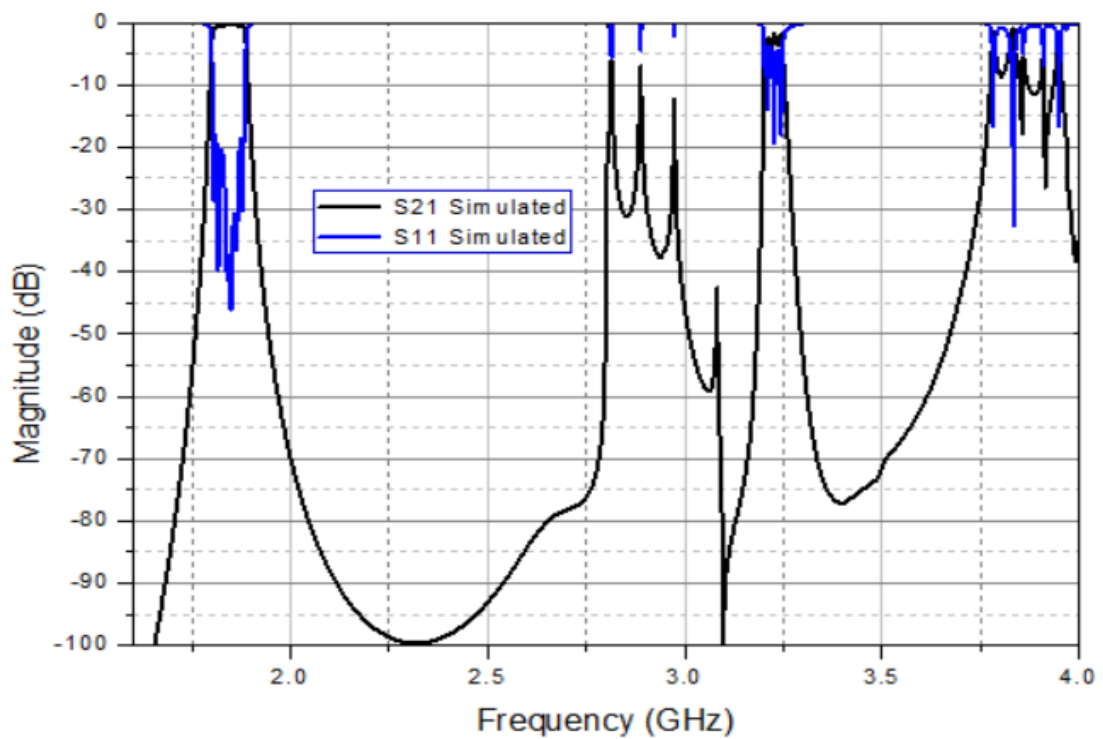


Figure 4.4: The full band response of ceramic waveguide filter

4.6 Inter resonator coupling

The rectangular ceramic waveguide filter consists of a metalized ceramic bar with various circular through-holes. These holes are placed in the broad dimension of a waveguide which provides inter-resonator coupling and design technique, as illustrated in [1]. These inductive posts designed as inductive shunt discontinuities between half wavelength resonators. It will be shown that these circular holes behave as impedance inverters over relatively broad bandwidths. When the susceptances (B) of a filter are known, the number of inductive holes and their required diameter can be calculated from the graph given in figure 4.5 [65].

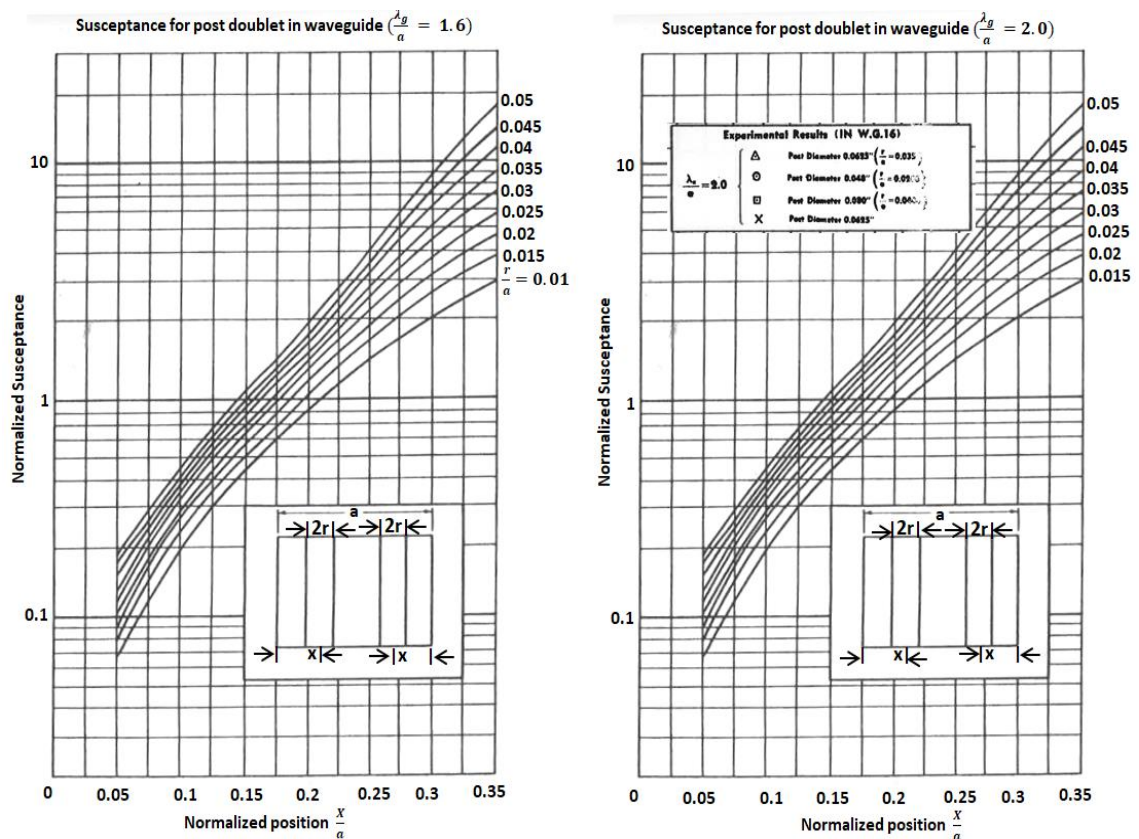


Figure 4.5: Normalized Susceptance of posts in a waveguide will change both this pictures later with good [65]

Inverter susceptances adjustments can also be made by varying the distance between inductive holes with a fixed diameter and a fixed number. The equivalent circuit of inductive posts in the ceramic rectangular waveguide is shown in figure 4.6.

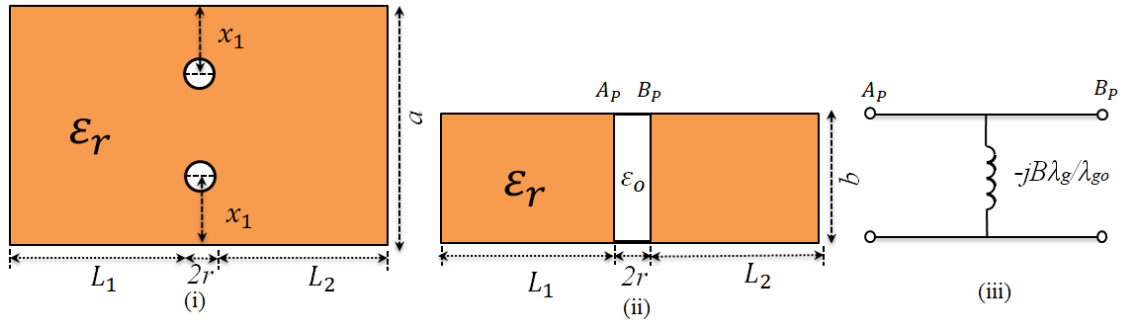


Figure 4.6: Shunt inductive through-holes in ceramic waveguide; (i) Top view (ii) Side view (iii) equivalent circuit

The inductive holes are placed symmetrically over the broad waveguide dimension to suppress the spurious modes. The section of waveguide can be represented by its transfer matrix, which is that of a transmission line with frequency-dependent propagation constant and characteristic impedance, i.e.:

$$Z_o = \frac{\eta_a \lambda_g}{\lambda_o} \quad \text{Eq 4.25}$$

$$Z_o = \frac{\eta_a}{\left[1 - \left(\frac{\omega_c}{\omega}\right)^2\right]^{\frac{1}{2}}} \quad \text{Eq 4.26}$$

And

$$\beta = \frac{2\pi}{\lambda_g} = \frac{\omega}{v} \left[1 - \left(\frac{\omega_c}{\omega} \right)^2 \right]^{\frac{1}{2}} \quad \text{Eq 4.27}$$

Thus, the transfer matrix for a length of waveguide can be written as:

$$[T] = \begin{bmatrix} A & B \\ C & D \end{bmatrix} = \begin{bmatrix} \cos \theta & j \sin \theta \\ j \sin \theta & \cos \theta \end{bmatrix} \quad \text{Eq 4.28}$$

Where

$$\theta = \beta l = \frac{2\pi l}{\lambda_g} \quad \text{Eq 4.29}$$

Or

$$\theta = \frac{\pi \lambda_{go}}{\lambda_g} \quad \text{Eq 4.30}$$

Where λ_{go} is proportional to guide length. Here, in this case, λ_{go} is set to be the guide wavelength when the waveguide is half the length of the wavelength, i.e.

$$l = \frac{\lambda_{go}}{2} \quad \text{Eq 4.31}$$

The discontinuities have been introduced in different ways in a waveguide to form an impedance inverter. Here, we use the inductive through-holes to realize a discontinuity in the broad dimension of the rectangular ceramic waveguide. The equivalent circuit of discontinuity with a reference plane is shown in figure 4.6.

The shunt inductor transfer matrix is given as:

$$[T] = \begin{bmatrix} 1 & 0 \\ \frac{-jB\lambda_g}{\lambda_{g0}} & 1 \end{bmatrix} \quad \text{Eq 4.32}$$

The reference plane A_p and B_p are normally within the diameter of the through hole. The number of inductive posts and their diameters determine the parameter B and reference plane locations.

The inductive iris section is also modified by symmetrically embedding them in a uniform section of waveguide of the electrical length:

$$\varphi = \frac{\varphi_0 \lambda_{g0}}{\lambda_g} \quad \text{Eq 4.33}$$

This iris embedded shunt inductive section of a waveguide is also shown in figure 4.7.

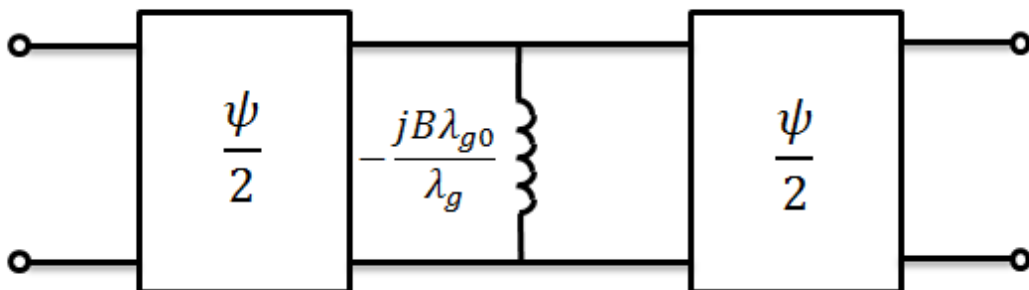


Figure 4.7: Iris embedded shunt inductive section of a waveguide

The transfer matrix of new section becomes

$$\begin{aligned}
[T] &= \begin{bmatrix} \cos\left(\frac{\varphi}{2}\right) & j \sin\left(\frac{\varphi}{2}\right) \\ j \sin\left(\frac{\varphi}{2}\right) & \cos\left(\frac{\varphi}{2}\right) \end{bmatrix} \begin{bmatrix} 1 & 0 \\ -\frac{jB\lambda_g}{\lambda_{go}} & 1 \end{bmatrix} \begin{bmatrix} \cos\left(\frac{\varphi}{2}\right) & j \sin\left(\frac{\varphi}{2}\right) \\ j \sin\left(\frac{\varphi}{2}\right) & \cos\left(\frac{\varphi}{2}\right) \end{bmatrix} \\
&= \begin{bmatrix} \cos\left(\frac{\varphi}{2}\right) + \frac{B\lambda_g}{\lambda_{go}} \sin\left(\frac{\varphi}{2}\right) & j \sin\left(\frac{\varphi}{2}\right) \\ j \sin\left(\frac{\varphi}{2}\right) - \frac{jB\lambda_g}{\lambda_{go}} \cos\left(\frac{\varphi}{2}\right) & \cos\left(\frac{\varphi}{2}\right) \end{bmatrix} \begin{bmatrix} \cos\left(\frac{\varphi}{2}\right) & j \sin\left(\frac{\varphi}{2}\right) \\ j \sin\left(\frac{\varphi}{2}\right) & \cos\left(\frac{\varphi}{2}\right) \end{bmatrix} \\
&= \begin{bmatrix} \cos^2\left(\frac{\varphi}{2}\right) - \sin^2\left(\frac{\varphi}{2}\right) + \frac{B\lambda_g}{\lambda_{go}} \sin\left(\frac{\varphi}{2}\right) \cos\left(\frac{\varphi}{2}\right) & j \left[2 \cos\left(\frac{\varphi}{2}\right) \sin\left(\frac{\varphi}{2}\right) + \frac{B\lambda_g}{\lambda_{go}} \sin^2\left(\frac{\varphi}{2}\right) \right] \\ j \left[2 \cos\left(\frac{\varphi}{2}\right) \sin\left(\frac{\varphi}{2}\right) - \frac{B\lambda_g}{\lambda_{go}} \cos^2\left(\frac{\varphi}{2}\right) \right] & \cos^2\left(\frac{\varphi}{2}\right) - \sin^2\left(\frac{\varphi}{2}\right) + \frac{B\lambda_g}{\lambda_{go}} \sin\left(\frac{\varphi}{2}\right) \cos\left(\frac{\varphi}{2}\right) \end{bmatrix} \\
&= \begin{bmatrix} \cos(\varphi) + \frac{B\lambda_g}{2\lambda_{go}} \sin(\varphi) & j \left[\sin(\varphi) + \frac{B\lambda_g}{\lambda_{go}} \sin^2\left(\frac{\varphi}{2}\right) \right] \\ j \left[\sin(\varphi) - \frac{B\lambda_g}{\lambda_{go}} \cos^2\left(\frac{\varphi}{2}\right) \right] & \cos(\varphi) + \frac{B\lambda_g}{2\lambda_{go}} \sin(\varphi) \end{bmatrix} \quad \text{Eq 4.34}
\end{aligned}$$

Now by equating the equation 4.24 above to an inverter with the transfer matrix

$$\begin{bmatrix} 0 & -\frac{j\lambda_g}{K\lambda_{go}} \\ -\frac{jK\lambda_g}{\lambda_{go}} & 0 \end{bmatrix} \quad \text{Eq 4.35}$$

Where K is the characteristic admittance when $\lambda_g = \lambda_{go}$. Hence

$$\cos(\varphi_o) + \frac{B}{2} \sin(\varphi_o) = 0 \quad \text{Eq 4.36}$$

That is

$$\varphi_o = -\tan^{-1}\left(\frac{2}{B}\right) \quad \text{Eq 4.37}$$

Now subtracting the parameter C_T from parameter B_T in each matrix and equating at λ_{go} we obtain

$$K - \frac{1}{K} = B \left[\sin^2\left(\frac{\varphi}{2}\right) + \cos^2\left(\frac{\varphi}{2}\right) \right] = B \quad \text{Eq 4.38}$$

The susceptance B of the inductive iris is positive. Therefore

$$\frac{1}{K} < K \text{ and } K > 1 \quad \text{Eq 4.39}$$

From equation 4.27 with a positive B, φ_o must be negative and the line cannot be realised in isolation. Practically, an impedance inverter connected to the waveguide lengths and negative lengths can be absorbed into these lengths of the waveguide. Therefore, we can say that a shunt inductive iris can be represented by an inverter with reference planes defined by equation 4.37 and the physical reference planes as shown in figure 4.6. It is very important to understand the iris approximation over broad bandwidths as the design equations are strictly valid at λ_{go} [1]. Examining the A parameter in equation 4.34

$$A = \cos\left(\varphi_o \frac{\lambda_{go}}{\lambda_g}\right) + \frac{B\lambda_g}{2\lambda_{go}} + \sin\left(\varphi_o \frac{\lambda_{go}}{\lambda_g}\right) \quad \text{Eq 4.40}$$

Moreover, from equation 4.37

$$\frac{B}{2} = -\frac{1}{\tan(\varphi_o)} \quad \text{Eq 4.41}$$

Hence

$$A = \cos\left(\varphi_o \frac{\lambda_{go}}{\lambda_g}\right) - \frac{\lambda_g}{\lambda_{go} \tan(\varphi_o)} \sin\left(\varphi_o \frac{\lambda_{go}}{\lambda_g}\right) \quad \text{Eq 4.42}$$

Differentiating A concerning λ_g we get

$$\begin{aligned} \frac{dA}{d\lambda_g} = & \varphi_o \frac{\lambda_{go}}{\lambda_g^2} \sin\left(\varphi_o \frac{\lambda_{go}}{\lambda_g}\right) - \frac{\lambda_g}{\lambda_{go} \tan(\varphi_o)} \sin\left(\varphi_o \frac{\lambda_{go}}{\lambda_g}\right) + \\ & \frac{\lambda_g}{\lambda_{go} \tan(\varphi_o)} \cos\left(\varphi_o \frac{\lambda_{go}}{\lambda_g}\right) \left(\varphi_o \frac{\lambda_{go}}{\lambda_g^2}\right) \end{aligned} \quad \text{Eq 4.43}$$

And if φ_o is relatively small

$$\frac{dA}{d\lambda_g} \approx \frac{\varphi^2 \lambda_{go}^2}{\lambda_g} - \frac{1}{\lambda_g} + \frac{1}{\lambda_g} = \frac{\varphi^2 \lambda_{go}^2}{\lambda_g} \quad \text{Eq 4.44}$$

Which is small for φ_o : hence A is approximately zero over a relatively broad bandwidth.

Furthermore, examining the parameter B in equation 4.34, we get

$$B = \sin\left(\frac{\varphi_o \lambda_{go}}{\lambda_g}\right) - \frac{2\lambda_g}{\tan(\varphi_o)\lambda_{go}} \sin^2\left(\frac{\varphi_o \lambda_{go}}{2\lambda_g}\right) \quad \text{Eq 4.45}$$

Again differentiating concerning λ_g , we get

$$\begin{aligned} \frac{dB}{d\lambda_g} = & -\frac{\varphi_o \lambda_{go}}{\lambda_g^2} \cos\left(\frac{\varphi_o \lambda_{go}}{\lambda_g}\right) - \frac{2}{\tan(\varphi_o)\lambda_{go}} \sin^2\left(\frac{\varphi_o \lambda_{go}}{\lambda_g}\right) \\ & + \frac{4\lambda_g}{\tan(\varphi_o)\lambda_{go}} \sin\left(\frac{\varphi_o \lambda_{go}}{2\lambda_g}\right) \cos\left(\frac{\varphi_o \lambda_{go}}{2\lambda_g}\right) \frac{\varphi_o \lambda_{go}}{2\lambda_g^2} \end{aligned} \quad \text{Eq 4.46}$$

Moreover, for small φ_o

$$\frac{dB}{d\lambda_g} = -\frac{\varphi_o \lambda_{go}}{2\lambda_g} \quad \text{Eq 4.47}$$

Now, the differential of the parameter B in equation is given by

$$\frac{dB}{d\lambda_g} = \frac{\lambda_{go}}{k\lambda_g^2} \quad \text{Eq 4.48}$$

Since φ_o is negative, the differential of two B parameters have the same functional behaviour with respect to λ_g . Hence, the inductive iris embedded in a waveguide is a good approximation to an inverter over a broad bandwidth.

4.7 Input/output Coupling

External coupling is achieved by placing the coaxial probe at the high electric field region of the first and last resonators of a filter. The ceramic waveguide resonator has

a maximum electric field at the center of the broad wall. Therefore, placing the probe at this position excites the highest energy inside the waveguide. The frequency, power handling and bandwidth can be controlled by different variables of probe position, like its diameter, its depth inside the waveguide and its distance from shorted ends [66]. The characteristic impedance of a coaxial probe can be calculated as [22]:

$$Z_{coax} = \frac{1}{2\pi} \sqrt{\frac{\mu}{\epsilon}} \ln \frac{d_{outer}}{d_{inner}} \quad \text{Eq 4.49}$$

Where d_{inner} and d_{outer} are the inner and outer diameter of conductor. The 50Ω impedance of the air-filled coaxial cable will be achieved by the ratio of $\frac{d_{outer}}{d_{inner}} = 2.3$.

The impedance of rectangular waveguide for TE mode can also be calculated from the following equation [67]:

$$Z_{wave} = \frac{2b}{a} Z_{TE} \quad \text{Eq 4.50}$$

Where

$$Z_{TE} = \frac{j\mu\omega}{\gamma} \quad \text{Eq 4.51}$$

Therefore,

$$Z_{wave} = \frac{2bj\mu\omega}{a\gamma} \quad \text{Eq 4.52}$$

The Q factor for the excited waveguide cavity can be calculated as [66]:

$$Q_e = \frac{\frac{\pi}{2} \left(\frac{\lambda_{go}}{\lambda_g} \right)^2}{\left(\frac{K_{01}}{\sqrt{Z_w Z_c}} \right)^2} \quad \text{Eq 4.53}$$

Where Z_w and Z_c represents the characteristic impedance of waveguide and coaxial cable respectively. Ceramic waveguide filters can be excited by the coaxial probes in the first and last resonators or by separate sections of waveguide can be added to couple energy into the filter. The probe is placed at the quarter wavelength distance from the shorted end, then the adjustment of probe depth into the waveguide helps to get a good return loss for the filter [68]. The input/output probes should be at the same distance from short circuited ends due to the symmetrical nature of the filter. The input and output probes are connected directly to the first and last resonator as it will help to achieve miniaturization, rather than to connect separate coaxial to the waveguide transitional cavity with the filter, which increases the overall volume of a filter.

4.8 Ceramic bandpass Waveguide Filters with posts

Two different designs of monolithic ceramic bandpass waveguide filter with posts are presented here. All six orders ceramic bandpass filters offer improved spurious performance and considerable miniaturization without having much effect on the selectivity of the filter.

4.8.1 Ceramic Resonator with Post

An integrated ceramic waveguide resonator having capacitive post consists of a high permittivity ceramic block, with a metal coated blind hole which acts as a post, placed at the center of its broad wall. The loaded post shifts down the fundamental frequency

without any change in the second resonant mode. The distance of fundamental mode and second mode is increased with the miniaturization of the resonator. The exterior surface of the ceramic resonator is coated with metallic silver paint. The Q factor and fundamental frequency of the resonator are readily computed from the Mitthaei [2], which is the same as the previous filter. The metal coated blind hole acts as an inner conductor like TEM resonator. Figure 4.8 shows the ceramic waveguide resonator with a metal coated blind hole act as a post. This ceramic resonator with post can also be termed as a *comblin resonator*, or *evanescent mode resonator* (waveguide below the cut-off frequency) depending on the capacitance between the metal rods in the center of the cavity and the top of the housing. The fundamental mode of the resonator is TEM_{00} , as shown in figure 4.9. The loading of ceramic resonator with post allows reducing the volume with the reduction in Q factor of the resonator, which makes it suitable for the wideband filters.

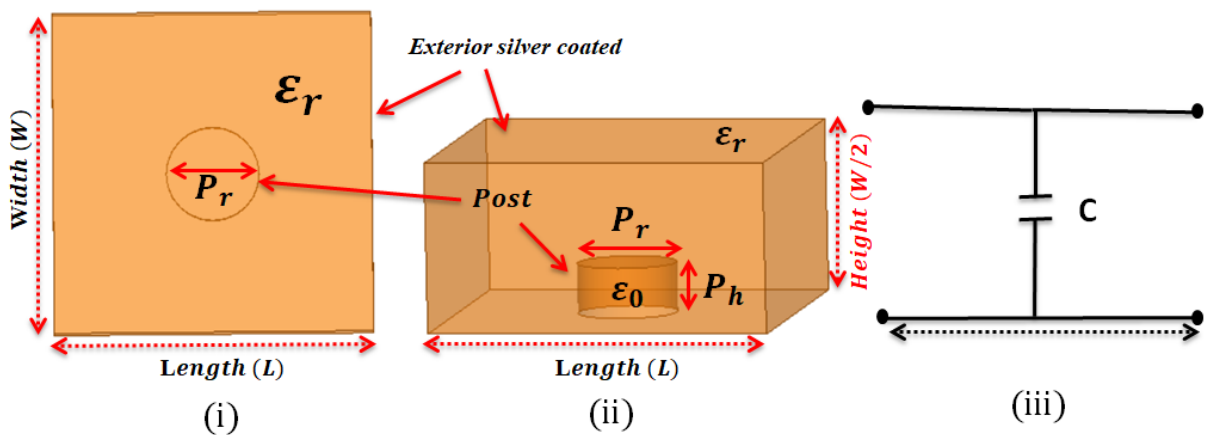


Figure 4.8: Ceramic waveguide resonator with metal post; (i) Top view (ii) 3D view (iii) equivalent circuit

The Eigen mode data for the ceramic resonator with a post height (P_h) = 1.9 mm and post radius (P_r) = 2.5 mm is given in table 4.3, which shows the fundamental mode, the Q factor and the spurious modes of the resonator.

Table 4-4 Eigen mode data (HFSS) for ceramic resonator with post

Mode #	Frequency (MHz)	Modes	Q-Factor
1	1841.04	TEM00	1911
2	2926.84	TEM02	2087
3	2964.72	TEM01	2497
4	3113.23	TEM11	1760
5	3186.55	TEM10	1810

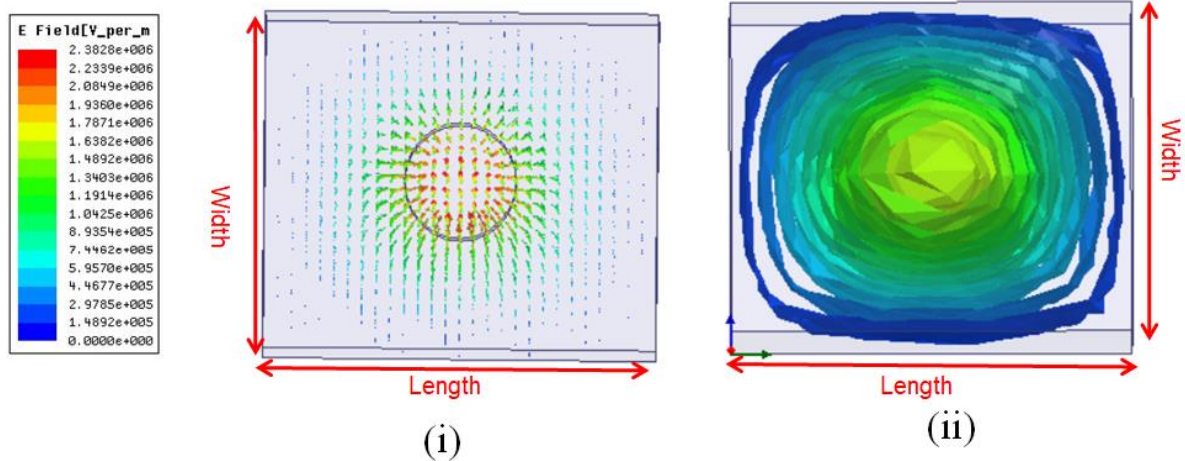


Figure 4.9: Electric field distribution of the ceramic waveguide resonator with a post for TEM00 mode (from HFSS) (i) Vector and (ii) Magnitude form

4.8.2 Ceramic bandpass waveguide filter with two Posts

A six order ceramic waveguide filter is designed by introducing the metallized post in the first and last resonators of the filter. These metalized posts improve the spurious performance by shifting down the fundamental mode and increasing its distance with the higher resonances but at the expense of a lower Q factor of the resonators. The low Q factor of these first and last resonators have very less effect on overall insertion loss of the filter [69] but it improves the overall spurious performance of a filter up to $1.73*f_o$ without affecting the selectivity of a filter. A filter with same layout but with dielectric permittivity of 45 is also published in [63]. Figure 4.10 shows the layout of a filter with the first and last ceramic resonators with posts. The pass band response and full band spurious performance of a filter shows in figure 4.11 and 4.12, shows the consonance between simulated results and theoretical concepts.

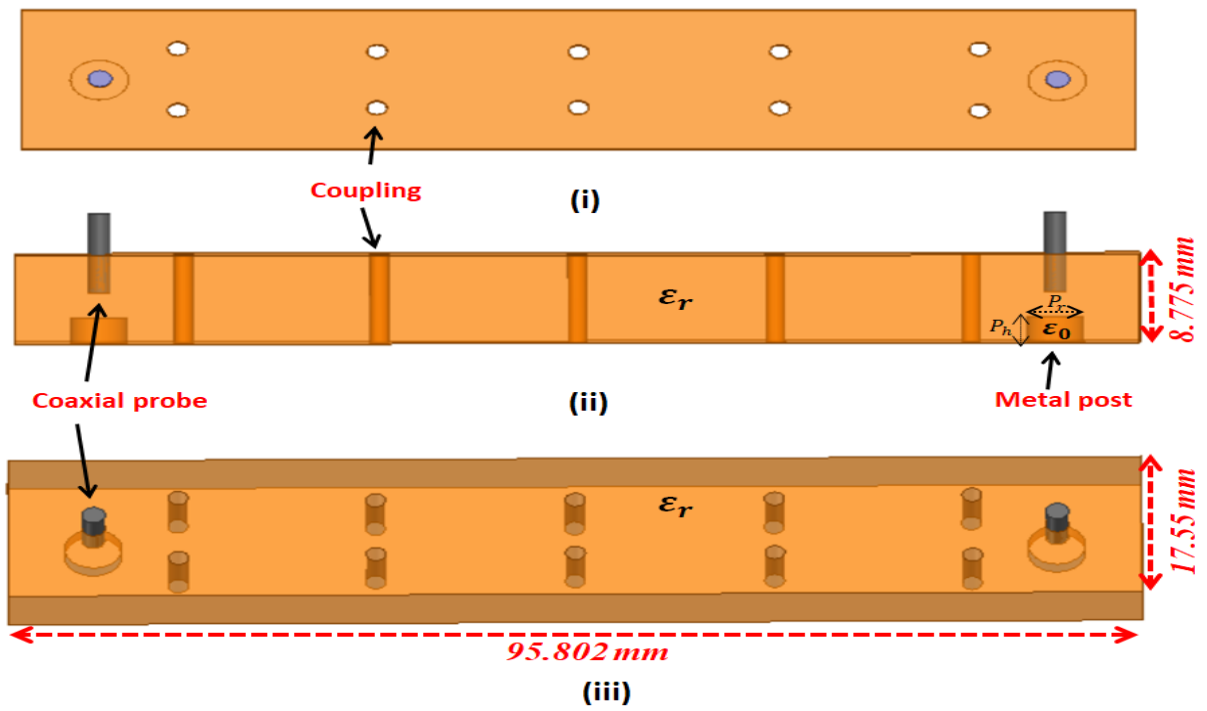


Figure 4.10: Ceramic bandpass waveguide filter with two posts (i) Top view (ii) Side view (iii) 3D view

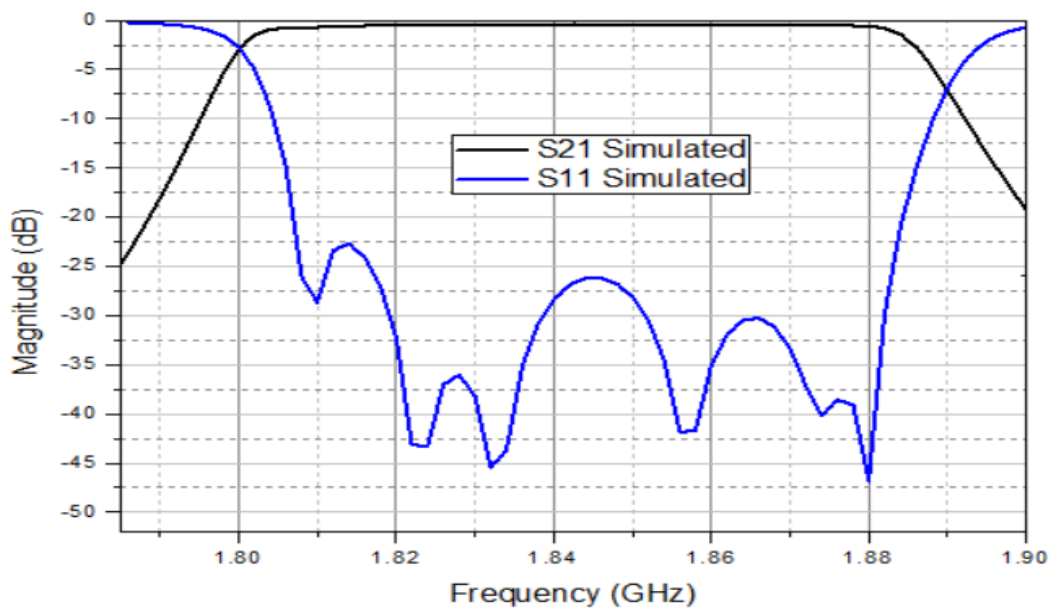


Figure 4.11: Simulated pass band response of ceramic bandpass waveguide filter with two posts

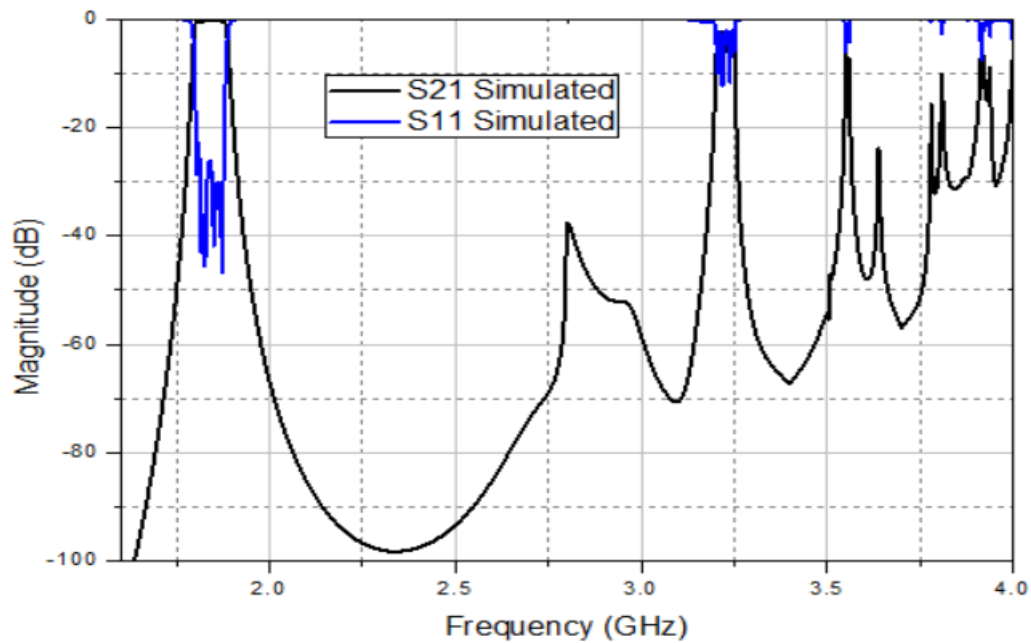


Figure 4.12: Full band spurious performance of Ceramic bandpass waveguide filter with two posts

4.8.3 Ceramic bandpass waveguide filter with all posts having same height

A six order ceramic bandpass waveguide filter is designed with all posts having same post height (P_h) and post radius (P_r) which offers improved spurious performance of up to $1.83 * f_o$ in comparison with the last two ceramic waveguide filters. Besides improving the spurious performance, these ceramic resonators also offer the merit of miniaturization. The overall volume of a filter is reduced by 29% compared to a ceramic waveguide filter (Test filter). The internal and external coupling follows the same procedure like the first filter. Figure 4.13 and 4.14 show the physical layout and pass band response of a filter. The out of band response which shows a 35 dB attenuation up to 3.37 GHz is shown in figure 4.15. The comparison of the spurious performance of ceramic bandpass filters with the test filter is shown in figure 4.16

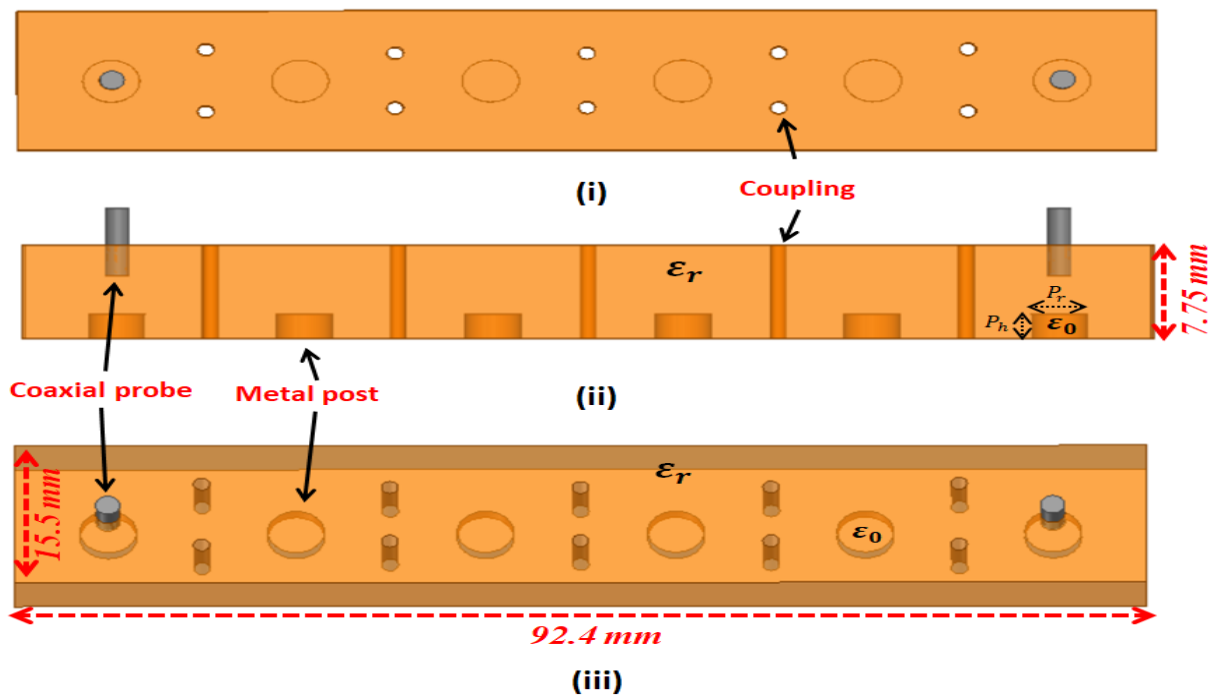


Figure 4.13: Physical layout of a ceramic bandpass filter with all posts having same height (i) Top view (ii) Side view (iii) 3D view

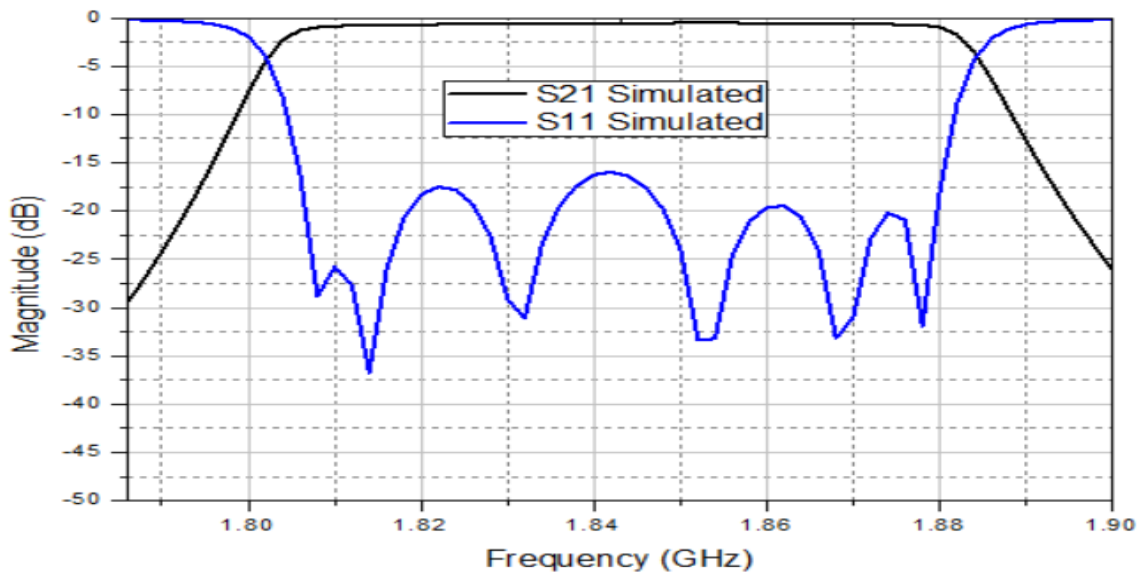


Figure 4.14: Simulated pass band response of a ceramic bandpass waveguide filter with all posts having same height

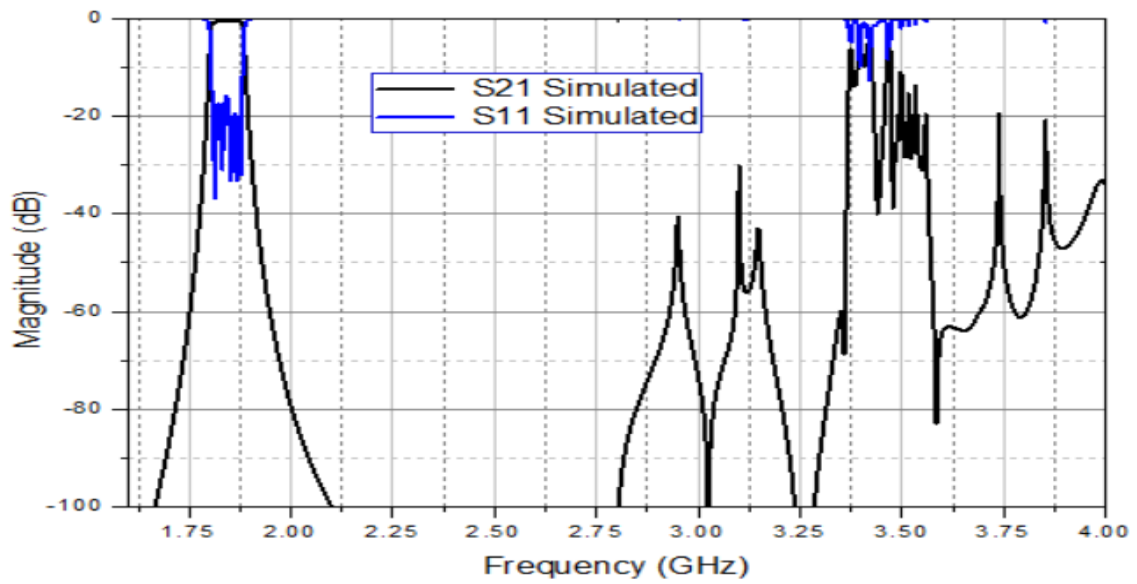


Figure 4.15: Full band simulated response of a ceramic bandpass waveguide filter with all posts having same height

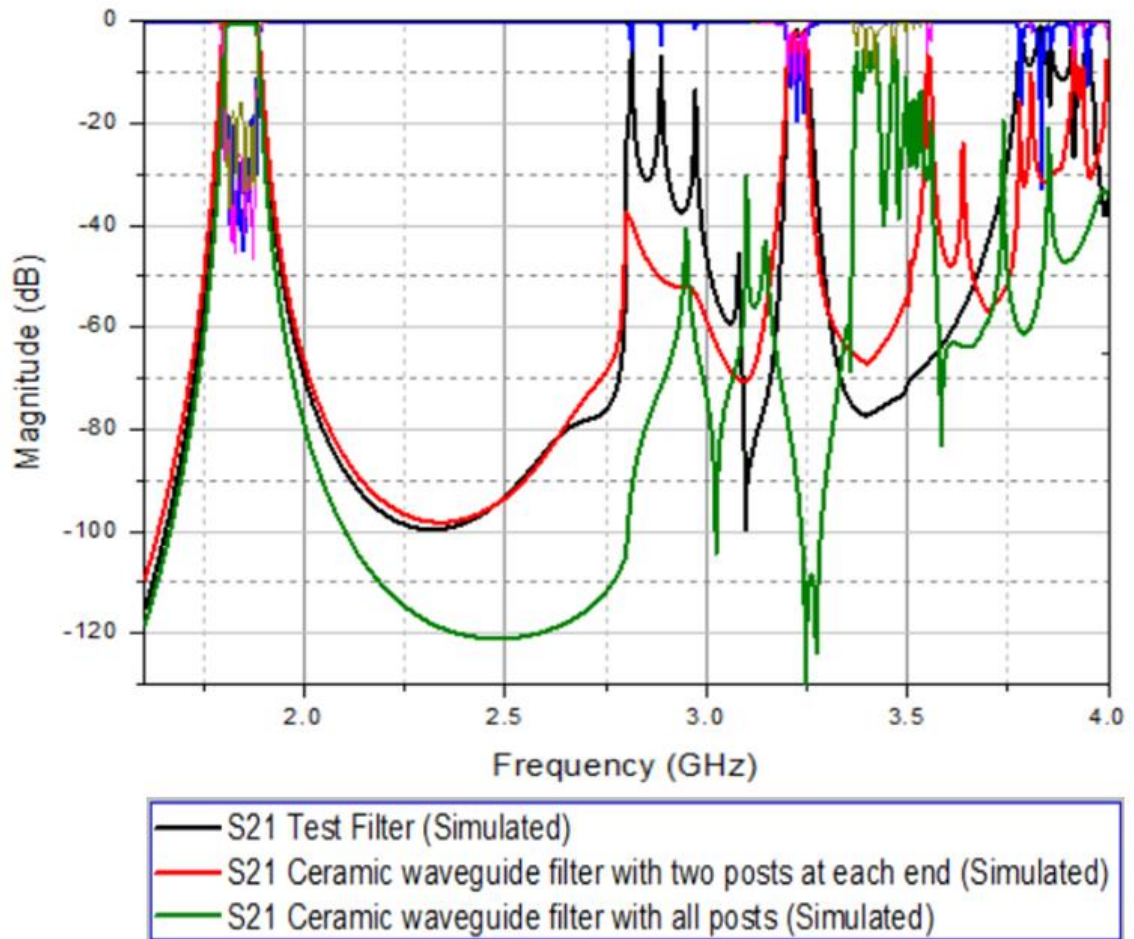


Figure 4.16: Comparison of spurious performance of test filter with ceramic bandpass waveguide filters having posts

4.9 High-Frequency Structure Simulator (HFSS)

HFSS is a tool for virtual prototyping and to model 3D passive devices by using the *Finite Element Method* (FEM). This FEM is used to solve Maxwell's equations in any arbitrary three-dimensional model and can provide a two-dimensional field solution for input and output ports [70]. The power behind HFSS lies in the mathematics of the finite element method and adaptive meshing technique. This allows the mesh to be precise and conformal to the three-dimensional structure and to be suitable for any electromagnetic problems[71]. By employing adaptive meshing, the mesh is automatically set to give the best and perfect mesh. Without adaptive

meshing, the responsibility of generating the correct mesh would be left to the user, which is tedious and also error prone. The mesh growth for each adaptive pass is controlled by the tetrahedron refinement in a setup solution. This will approximate the actual field in the problem space by discretizing the field domain into tetrahedral volume elements in the three-dimensional problem. The advantage of these simple elements is their flexibility to subdivide any arbitrary geometry shown in figure 4.17. After refinement, a full solution is performed and the process is repeated until convergence. The delta S is a default criterion used to determine mesh convergence.

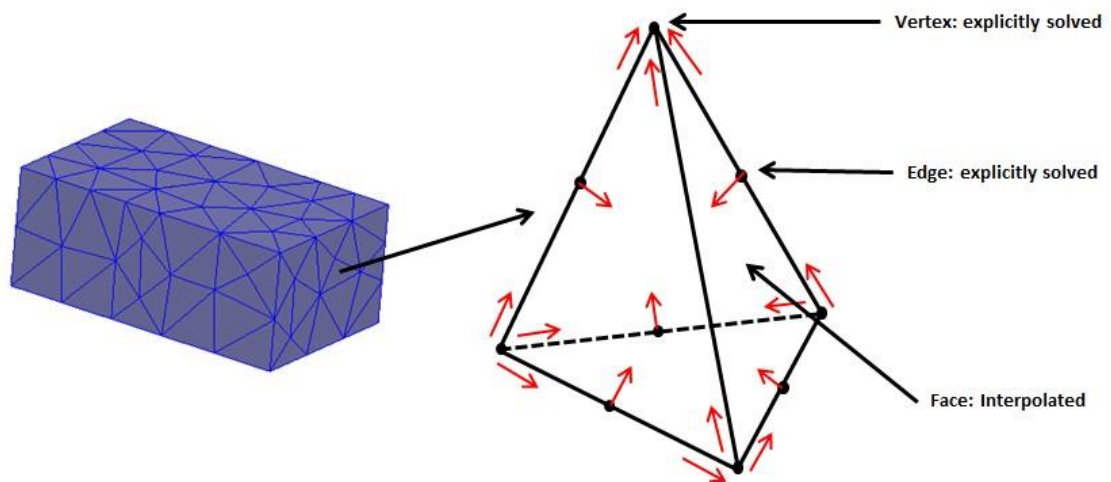


Figure 4.17: Mesh with tetrahedral elements to approximate the shape and 3D object

It is defined as the maximum change in the magnitude of the s-parameters between two consecutive passes. In general Delta S is set at 0.02 (2%), or if we set it at 0.01, then we need to increase the number of passes for accurate results. HFSS is based on several advanced solvers, allowing users to use any solver for their specific simulation need. After getting the user input of geometry, material properties and range of frequencies, HFSS generates the most appropriate, efficient and accurate mesh for the simulation by the use of these solvers.

HFSS is used to design several electromagnetic structures such as a waveguide, filters, antenna, transmission lines and plenty of other microwave components. It provides the user with the choice to select materials of any permittivity, loss tangent and permeability, and also includes the materials of any of these properties. HFSS has three solution types, named as driven modal, driven terminal and Eigen mode. In a driven problem, an external source of energy is applied at a physical access port, and a matrix is built and inverted to find the solution at each frequency of interest, at which point the scattering parameters are calculated. The sourceless problem of any three-dimensional structure can also be solved using an Eigen mode solution type with defined short circuit planes. This solution type calculates the resonant frequencies and Q-factor of a three-dimensional structure and plots its field patterns at those resonant frequencies. The terminal based s-parameters of multi-conductor transmission line ports are calculated in a driven terminal solution type of the HFSS [72]. The meshing algorithm helps to predict the required mesh density for particular boundary configurations. The resolution of the mesh can be increased to improve the accuracy of the design at the expense of greater simulation times. Also, to ensure the convergence of each adaptive mesh, a convergence value is required that is also a trade-off between computational time and accuracy of the design. An example of a ceramic waveguide resonator with different mesh resolution is shown in Figure 4.18.

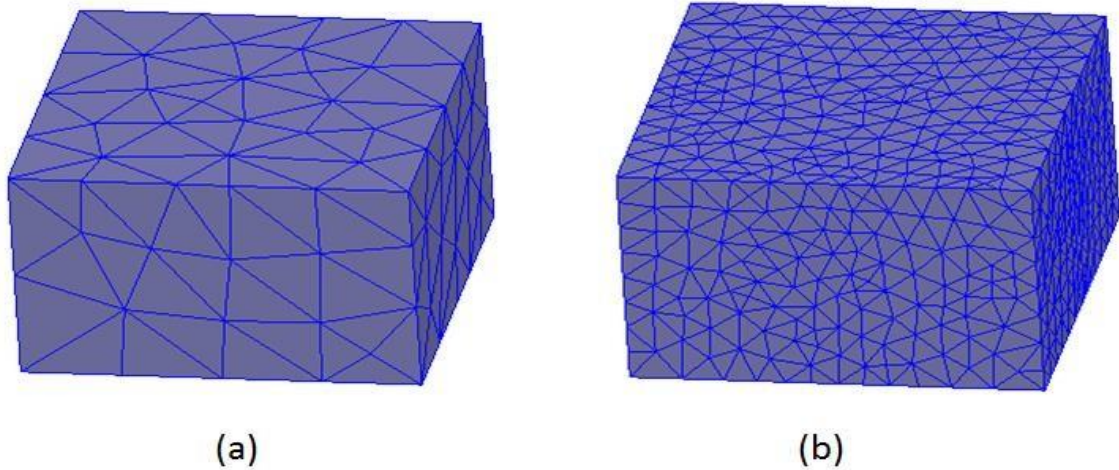


Figure 4.18: Finite element method analysis of integrated dielectric resonators; (a) mesh with 0.6λ (b) mesh with 0.2λ

With these benefits, there are also some drawbacks to using HFSS. It requires high computational time and significant system memory to simulate complicated designs with high accuracy. It also does not calculate the impedance itself unless impedance lines are defined by voltage integration lines on the ports. These lines connect the maximum voltage difference points at each port and are different for each mode. Though HFSS is very accurate in three-dimensional simulations for dielectric filters, tunings screws are usually required to compensate some practical imperfections.

4.10 Summary

Two different integrated ceramic bandpass filters with posts are designed with a dielectric permittivity of 43. They offer better spurious performance and considerable size reduction in contrast to a ceramic waveguide filter (test filter). The filter design is based on a low pass prototype ladder network and insertion loss filter design method. The inter-resonator coupling and input/output coupling is achieved through a coaxial probe and metal coated through holes. The silver conductivity of $4e7$ is used to metallize the exterior walls of the filters. The simulated results are in good agreement with the theoretical concepts. The brief overview of Ansoft (Ansys) HFSS simulator is also presented.

5

CERAMIC BANDPASS WAVEGUIDE

FILTERS WITH NON-UNIFORM WIDTH

RESONATORS

5.1 Introduction

Ceramic waveguide resonators with non-uniform widths are used to improve the overall spurious performance of a ceramic waveguide filter. A waveguide resonator's resonances are a function of its physical dimensions i.e. length, width, and height. These dimensions are chosen in such a manner that the passband of a filter must lie as close to the center of the fundamental mode. In standard waveguide filter, with a uniform width, the length ' l ' determines the fundamental resonant mode, higher order mode and also the higher resonant frequencies. Some of these frequencies would lie at those points where good out of band rejection is required. Thus the use of low pass filter and stop band filter becomes essential to overcome this problem. Therefore, different techniques were proposed to control the out of band resonances without the use of low pass filter and stop band filter. One such technique is by altering the resonator geometry; in which by changing the length and width ratio of resonator, the distance between fundamental and higher order modes would also be changed. The change in width spreads out the higher order resonances, so they will not contribute as strongly as they did in a conventional waveguide

filter. Riblet firstly patented this idea in air-filled waveguide filters [13]. In all standard waveguide filters the width is common for all resonators but the length is adjusted to get the required amount of coupling. Therefore, these lengths are quite similar for all resonators which generates the re-resonances very close to each other. The spurious pass bands are the results of these resonances and the resonant frequencies of higher order modes. This issue can be compensated by the use of non-uniform width resonators. As, they allow to change the second resonant frequency for each resonator. These non-uniform widths resonators will be designed in such a way that their fundamental frequency remain same, but their higher resonances can be controlled by the non-uniform widths ' W_n ', if chosen carefully. As both resonators have different physical dimension, their lengths and widths can be computed using the following equations [15]:

$$W_n = \frac{1}{\sqrt{\epsilon_r}} \left(\frac{c}{2} \sqrt{\frac{3}{4(f_o)^2 - (f_{1n})^2}} \right) \quad \text{Eq 5.1}$$

$$L_n = \frac{1}{\sqrt{\epsilon_r}} \left(\frac{W_n}{\sqrt{\left(\frac{f_o}{f_{1n}}\right)^2 - 1}} \right) \quad \text{Eq 5.2}$$

Where W_n , L_n are the widths and lengths of resonators and f_c , f_{1n} and f_o are the cut-off, spurious frequencies and fundamental frequencies, respectively. The two non-uniform width resonators consist of a mono block ceramic ($\epsilon_r = 43$) is shown in figure 5.1. Their dimensions and Eigen mode data (HFSS) for Q factor and resonant frequencies are also given in table 5-1

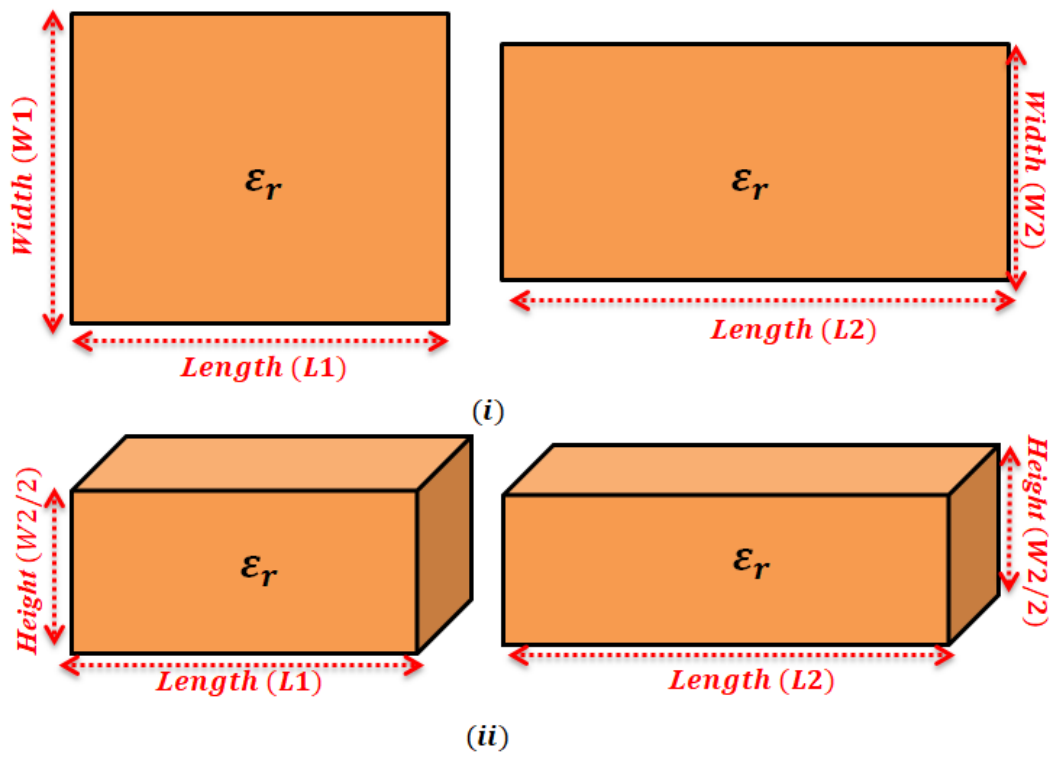


Figure 5.1: Non-Uniform width resonators (i) Top view (ii) 3D view

Table 5-1 Dimensions and Eigen mode data for two non-uniform width resonators

Parameters	Resonator 1		Resonator 2	
Dimensions (in mm)	W=18.627	L=16.64	W=14.91	L=22.39
Q factor of fundamental mode	2081		2039	
Fundamental Mode frequency (in GHz)	1.842 (TE ₁₀₁)		1.843 (TE ₁₀₁)	
First spurious frequency (in GHz)	2.74 (TE ₂₀₁)		2.55 (TE ₀₁₁)	
Second spurious frequency (in GHz)	2.80 (TE ₁₀₂)		3.23 (TE ₂₀₁)	

5.2 Ceramic Waveguide Filter with Two Non-Uniform Width Resonators

The six order ceramic waveguide filter with two non-uniform width resonators have been designed with the following specification given in table 4.1. The input/output coupling and inter-resonators coupling are achieved through the coaxial probe and metal plated through holes same as previous filters. The physical layout of the non-uniform width ceramic waveguide filter is shown in figure 5.2, where both the widths and lengths are divided by a dielectric value (43) to get the miniaturized size. The different widths provide more freedom to spread the spurious resonances for achieving good stop band performance. The pass band response and stop band attenuation of 40 dB is achieved up to

$1.85 * f_0$ as shown in figure 5.3 and 5.4. The same design technique and results of the ceramic non-uniform width filter is also published by the author in [73]. where 40 dB attenuation is achieved upto 3.3 GHz shows around 60% improvement in the spurious performance as in comparison of ceramic waveguide filter.

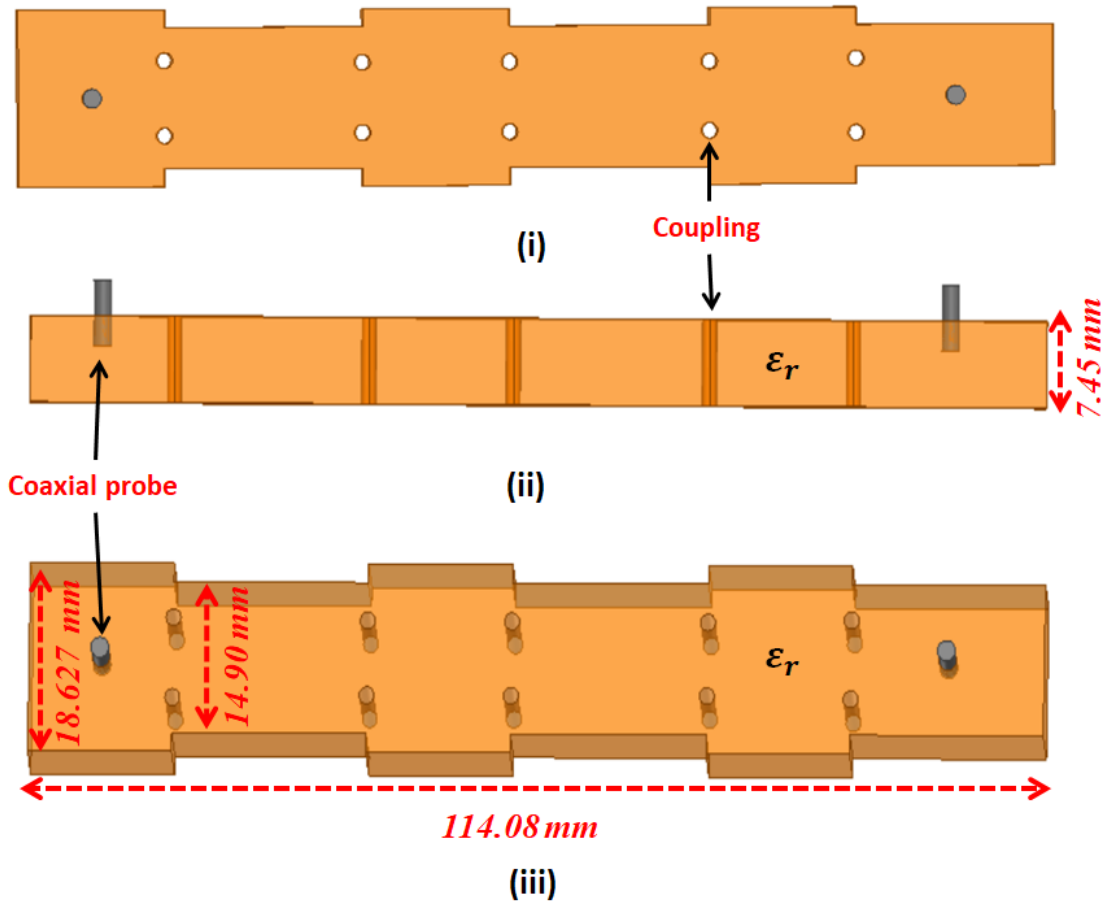


Figure 5.2: Ceramic waveguide filter with non-uniform width resonators (i) Top view (ii) Side view (iii) 3D view

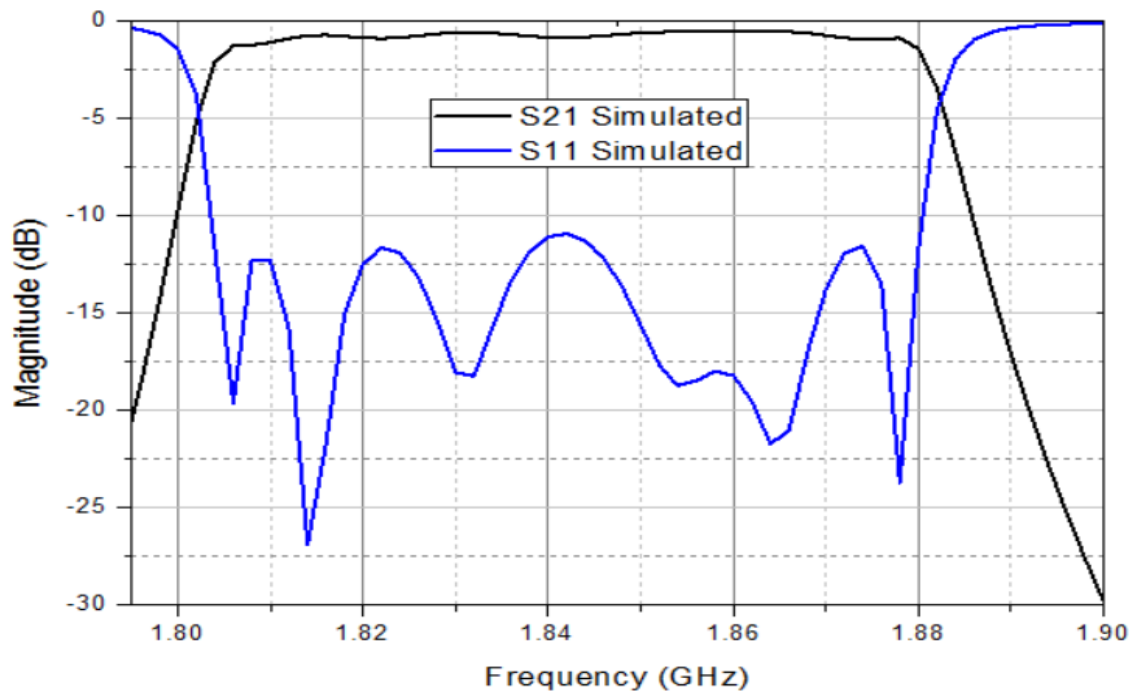


Figure 5.3: Simulated pass band response of ceramic waveguide filter with two non-uniform width resonators

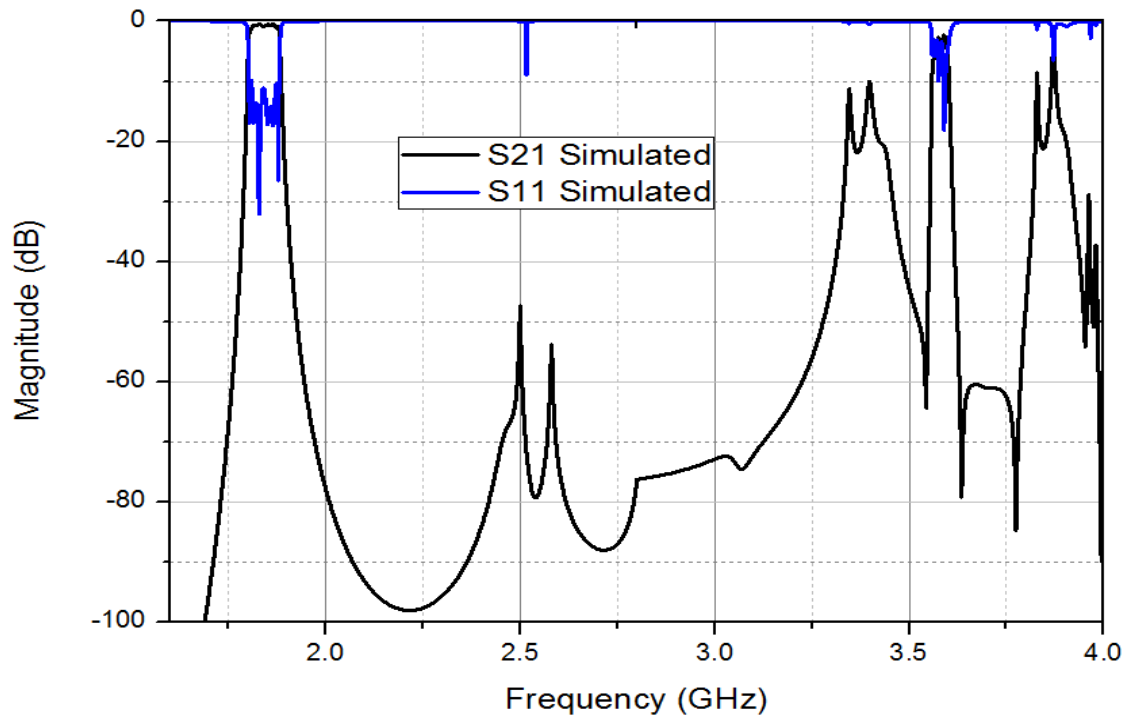


Figure 5.4: Broad band simulated response of ceramic waveguide filter with two non-uniform width resonators

Another seventh order filter with same two non-uniform width resonators is designed and optimized to show the performance while maintaining the symmetrical structure of a filter which gives stop band attenuation of 30 dB up to 3.55 GHz. The filter physical structure and full band response is shown in figure 5.5 and 5.6.

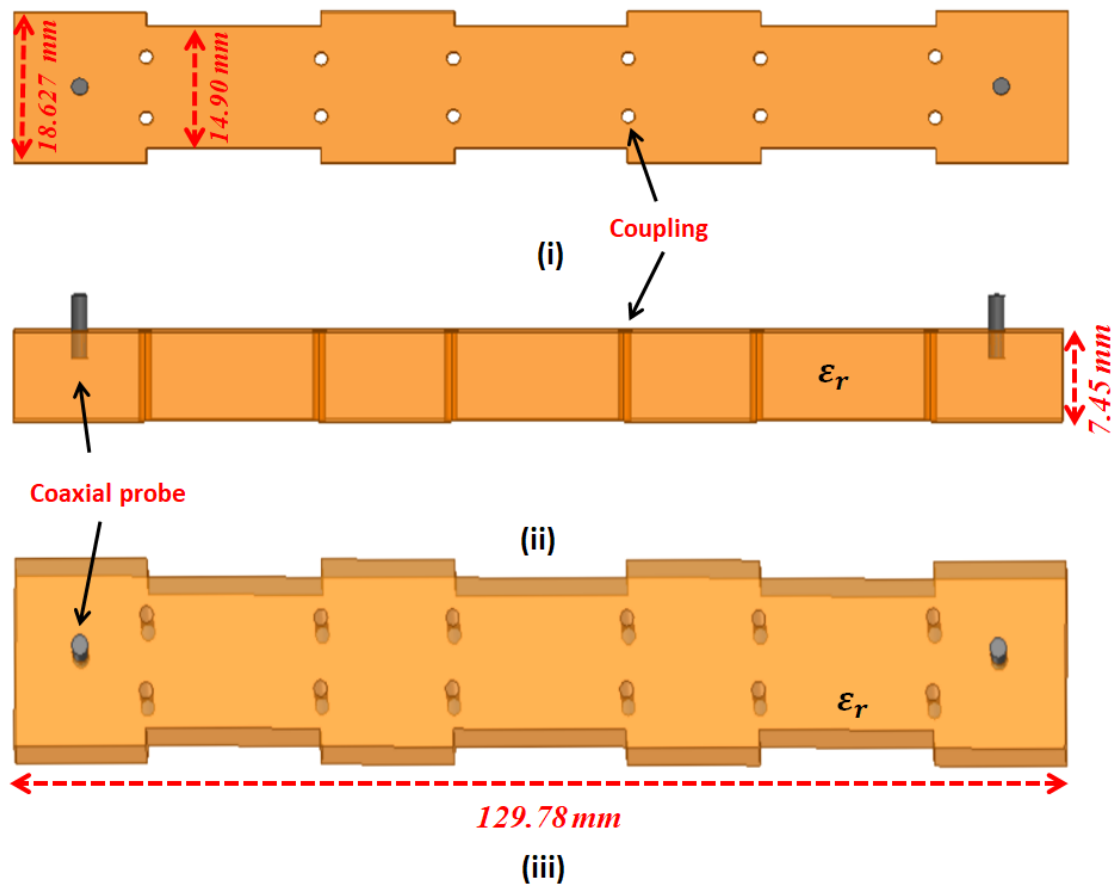


Figure 5.5: Physical layout of 7-pole ceramic waveguide filter with two non-uniform width resonators (i) Top view (ii) Side view (iii) 3D view

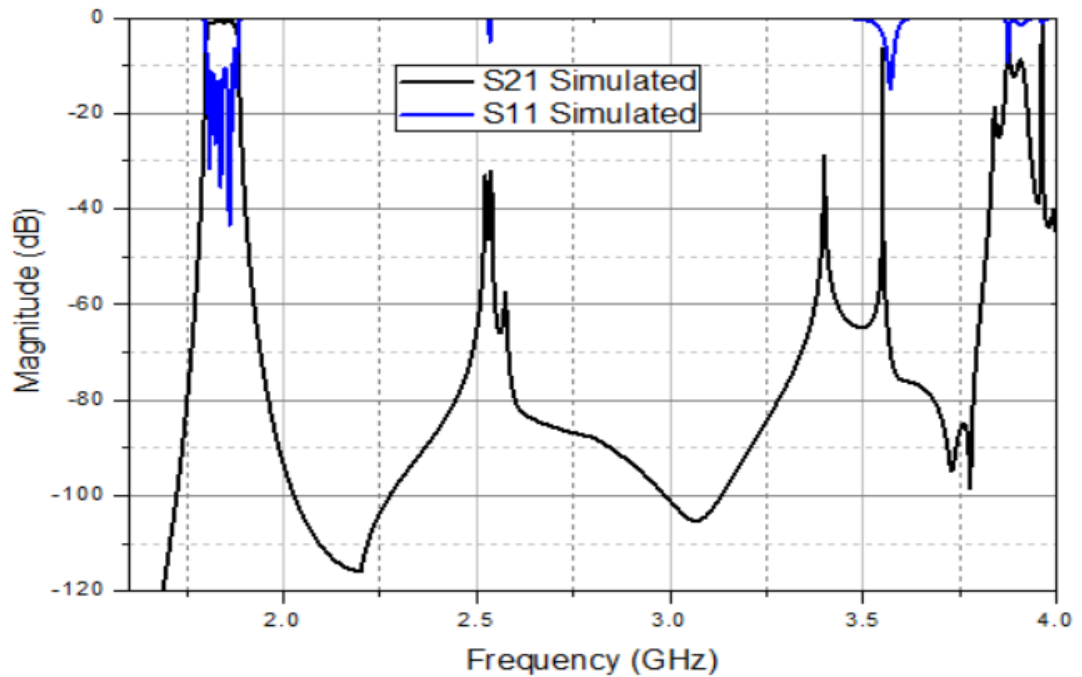


Figure 5.6: Broad band simulated response of 7-pole ceramic waveguide filter with two non-uniform width resonators

5.3 Ceramic Waveguide Filter with Three Non-Uniform Width Resonators

A ceramic waveguide filter is designed with three non-uniform width resonators and same specification of table 4.1. The resonators widths of three resonators are set with an equal gap and optimized their lengths to achieve the same fundamental frequency but with different spurious resonances. The three non-uniform widths allow us to spread out the spurious resonances well apart, that they cannot contribute significantly in out of band region. The physical layout of all three non-uniform width resonators and full filter is shown in figure 5.7 and 5.8. The input and output coupling is same as previous filters, and same inductive posts are used for inter-resonators couplings. The pass band and out

of band performance of a filter is shown in figure 5.9 and figure 5.10 with 33 dB out of band rejection up to 3.46 GHz.

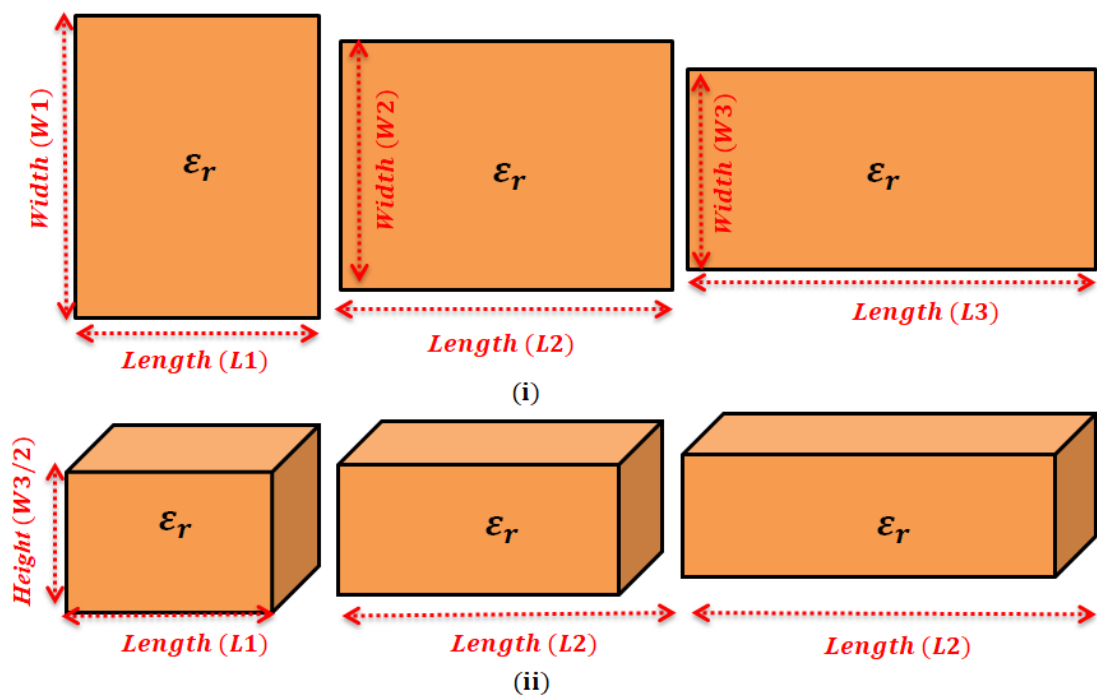


Figure 5.7: physical layout of three different width ceramic waveguide resonators (i) Top view (ii) 3D view

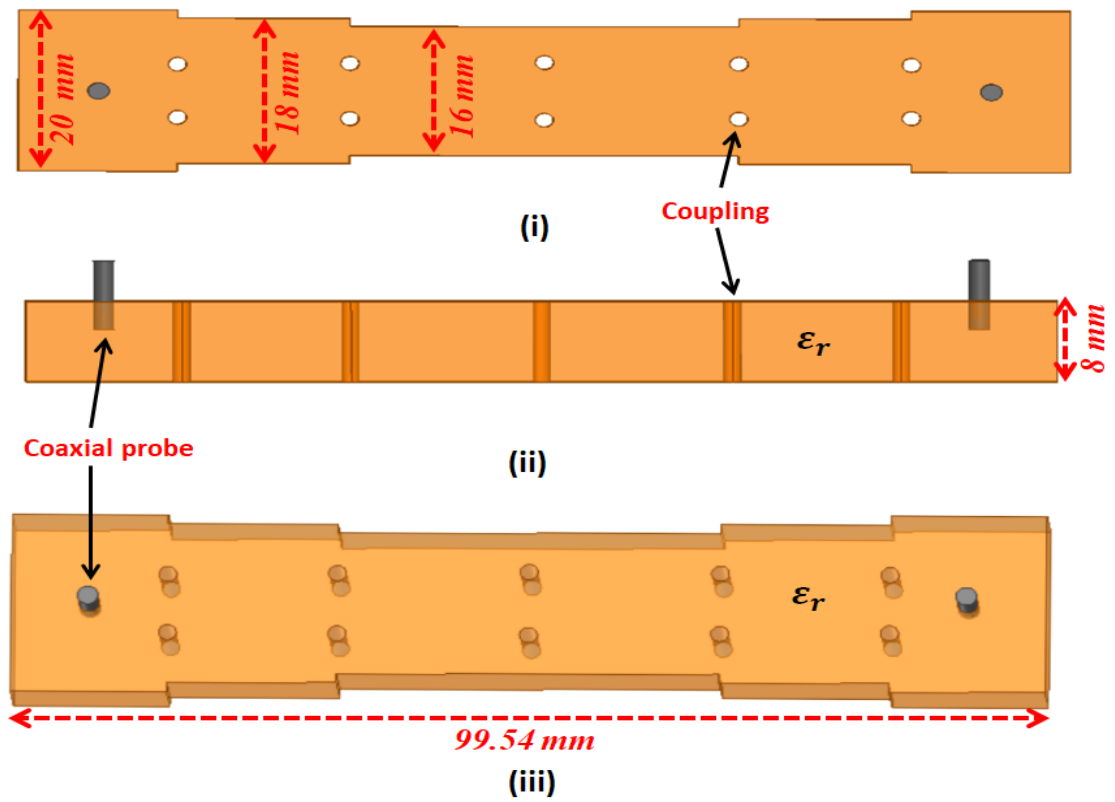


Figure 5.8: Physical layout of ceramic waveguide filter with three non-uniform width resonators (i) Top view (ii) Side view (iii) 3D view

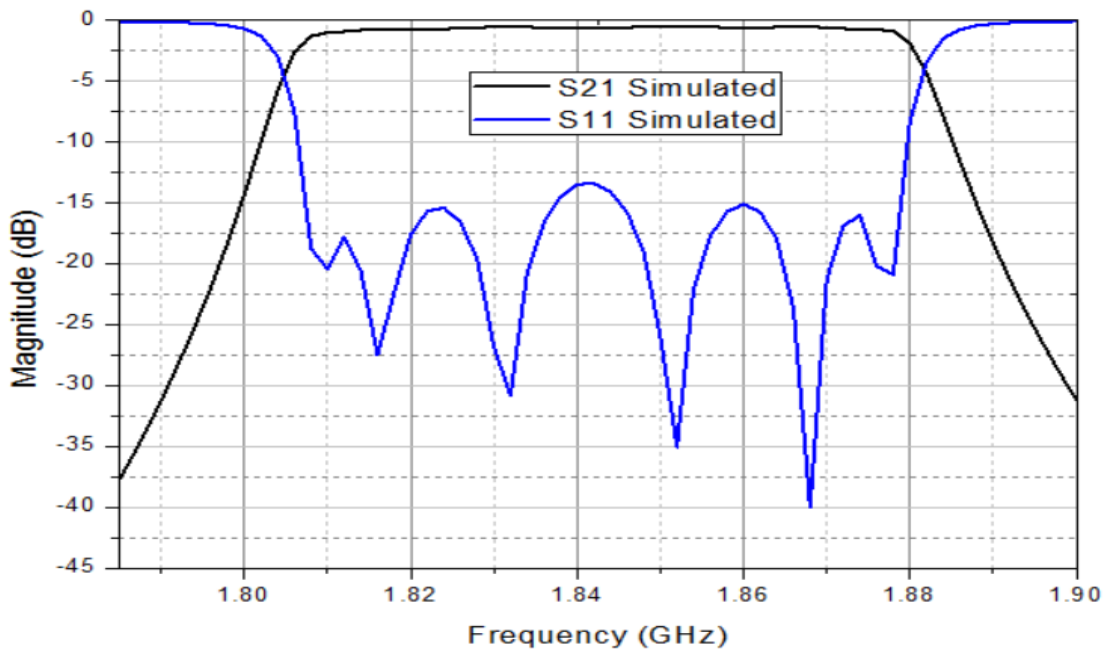


Figure 5.9: Simulated pass band response of ceramic waveguide filter with three non-uniform width resonators

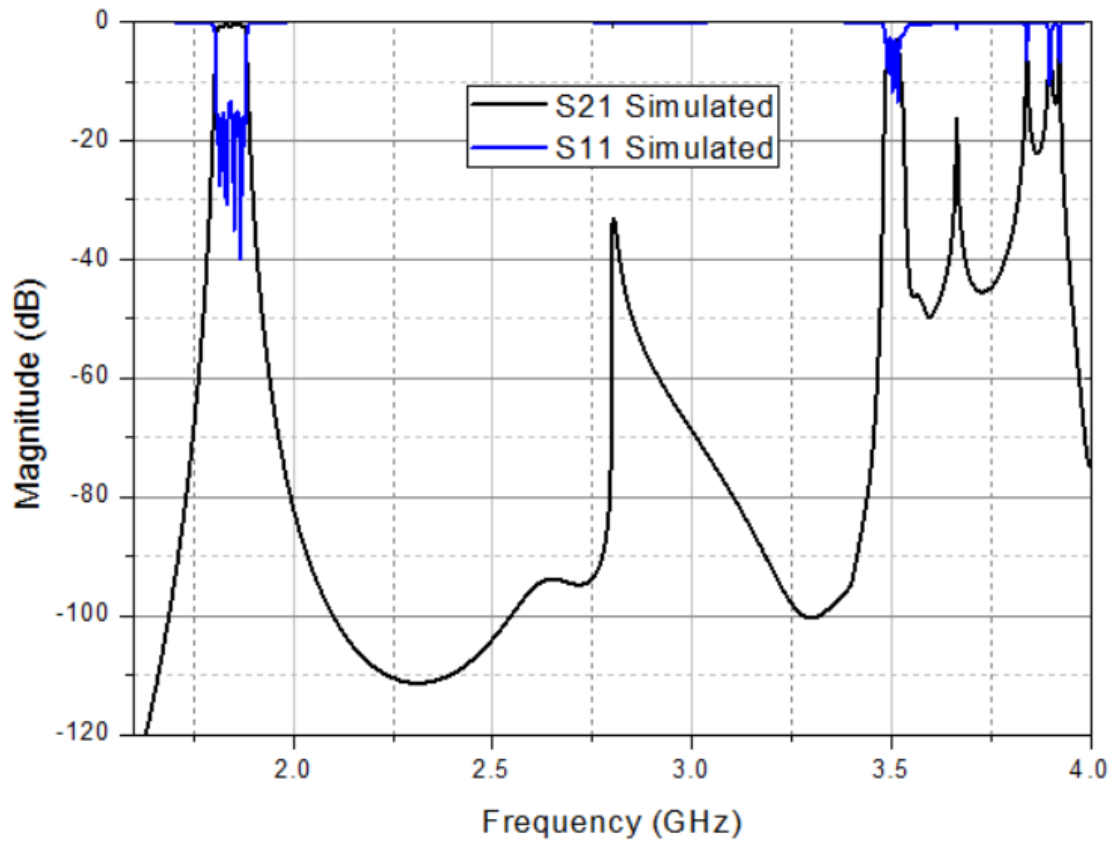


Figure 5.10: Simulated broad band response of ceramic waveguide filter with three non-uniform width resonators

The comparison of spurious performance of both the six order non-uniform width filters with test filter is shown in figure 5.11. The seventh order filter is included just to analyse the symmetry, so not needed to put here for comparison as test filter and all other filters are of six orders. The 30 dB attenuation is achieved up to 3.45 GHz in stop band.

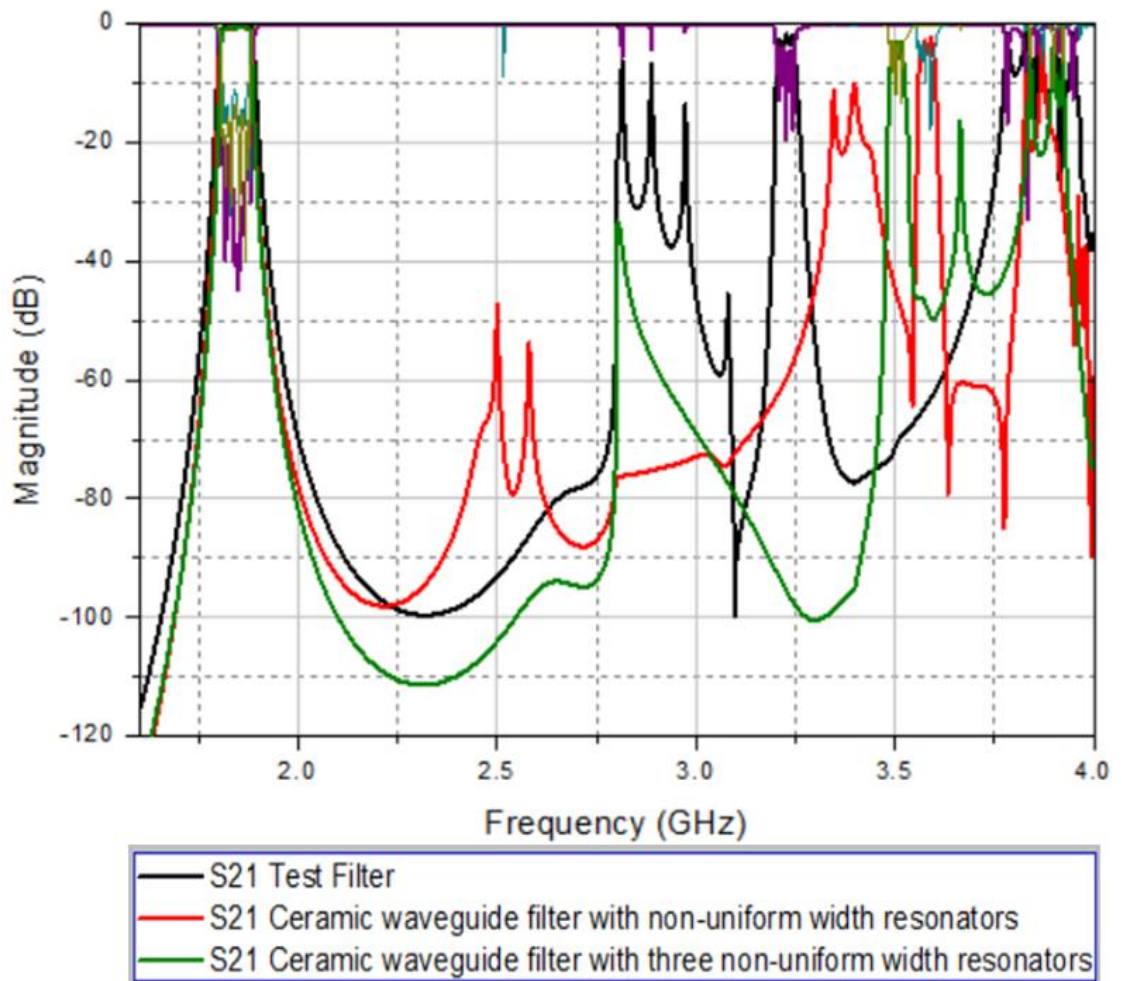


Figure 5.11: Comparison of spurious performance of both six order ceramic non-uniform width resonator filters with test filter

5.4 Summary

In this chapter, two different design techniques have been presented to improve the spurious performance of integrated ceramic waveguide filter (test filter). The design of a ceramic waveguide filter has been made more flexible by considering the width of a resonator as a design parameter.

In this way, a better spurious performance has been achieved by controlling the second resonance of a fundamental frequency. Filter design techniques with two and three non-uniform width resonators have been given and simulated response of corresponding filters shows good improvement over uniform width

ceramic waveguide filter. The insertion loss of the ceramic non-uniform width filter is also comparable with the test filter as the average Q factor and volume of a filter does not change significantly.

6 CERAMIC BANDPASS WAVEGUIDE FILTERS WITH METAL POSTS AND NON-UNIFORM WIDTH RESONATORS

6.1 Introduction

In this chapter, further new design techniques to improve the out of band performance of integrated ceramic waveguide filters are presented. The new technique uses the ceramic resonators with posts and ceramic non-uniform width resonators. In the integrated configuration of filters, a single monolithic metal coated ceramic block is used. Rectangular ceramic waveguide resonator geometry is modified to make it resonate at an evanescent mode frequency (Capacitive loaded ceramic cavity) by introducing silver coated blind holes at the Centre of the broad wall. The ceramic resonator with post allows significant size reductions with improved spurious performance, whereas resonators with different widths offer spurious suppression without degradation in the Q-factor. Different design techniques for chebyshev monolithic integrated ceramic filter are presented in this chapter to improve the spurious performance of a integrated ceramic waveguide filter.

6.2 Ceramic bandpass waveguide filter with all posts having different post height

A six order ceramic bandpass waveguide filter is designed with all ceramic resonator with posts having the different post heights (P_h), which allows to change the length and width of a filter to spread out the higher order resonances of resonator. Figure 6.1 shows the all three resonators with different post heights. This variation in post heights gives more freedom to alter the shape of resonators which helps to spread out the higher order resonances that will not then contributed so significantly to make any pass band near desired pass band. The post radius ($P_r = 2.5mm$) remains same, while offering improved spurious performance up to $1.955 * f_o$ by altering the height of the posts.

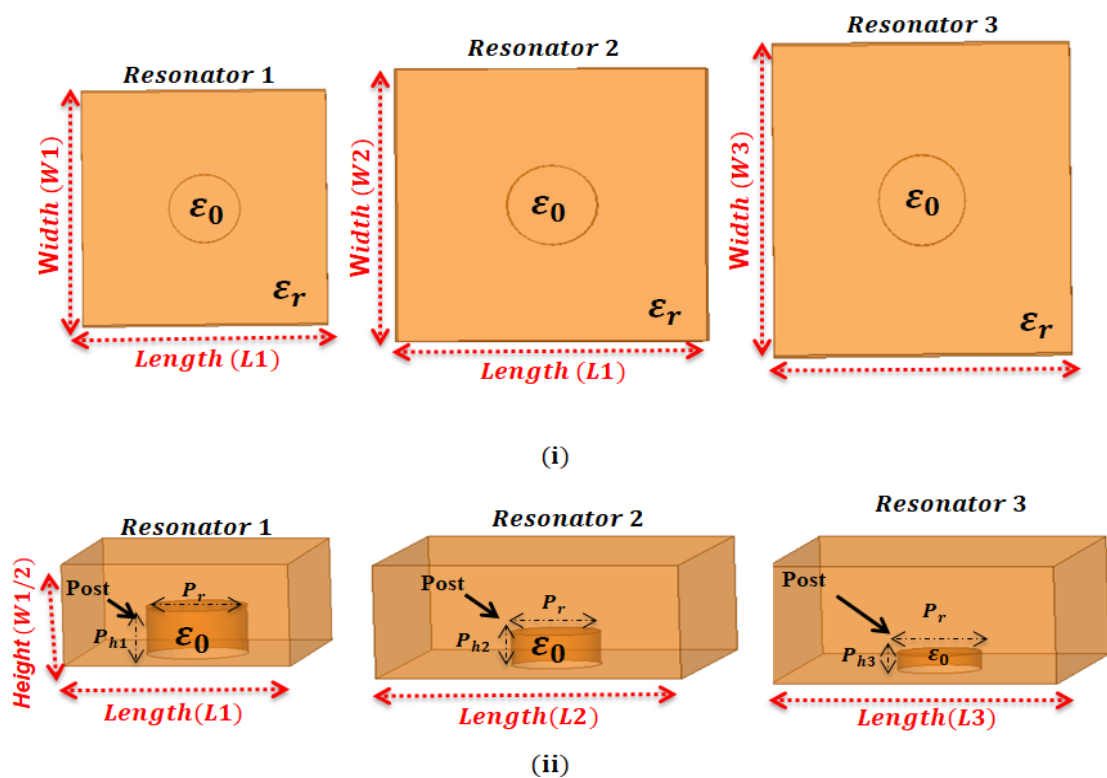


Figure 6.1: Three resonators with different post heights (i) Top view (ii) 3D view

More miniaturization has been achieved by reducing the overall volume of a filter by 29% in comparison of ceramic waveguide filter (test filter). The inter-resonator coupling achieved through the use of inductive through holes and I/O coupling is realised by having the coaxial probe at the center of first and last resonators of filter. Figure 6.2 shows the physical layout of a filter which shows the capacitive posts with different heights in respective resonators. The increase in post height also decrease the Q factor of the resonators, so, the resonators with lower Q factor have been used as first and last resonators to minimize the effect of lower Q factor on overall insertion loss of a filter[69]. The HFSS simulated pass band and out of band response of a filter shown in figure 6.3 and figure 6.4. The stop band performance of a filter shows 40 dB attenuation up to 3.60 GHz which is 1.955 times the fundamental frequency. This filter design technique with same specifications is also published in [74]. The details of the resonators unloaded quality factor, volume and post size are also given in table 6-1.

Table 6-1 Details of Quality factor, post heights and volume of resonators

Resonator	Post height (mm) / Electrical length (degrees)	Volume (Cm ³)	Unloaded Q Factor
Resonator 1 & 6	2.6 mm / 18.9°	1.372	1559
Resonator 2 & 5	2.1 mm / 15.3°	1.638	1732
Resonator 3 & 4	1.6 mm / 11.6°	1.837	1859

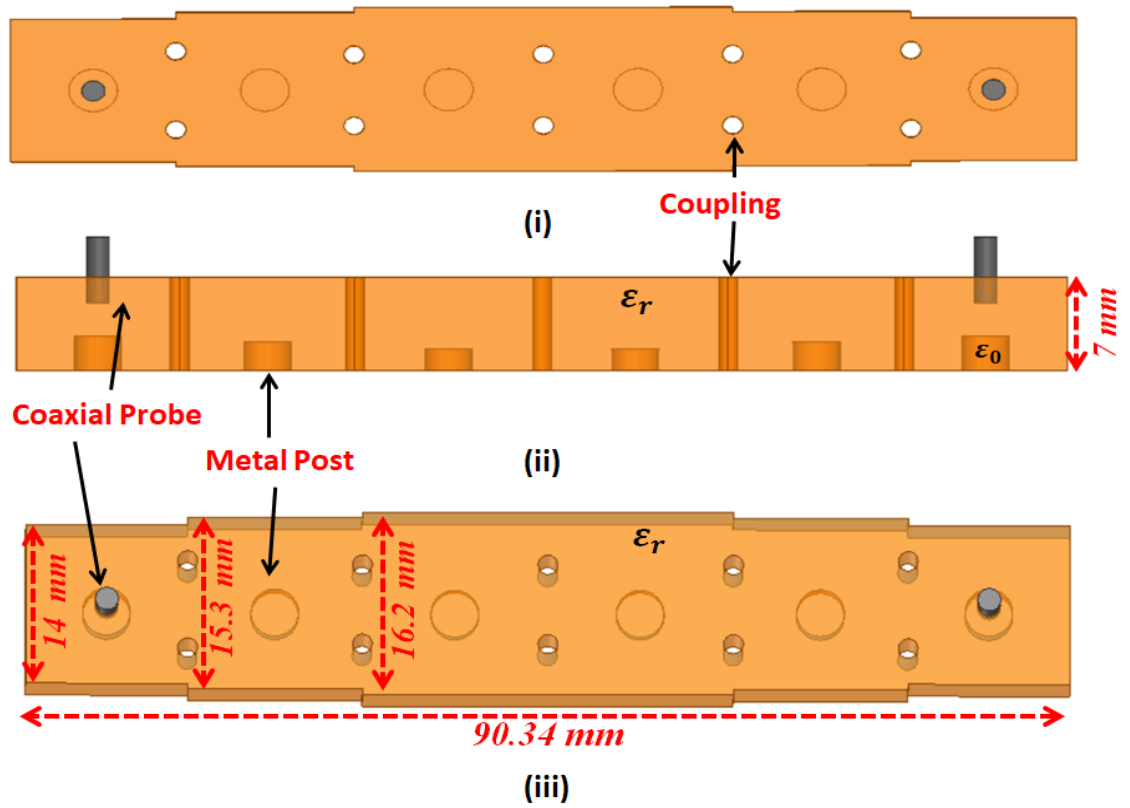


Figure 6.2: Physical layout of a filter with all posts resonators having different posts heights (i) Top view (ii) Side view (iii) 3D view

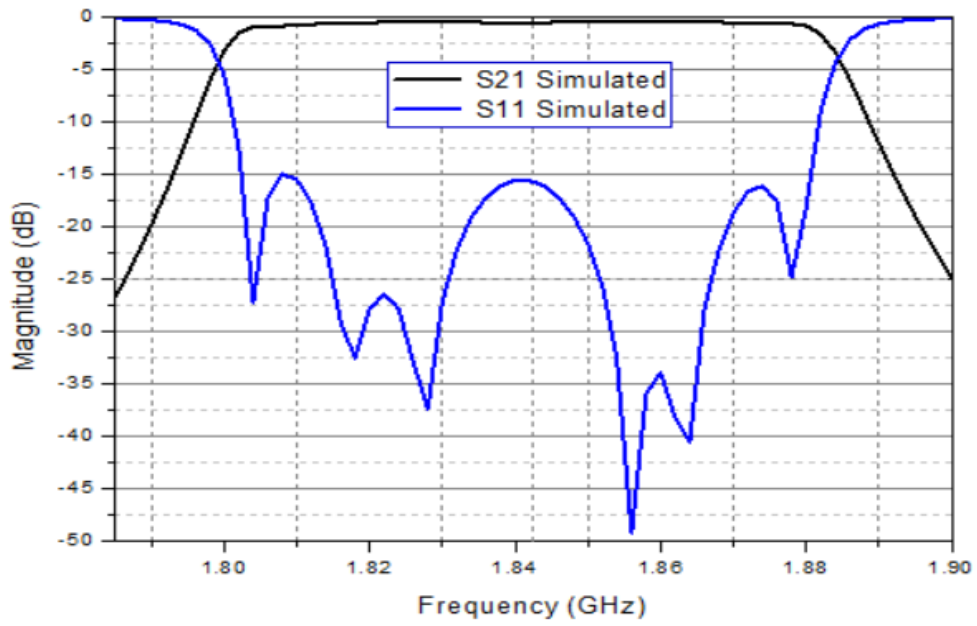


Figure 6.3: Simulated (HFSS) Pass band response of a ceramic waveguide filter with all posts having different height.

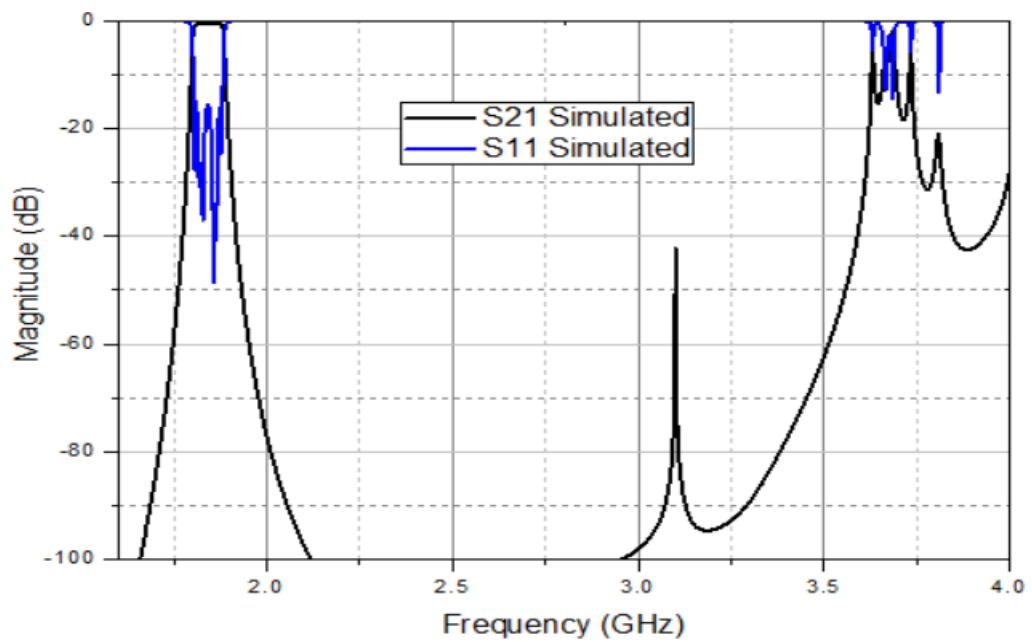


Figure 6.4: Full band simulated (HFSS) response of a ceramic waveguide filter with all posts having different height

6.3 Ceramic non-Uniform width filter with metal posts

This filter design technique uses the two non-uniform width resonators loaded with TEM posts having equal height. It offers good improvements in the spurious performance but with the slight degradation of Q factor of a filter. This six order Chebyshev ceramic filter with non-uniform width and posts improves the spurious performance by suppressing the higher order modes. This mix resonators approach also provides further reduction in volume at the cost of increased insertion loss. The input/output coupling realized with the coaxial probe at the center of first and last resonator and inductive through holes is used for inter-resonator coupling same as before. Figure 6.5 and 6.6 shows resonator structure and filter layout of ceramic bandpass filter with non-uniform width and posts.

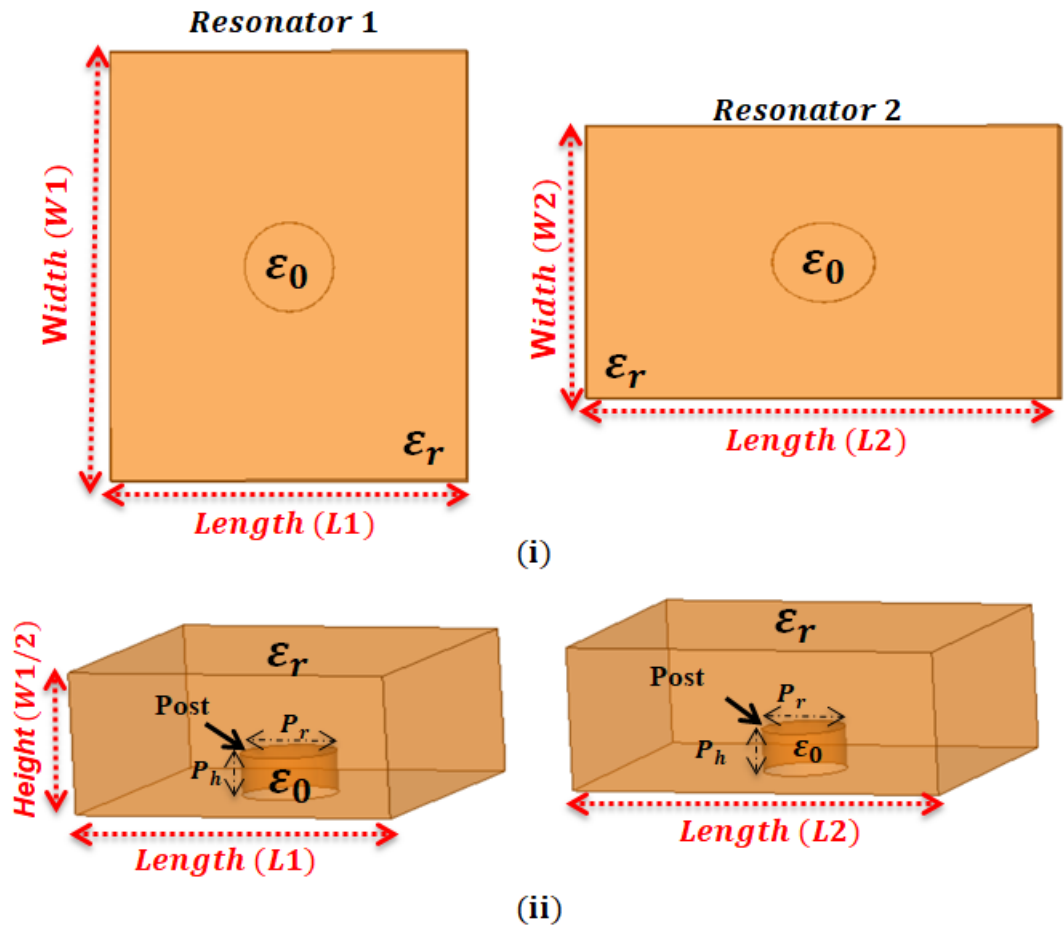


Figure 6.5: Two non-uniform width resonators posts having equal height (i) Top view (ii) 3D view

This design technique allows us to achieve the spurious free window up to 3.45 GHz with the attenuation of 72 dB, which makes it 1.87 times the fundamental frequency. The pass band and stop band response showed in figure 6.7 and 6.8. The details of volume, Q factor and post height of resonators are also given in table 6.2. This proposed technique have also been published in [73].

Table 6-2 details of Q factor, post height and volume of two non-uniform width resonators

Resonator	Post height (mm) / Electrical length (degrees)	Volume (Cm ³)	Unloaded Q Factor
Resonator 1	2.1 mm / 15.3°	1.81	1699
Resonator 2		1.67	1716

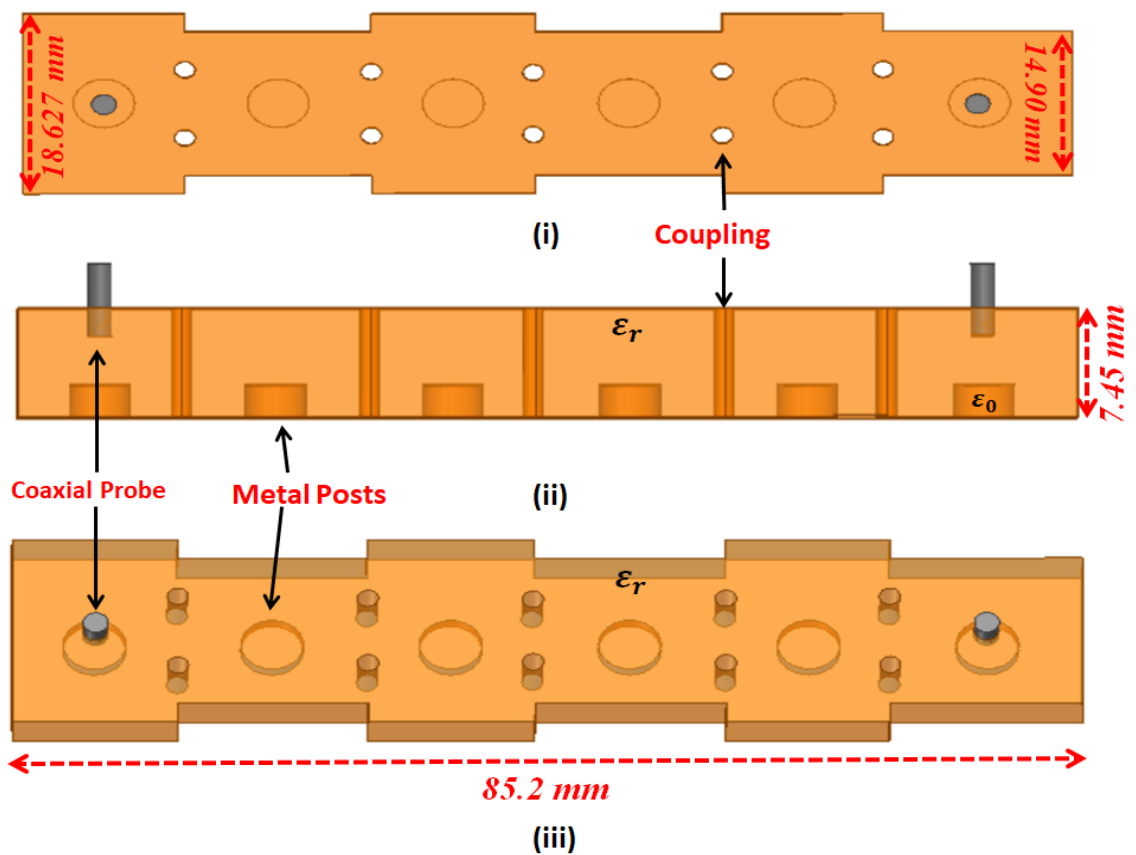


Figure 6.6: Physical layout of ceramic bandpass filter of non-uniform width resonators having posts of equal height (i) Top view (ii) Side view (iii) 3D view

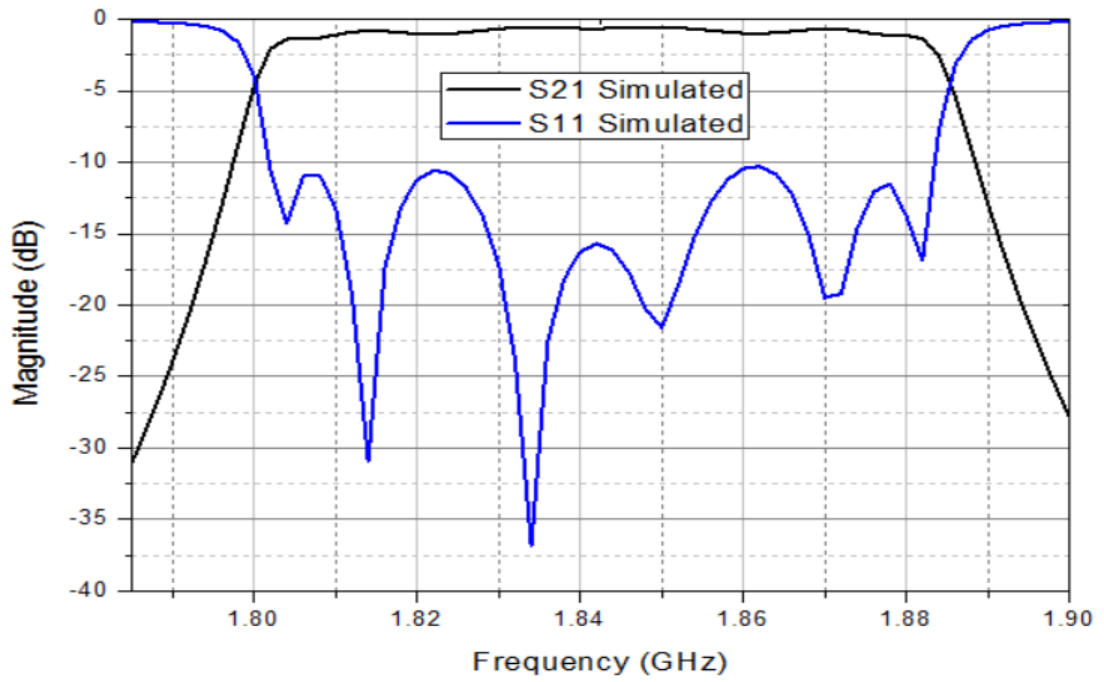


Figure 6.7: Simulated (HFSS) pass band response of ceramic bandpass filter of non-uniform width resonator having posts of equal height

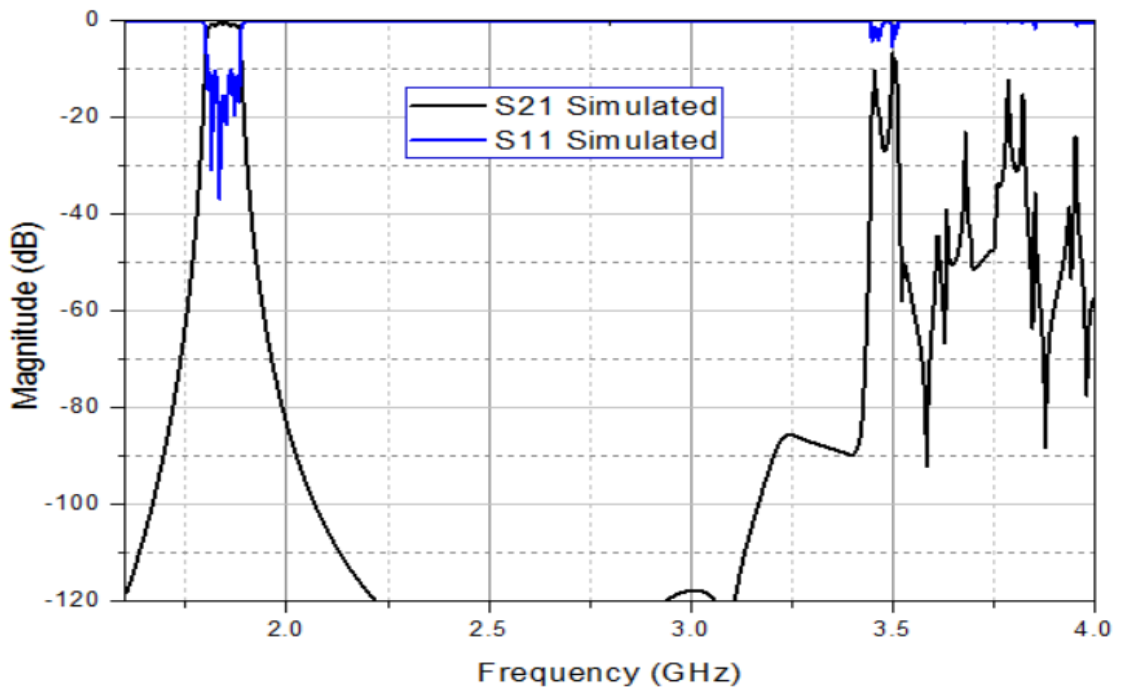


Figure 6.8: Simulated (HFSS) Broadband response of ceramic bandpass filter of non-uniform width resonator having posts of equal height

6.4 Ceramic non-uniform width filter with two metal posts

This design technique combining both capacitive loaded resonator and non-uniform width resonators in such a way to get the advantages of both individual resonators types. The author have published the idea of a mixed resonator approach using HFSS simulations of a ceramic waveguide filter with given specifications in [74]. The proposed design consists of a mono block ceramic structure having both non-uniform width resonators and ceramic resonators with posts. Non-uniform width resonators have different cut-offs and at the same time capacitive loaded resonator further enhances the out of band performance of a filter. This capacitive loaded resonator offers low Q factor but good spurious performance. So, they can be used as first and last resonators to have a negligible effect on the overall insertion loss of a filter[69]. The couplings of a filter are achieved in a same manner like previous filter designs. The resonator structures and simulated filter design of ceramic bandpass filter are shown in Figure 6.9 and 6.10 respectively. Initially the filter is designed with mono block ceramic structure of permittivity of 43. Their simulated s-parameters response shown in figure 6.11 and figure 6.12, indicates that the spurious free region extends up to $1.99 * f_o$ having 30 dB stop band attenuation up to 3.66 GHz. The same filter is re-designed, simulated and then fabricated in air filled structure to validate the concept and EM simulations of the design. The simulated pass band and out of band response of air filled filter is depicted in figure 6.13 and 6.14. The comparison of all filter responses shown in figure 6.15.

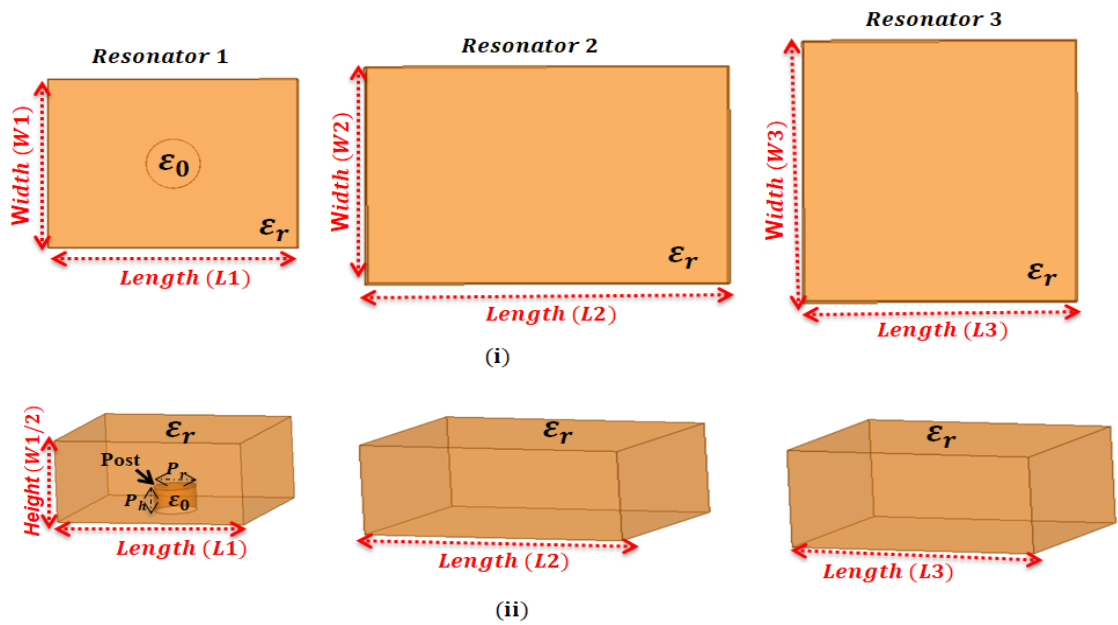


Figure 6.9: Structural layout of TEM and non-uniform width resonators (i) Top view (ii) 3D view

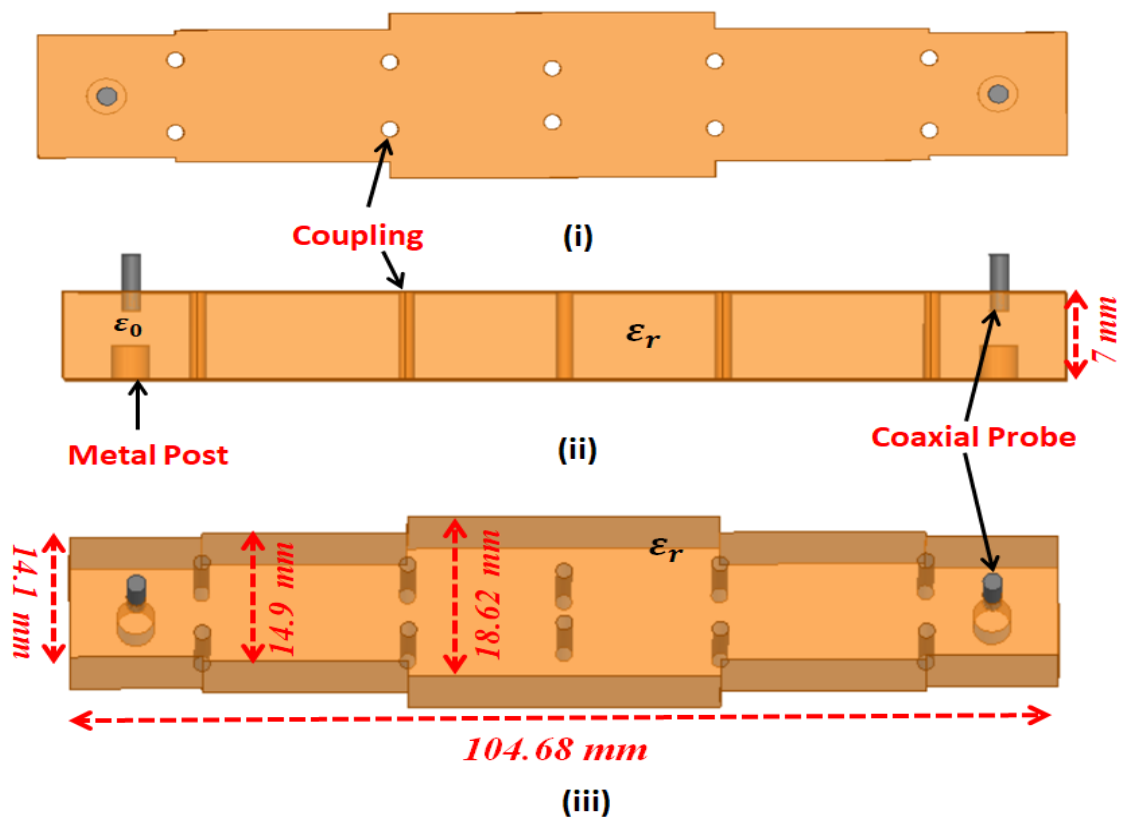


Figure 6.10: Simulated design of ceramic waveguide filter with two posts and non-uniform width resonators (i) Top view (ii) Side view (iii) 3D view

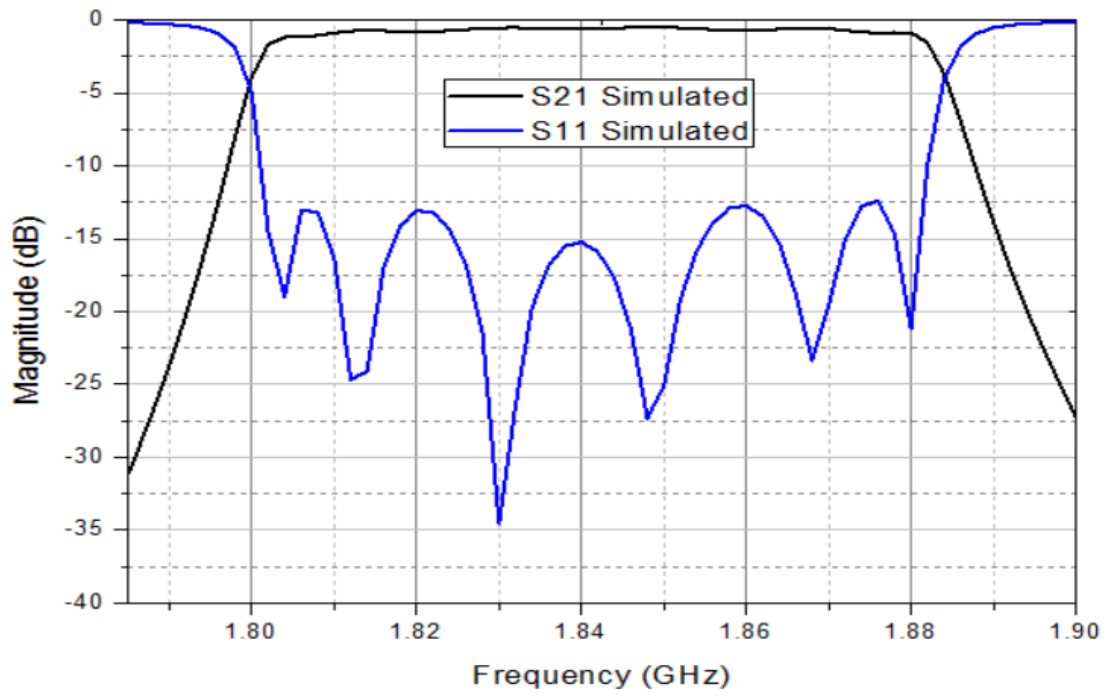


Figure 6.11: Simulated pass band response of ceramic TEM and non-uniform width filter

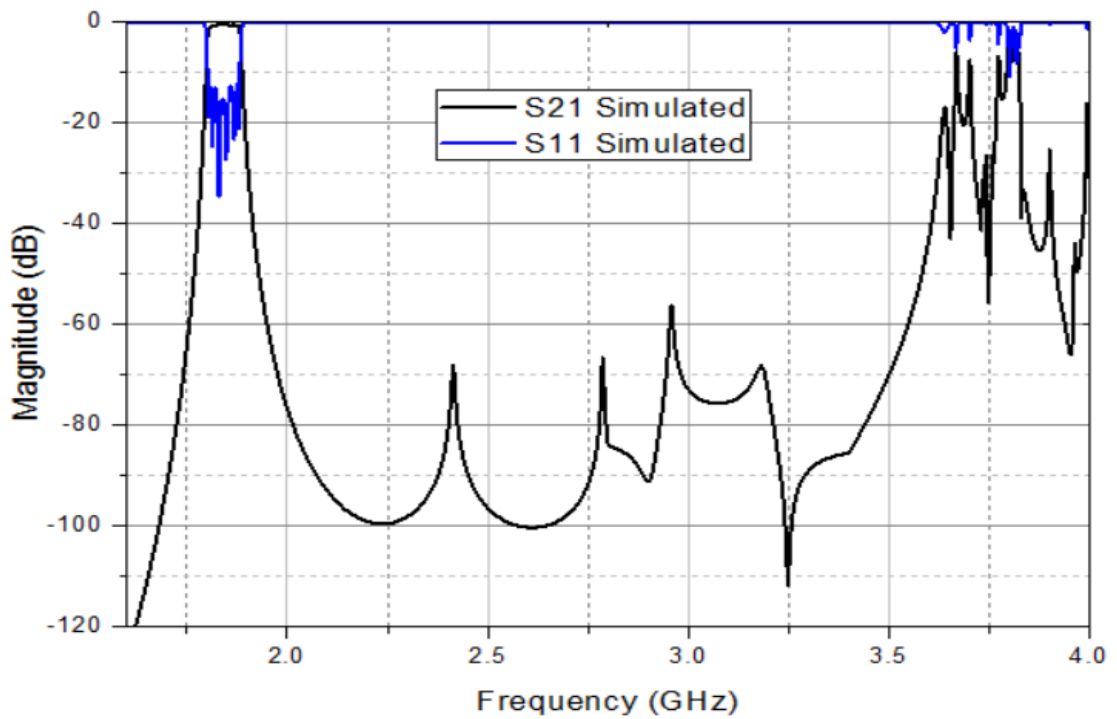


Figure 6.12: Simulated Broadband response of ceramic TEM and non-uniform width filter

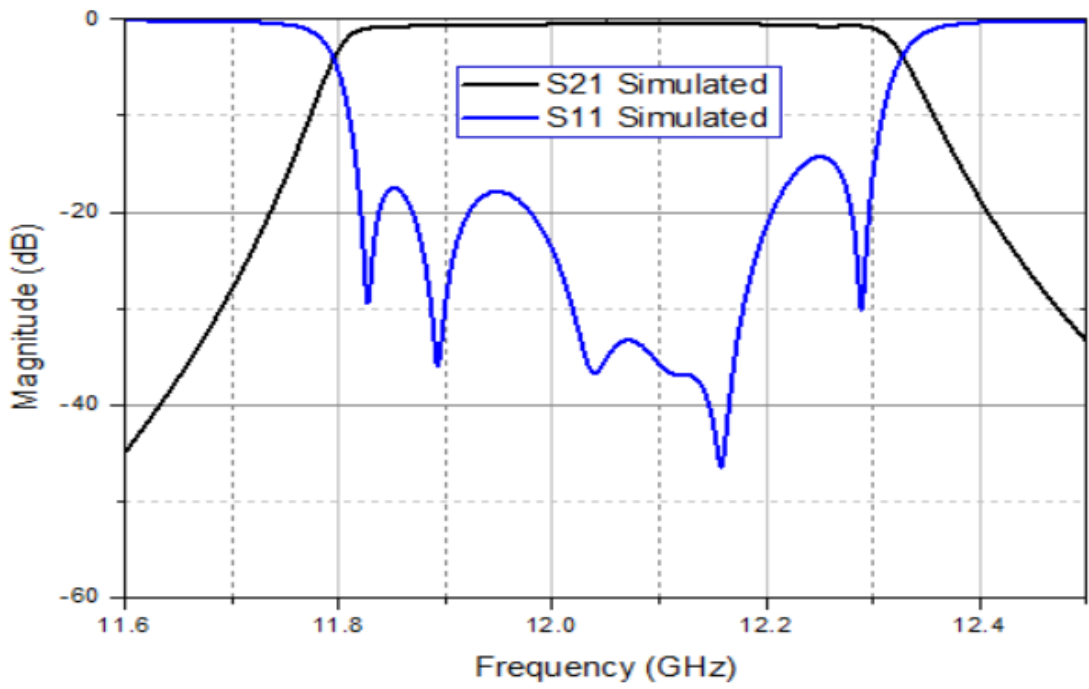


Figure 6.13: Simulated pass band response of air filled TEM and non-uniform width filter

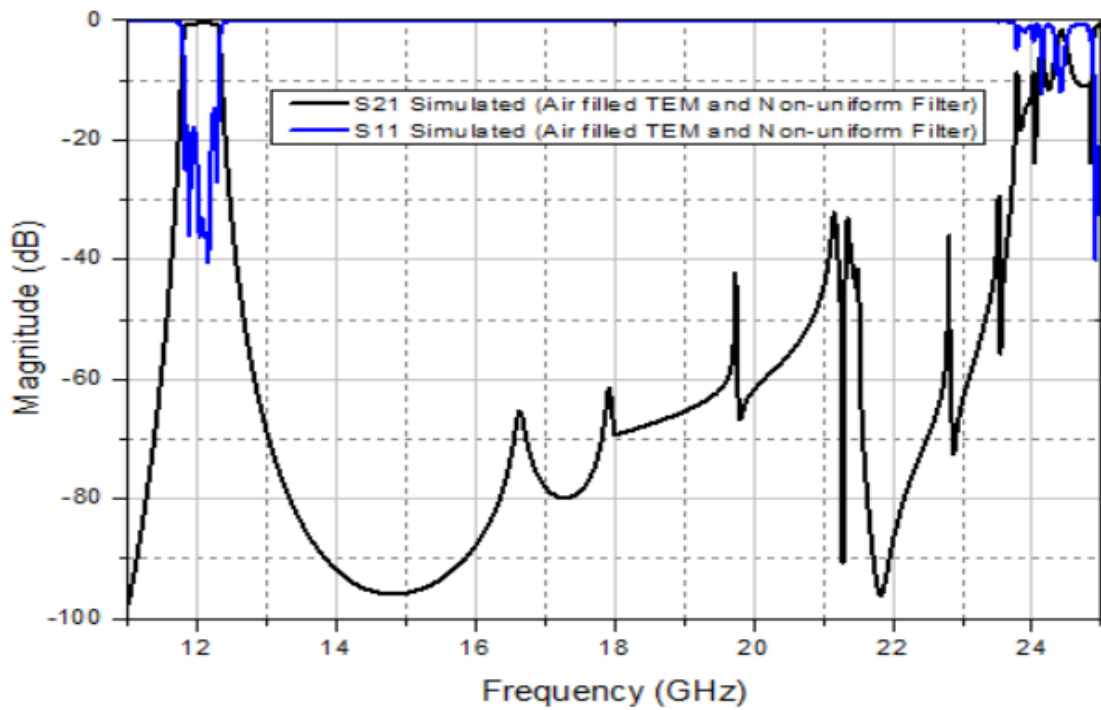


Figure 6.14: Broadband simulated response of air filled TEM and non-uniform width filter

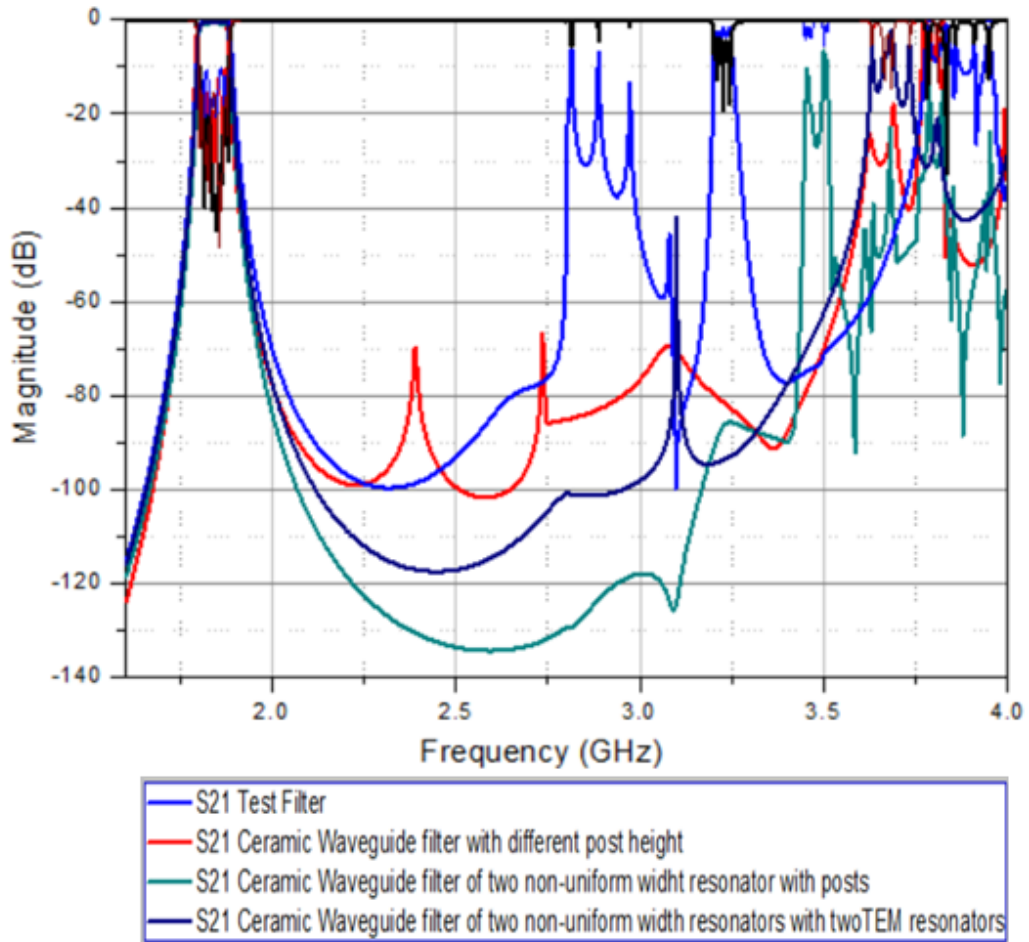


Figure 6.15: Comparison of broadband response of all simulated ceramic filters with test filter

6.4.1 Fabrication Details

The proposed filter design is fabricated in air filled configuration. Therefore, for the same size, the fundamental frequency is shifted up by a factor of $\sqrt{\epsilon_r}$. The scaled fundamental frequency is now 12.07 GHz, and spurious free region extends up to 24 GHz ($1.99 \cdot f_0$) which is same as in simulated design. The tuning screws are introduced in the fabricated design to mitigate the effects of physical dimension tolerances and material discrepancies. 1mm diameter screws are placed at the center of each resonator to perturb the E-field of the fundamental mode which is maximum at the center, except for the first and last

resonators. A photograph of fabricated air filled capacitive loaded and non-uniform width resonator filter with tuning screws is shown in figure 6.16. A comparison of simulated and measured results of air filled capacitive loaded and non-uniform width resonator filter is shown in figure 6.18, 6.19 and 6.20 respectively. The slightly degraded response is due to possible air gap between the inductive coupling posts and the top lid. The simulated and measured results show an excellent agreement of stop band attenuation of 30 dB up to $1.99*f_o$.

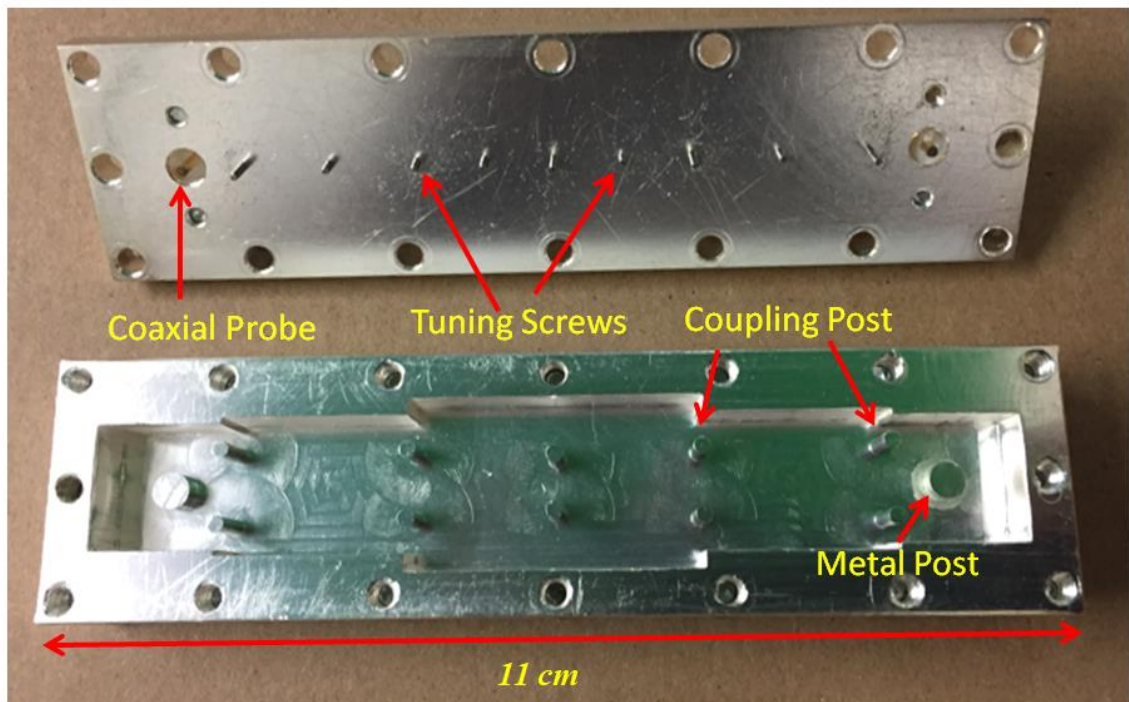


Figure 6.16: Fabricated silver plated air filled TEM and non-uniform width filter with tuning screws

6.4.2 Filter Tuning

The best way to tune the resonant frequency of a waveguide resonator is to perturb its electric field by placing the metallic screw at the center of its broad

wall as shown in figure 6.17. Manufacturing discrepancies and tolerances can lead to a shift in frequency, where tuning becomes essential to get the fabricated response of filter as close to simulated response. This tuning mechanism also allows reducing the overhead time to optimize the measured response in very stringent limits. The amount of tuning can be controlled by diameter and depth of a screw. The maximum tuning will be achieved at the center of a resonator where the electric field is maximum for TE_{101} mode.

Tuning screws are also used for having adjustable susceptances. A tuning screw with less the quarter wavelength length produces an effective capacitive susceptance, whose value increases with the depth of penetration. When the penetration depth is approximately a quarter wavelength the screw is series resonant, and further penetration causes the susceptance to become inductive[68, 75]. The coupling between the resonator realized by inductive posts or inductive irises can also be controlled by placing the metal screws between the post or irises.

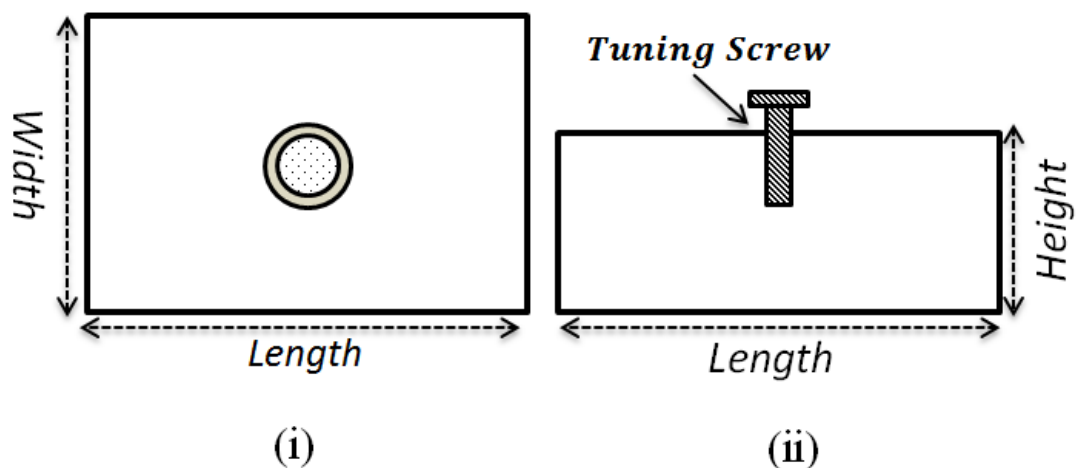


Figure 6.17: Resonator with tuning Screw (i) Top view (ii) Side view [68]

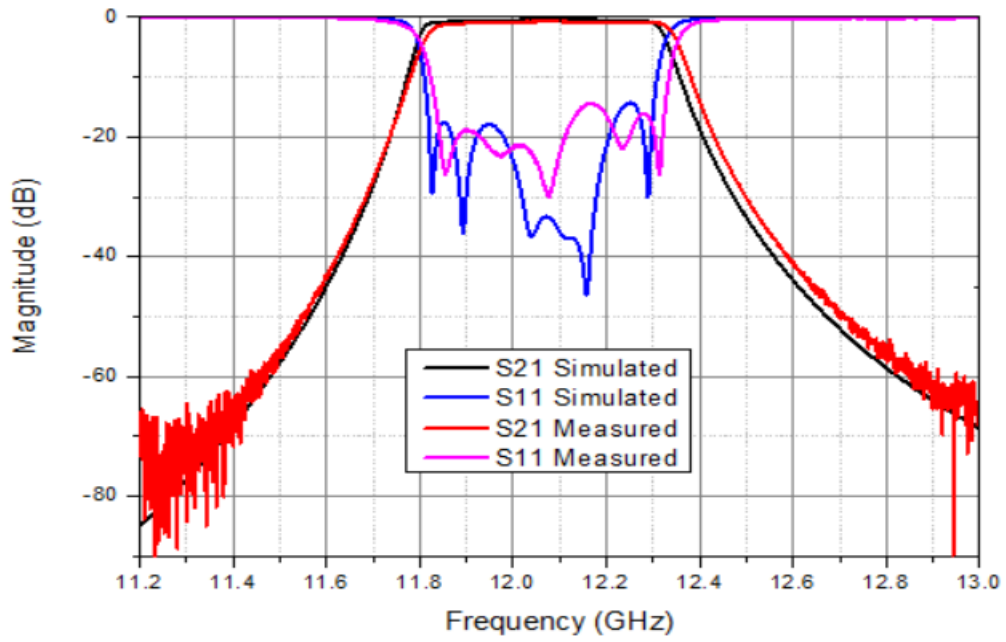


Figure 6.18: Comparison of simulated and measured passband response of air-filled waveguide filter having two metal posts and non-uniform width resonators

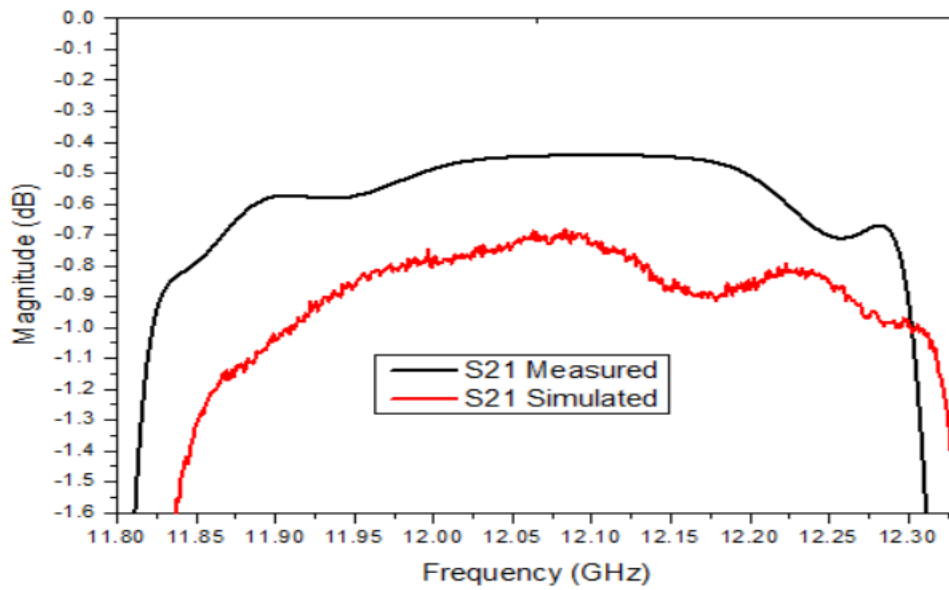


Figure 6.19: Detailed comparison of simulated and measured passband response of air-filled waveguide filter having two metal posts and non-uniform width resonators.

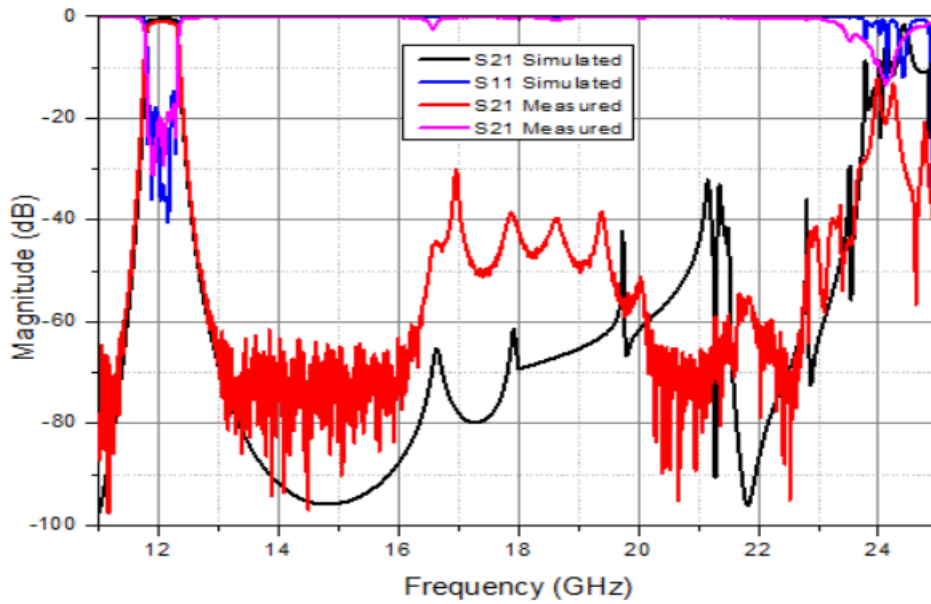


Figure 6.20: Comparison of simulated and measured broadband response of air-filled waveguide filter with post and non-uniform width resonators

The bandwidth of the filter also extended from 75 MHz to 492 MHz, when fabricated as air filled filter. The comparison of all simulated ceramic filter with test filter is shown in figure 6.15, which shows the significant improvement in the stop band performance of an integrated ceramic filter.

6.5 Summary

The novel design techniques used to improve the spurious performance of the integrated ceramic waveguide resonator filters are presented. The integrated ceramic rectangular waveguide resonator geometry is modified to increase the separation between first and higher order resonances. The combination of the non-uniform width resonators with ceramic resonators with posts results in significantly improved spurious performance without much degrading the Q-factor of a filter. Three design techniques are used to improve the spurious performance of ceramic waveguide filters. The ceramic filter design with

capacitive loaded and non-uniform width resonators is scaled, simulated and fabricated in air filled configuration and measured. The fabricated filter results are in good agreement with the simulated results.

7 CERAMIC WAVEGUIDE FILTERS WITH STEPPED IMPEDANCE RESONATORS AND CERAMIC LOADED RESONATORS

7.1 Introduction

In this chapter, a ceramic waveguide filter is designed with monolithic ceramic step impedance resonators and ceramic loaded resonators. This stepped impedance resonator consist of a low impedance (Z_1) transmission line alternately connected with high impedance (Z_2) transmission line. The high impedance transmission line act as a series inductor, while a low impedance transmission line behaves like a shunt capacitor. The low impedance transmission line has a wider width and a shorter length as in comparison of high impedance transmission line which has a narrower width a longer in length. The too short transmission line can have an extra inductance where a too longer transmission line can have an extra capacitance. The additional required capacitance and inductance can be made by making the transmission line wider and narrower. The larger the difference between two widths the shorter the size of the resonator shown in table 7-1. This difference of impedances in transmission line has a significant effect on the stop band performance of a filter[37, 76]. To further improve the band stop performance of a filter, a filter can be designed with resonators of different impedance ratio. In this way the

spurious resonances can be spread over the stop band and will not contribute significantly.

Table 7-1 Different Resonator impedance Dimensions-ratios for Improved Stop band[37]

	$Z_2 / Z_1 < 1$	$Z_2 / Z_1 > 1$	$Z_2 / Z_1 = 1$
Length	Shorter	Longer	Reference
Spurious	$> 2 \times f$	$< 2 \times f$	$2 \times f$

7.2 Ceramic Bandpass Filter with Stepped Impedance Resonator

The Uniform Impedance resonator (UIR) controlled its resonant frequencies by changing the length of resonator, which is the only freedom of structure. The fundamental frequency F_o , can be controlled by the length of resonator, hence, all the higher order modes are fixed. In Stepped impedance resonator (SIR), the more degree of freedom is available to control the fundamental frequency and higher order modes by changing the length and ratio between two impedance of resonator. The different impedance of quarter wave and half wave resonators have shown in figure 2.13. In [16] Morelli et al introduces the use of Uniform Impedance resonator (UIR) and Stepped impedance resonator (SIR) for a wide spurious performance of wave guide filters. He achieved the more than an octave wide spurious performance in waveguide filter by employing UIR and SIR resonators. As UIR have same impedance across its length of resonator, the SIR impedance ratio can be determined by the following equation.

$$K = \frac{Z_2}{Z_1} \quad \text{Eq 7.1}$$

In rectangular waveguide resonator, the Stepped impedance resonator (SIR) can be realized by E-plane and H-plane steps. In H-Plane SIR, the cut off frequencies are different for inner and outer sections. In each section resonator, the fundamental mode is propagating in centre of each section and to prevent the higher order modes for propagation, the ratio between the two broad dimensions is limited in H-plane SIR. While in E-plane SIR, this constraint is not hold valid and a wide variety of impedance ratios can be achieved. Hence the E-plane SIR, is focused to design a waveguide filter which make possible to achieve a wide spurious performance. The better stop band performance is achieved by employing SIR in two different ways; firstly the all resonators have same fundamentals frequencies but different first spurious frequency. In this way, the second spurious is arising around first spurious will be spread over frequency range. Secondly, it is also possible to design resonator with same fundamental frequency and same first spurious frequency placed well beyond the fundamental frequency where good attenuation is required. The second method is employed here to design a Stepped impedance resonator (SIR) ceramic filter to attain a very good spurious performance. The E-plane Stepped impedance resonator (SIR) is designed with fundamental frequency of 1.84 GHz is given below

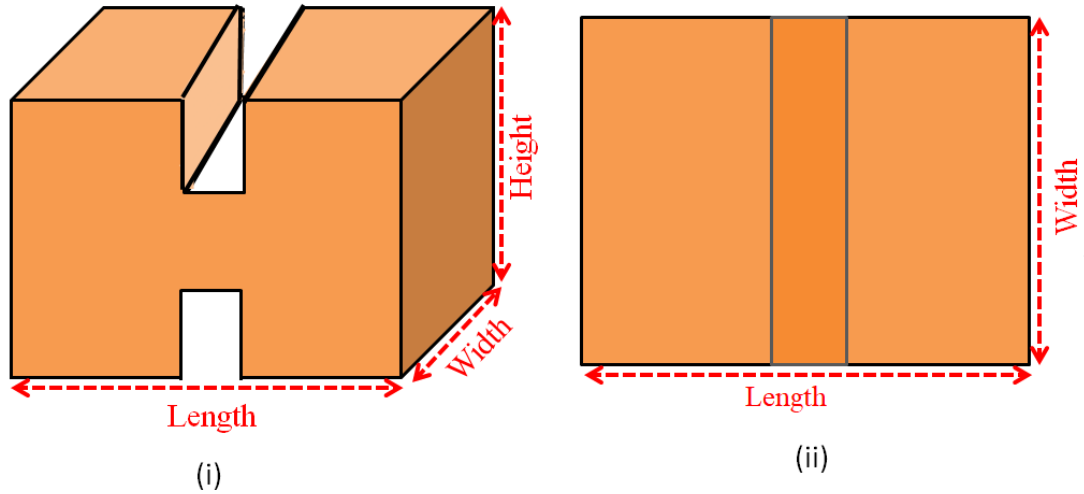


Figure 7.1: Stepped impedance resonator (i) 3D view (ii) Top view

The fundamental frequency and first spurious with Q factor of Stepped Impedance resonator is given below in table 7.2

Table 7-2 Frequencies and Q factor of Stepped impedance resonator

S #	Frequency	Modes	Q Factor
1	1.843 GHz	TE ₁₀₁	1302
2	2.914 GHz	TE ₂₀₁	1485
3	3.0096 GHz	TE ₁₀₂	1527

The ceramic stepped impedance filter is designed with 4 stepped impedance resonators with first and last uniform impedance resonators. The first and last resonators are selected to be uniform impedance resonators to facilitate the input and output coupling through coaxial probes. The stepped impedance resonator helps to push the spurious resonance beyond the cut-off frequency of TE₃₀ mode. The Spurious free window of up to 2.02*fo is achieved with the

significant reduction in the physical length of the filter in comparison with ceramic uniform impedance resonator filter. The simulated unloaded Q-factor of the ceramic stepped impedance resonator is 1342. Both the merits of superior and better spurious performance and miniaturization of the resonators are achieved at an expense of lower unloaded Q-factor. The simulated design of ceramic stepped impedance resonators filter is shown in figure 7.2.

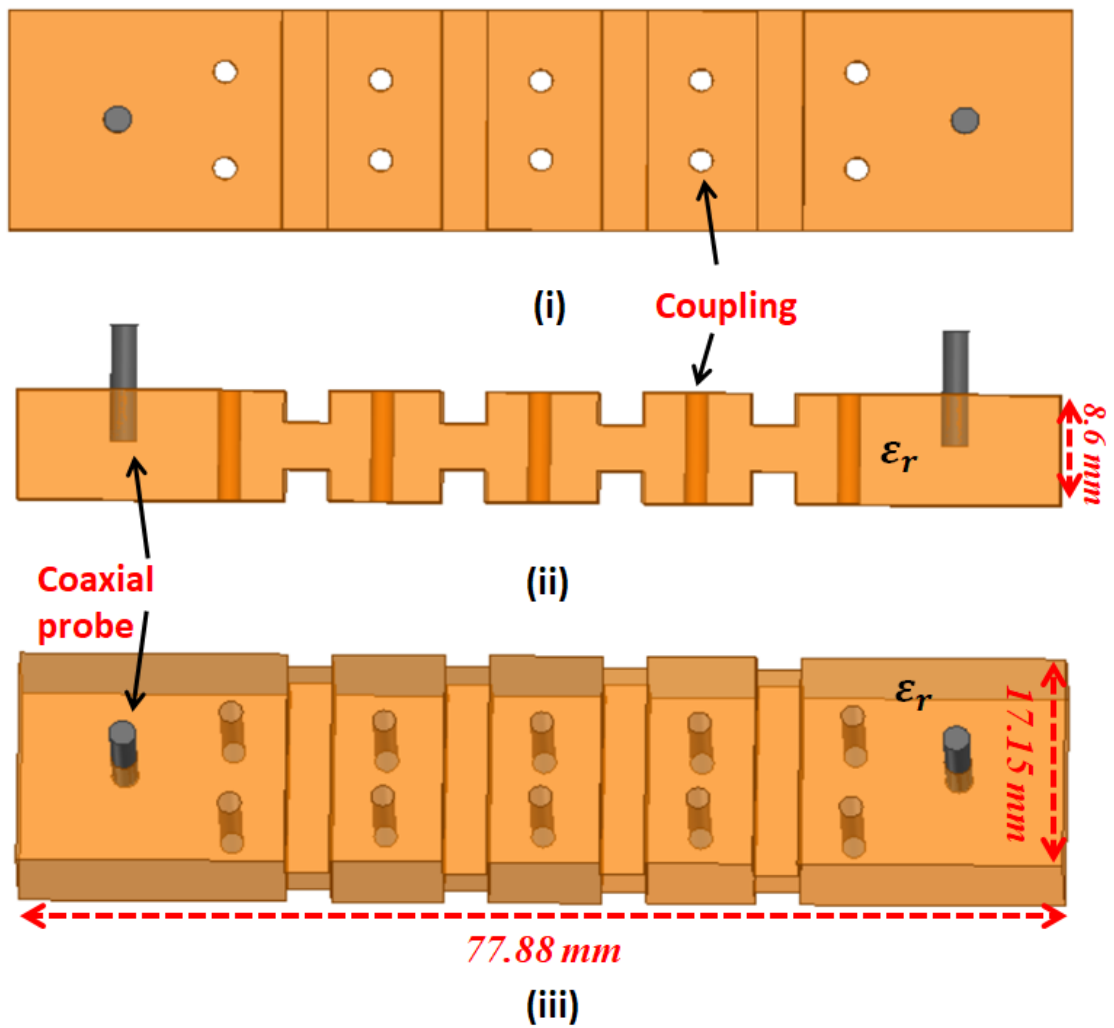


Figure 7.2: Ceramic Stepped impedance resonator filter (i) Top view (ii) Side view (iii) 3D view

In figure 7.3 and 7.4, the pass band and broad band performance of a ceramic stepped impedance resonator filter is shown below. It shows the considerable improvement in the spurious performance in comparison of the uniform impedance ceramic band pass filter.

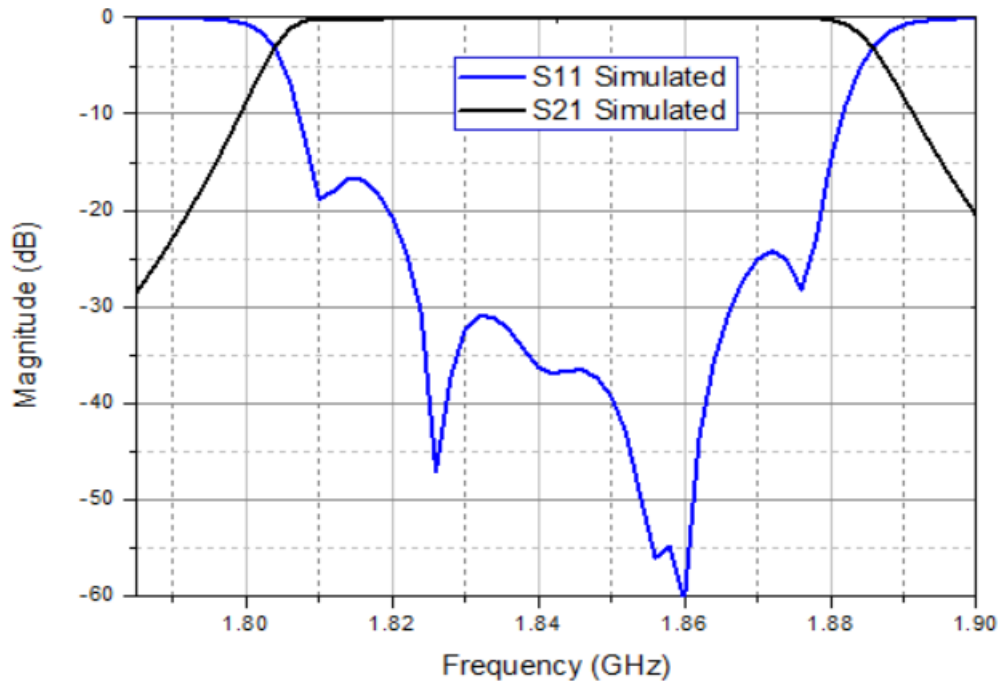


Figure 7.3: Simulated pass band response of a ceramic stepped impedance resonator filter

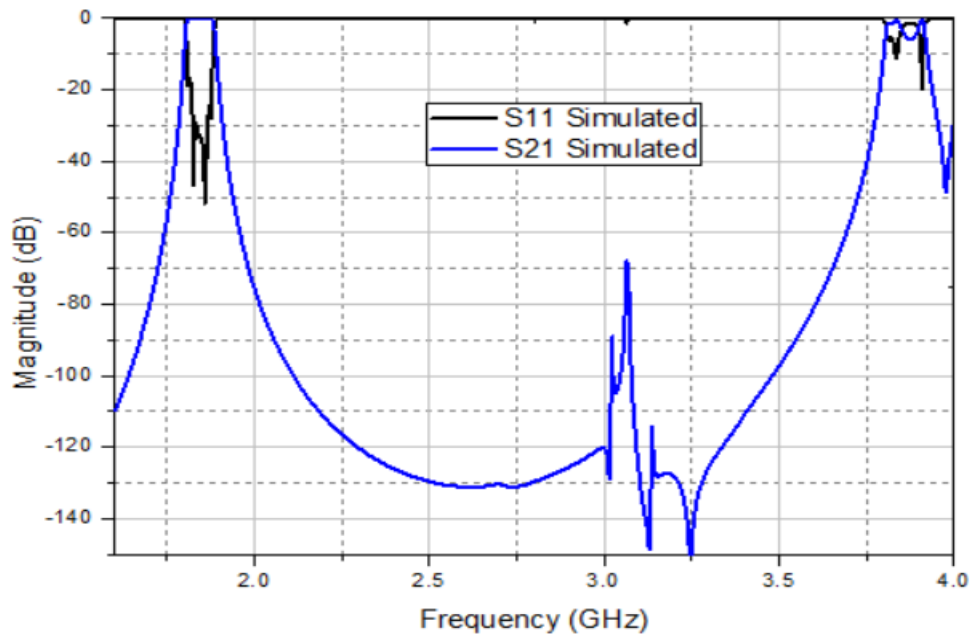


Figure 7.4: Simulated Broadband response of a ceramic stepped impedance resonator filter

7.3 Ceramic Bandpass Filter with Ceramic Loaded Resonators

Ceramic loaded resonator filters offer high Q with miniaturized volume for narrow band applications. Optimal Q/volume ratio can be achieved with the partial ceramic loading, localised at the center of the cavity. Ninety nine percent of electric field stored in the centre ceramic, thus the magnetic field around ceramic is used for the coupling of a filter. The idea of cross-coupled ceramic loaded high-Q resonator filter was implemented in [1, 51]. Here we designed a six order chebyshev ceramic loaded bandpass filter with ridge and non uniform ceramic blocks. The excellent out of band performance is achieved by mixing different kinds of ceramic blocks localised at the center of the cavity. The structural layout and mode chart of ceramic resonator is shown in the figure 7.5 and in table 7.3.

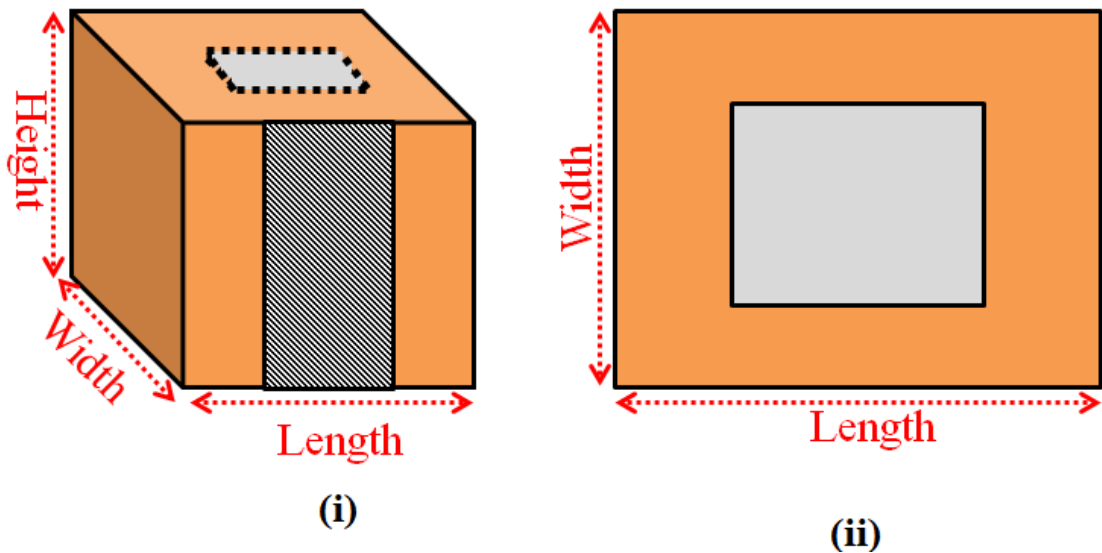


Figure 7.5: ceramic loaded resonator with centralized ceramic block (i) Side view (ii) Top view

Table 7-3 Mode chart for ceramic loaded resonator

Eigen Mode	Frequency (GHz)	Modes	Q factor
Mode 1	1.843	TE ₁₀₁	2971
Mode 2	3.271	TE ₂₀₁	4467
Mode 3	3.272	TE ₁₀₂	4464
Mode 4	3.692	HE ₀₁	3529
Mode 5	3.693	HE ₁₀	3533
Mode 6	4.441	HE ₁₁	6680

The top and bottom surfaces of the resonator are metallized with silver paint and have the conductivity value of $4e7$ s/m. The variation in height can change the Q factor but, the spurious performance remains same for the resonator as shown in table 7.4. The resonator consisted of a rectangular ceramic block

placed inside a metal cavity where the top and the bottom surface of the resonator were touching the cavity. The ratio of widths of the ceramic blocks can be calculated as described by Morelli[15].

Table 7-4 Details of height and Q factor for dielectric loaded resonator

Change in Height (in mm)	Q factor	Spurious (in GHz)
8	2771	3.27
9	2971	3.27
10	3156	3.27
11	3321	3.27
12	3478	3.27

These ceramic blocks same like before, placed at the center of each metallic resonator with the top and bottom metal coated faces. Inductive couplings are introduced between resonators through irises, and input/output coupling is achieved through the coaxial cable by perturbing the magnetic field around the ceramic blocks of external resonators as [51]. A six degree dielectric loaded chebyshev filter is first designed with ceramic blocks with TEM post and with non-uniform width. The structural layout of resonators and filter are shown in figure 7.6 and figure 7.7. But, after some mechanical limitation of ceramic TEM post, the same resonator is optimized with a one side ridge in ceramic block. The structural layout of ceramic loaded resonators with ceramic ridge and non-uniform width blocks is shown in figure 7.8. The ridge ceramic resonator is optimized in such a way to get a quite similar spurious performance and slightly good Q factor like TEM shown in table 7.5. Then, same sixth-degree dielectric

loaded Chebyshev filter is designed with ceramic non-uniform widths and ridged blocks, as shown in fig. 7.9, where the dimensions, Q factor and spurious details of the ridged and non uniform width ceramic blocks are shown in table 7.6.

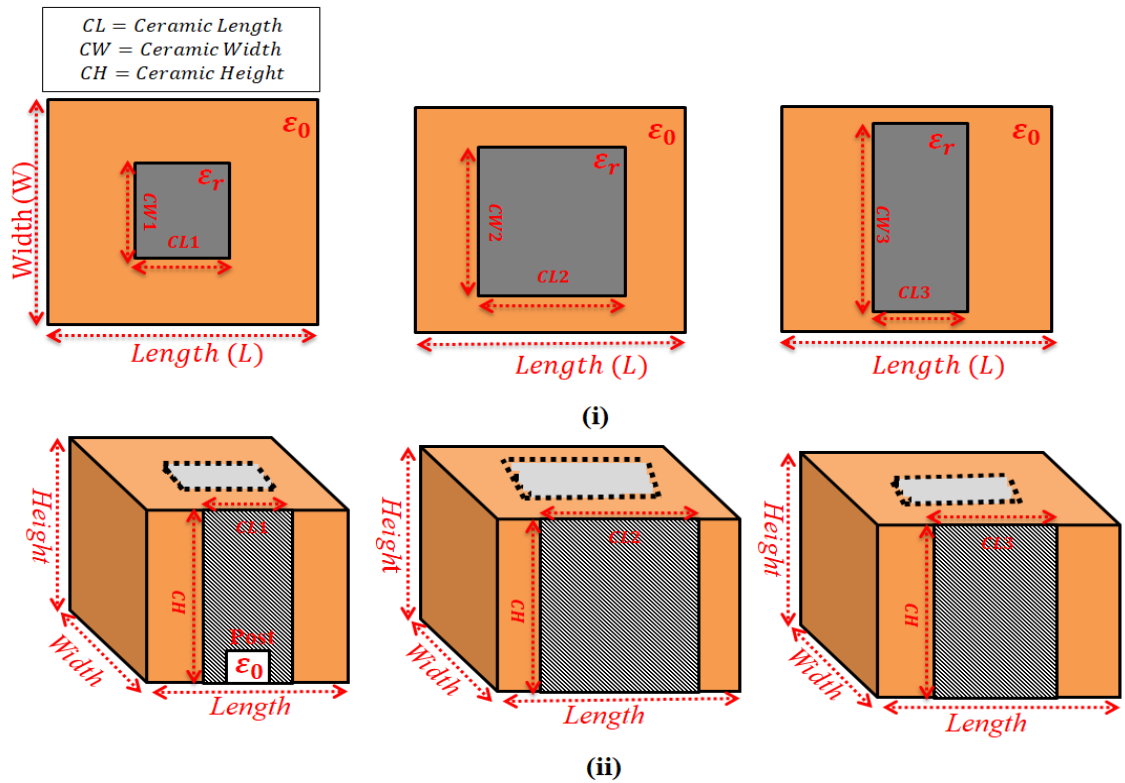


Figure 7.6: structural layout of ceramic loaded resonators with ceramic TEM and non-uniform width blocks (i) Top view (ii) 3D view

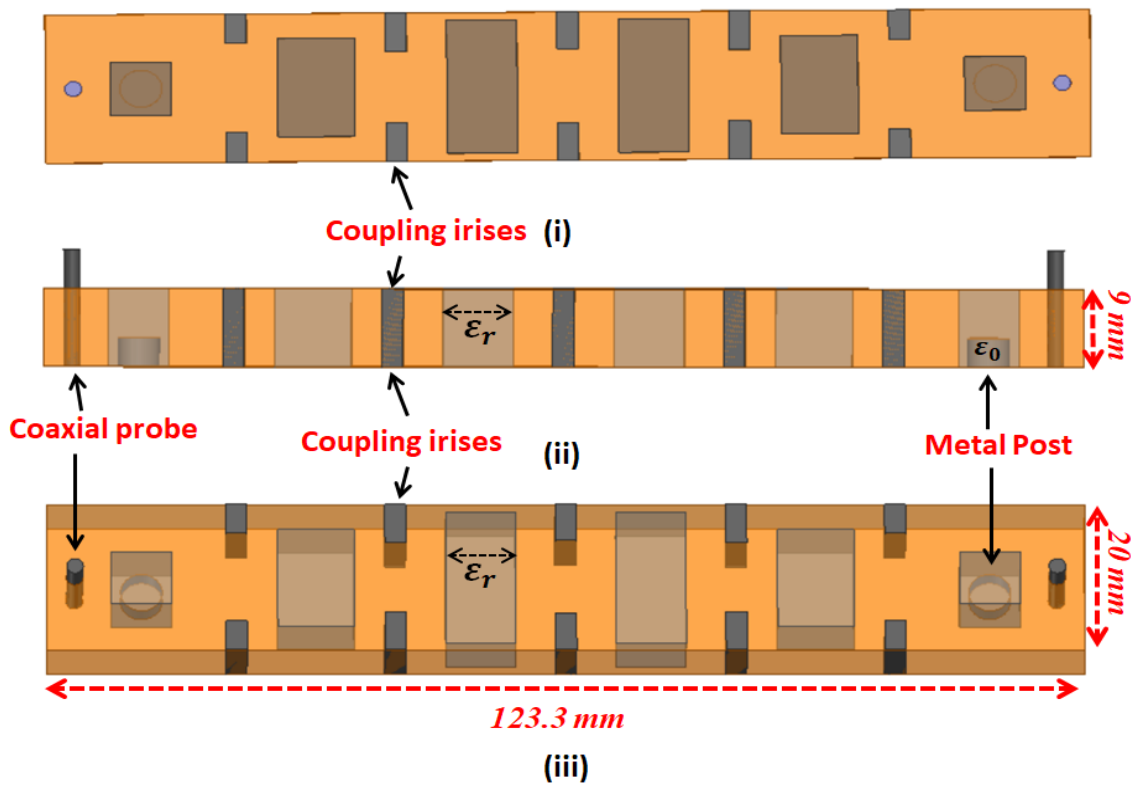


Figure 7.7: Structural layout of ceramic loaded filter with ceramic TEM and non-uniform width blocks (i) Top view (ii) Side View (iii) 3D view

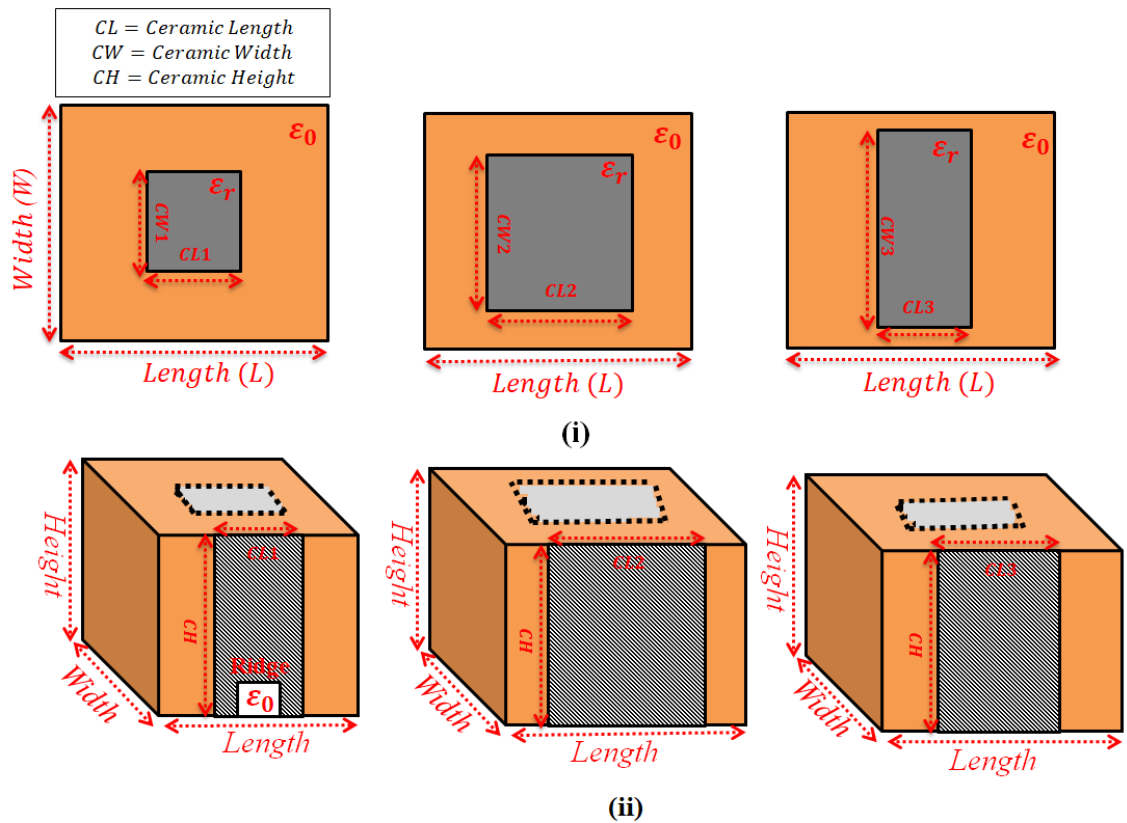


Figure 7.8: Structural layout of a ceramic loaded resonators with ceramic ridge and non-uniform width blocks (i) Top view (ii) 3D view

Table 7-5 Comparison of Ceramic TEM resonator and Ceramic Ridge resonator

Resonator Type	TEM Ceramic Block	Ceramic Block with Single Ridge
Dimensions in mm	7.2 x 7.2 x 9	6.8 x 6.8 x 9
Q Factor	1989	2264
First Spurious in GHz	4.284	4.280
Second Spurious in GHz	4.284	4.646

The low Q factor of these ridged ceramic resonators can be compensated by putting them as the first and last resonators, as their low Q factor would not contribute as significantly as others in the filter insertion loss [69]. The simulated broadband response of a filter with TEM post and non-uniform width ceramic block is shown in figure 7.10, and after the introduction of ridge ceramic block the simulated passband and broad band response of a filter is shown in figure 7.11 and 7.12. Both the filters with ceramic TEM post and ceramic ridge block showing an excellent improvement in spurious performance of a dielectric loaded filter. The stop band attenuation of more than 80 dB is achieved upto 4.5 GHz. This exhibits the spurious free window of $2.44 * f_o$. The comparison of ceramic loaded filter, ceramic stepped impedance filter with test filter shown in figure 7.13.

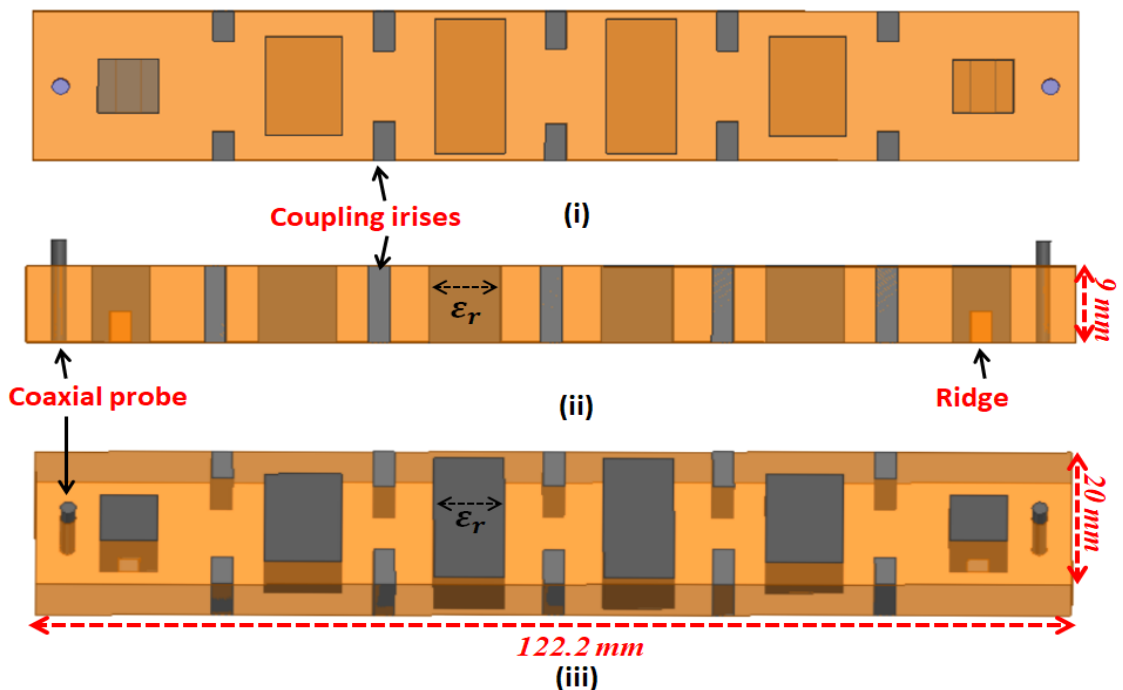


Figure 7.9: Structural layout of a ceramic loaded filter with ceramic ridge and non-uniform width blocks (i) Top view (ii) Side view (iii) 3D view

Table 7-6 details of ceramic loaded resonators with ridge and non-uniform width ceramic blocks

Ceramic Resonator Type	Ridge Block	Non-uniform width Block -I	Non-uniform width Block -II
Dimensions in mm	6.8 x 6.8 x 9	13.25 x 9.1 x 9	8.3 x 18 x 9
Q Factor	2264	2916	2637
Fundamental frequency in GHz	1.842	1.842	1.842
First Spurious frequency in GHz	4.280	3.023	2.844
Second Spurious frequency in GHz	4.646	3.507	3.363

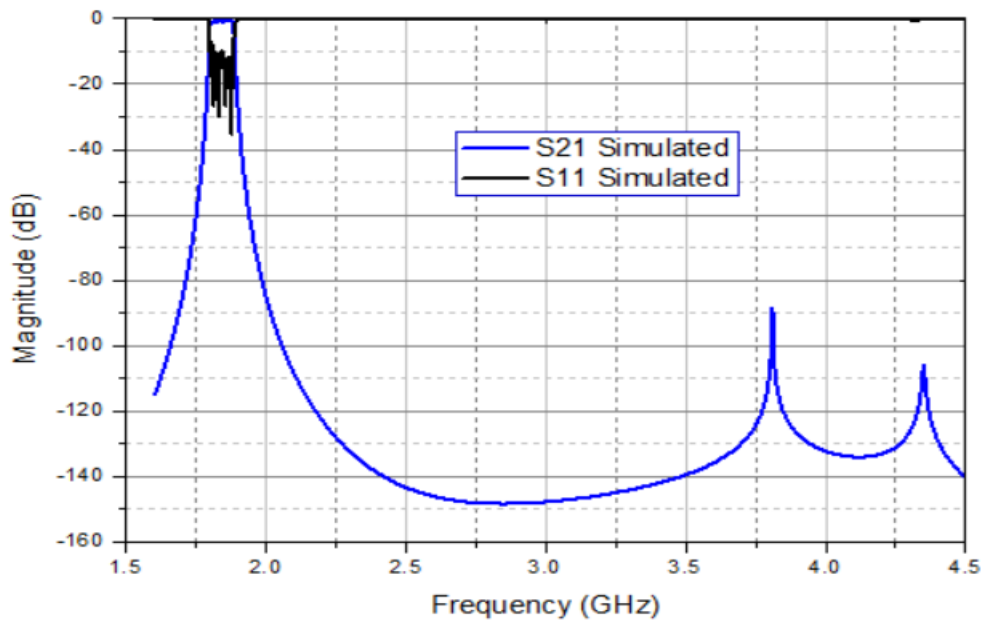


Figure 7.10: Resonators with non-uniform width and TEM Ceramic Blocks (i) Top view (ii) Side View

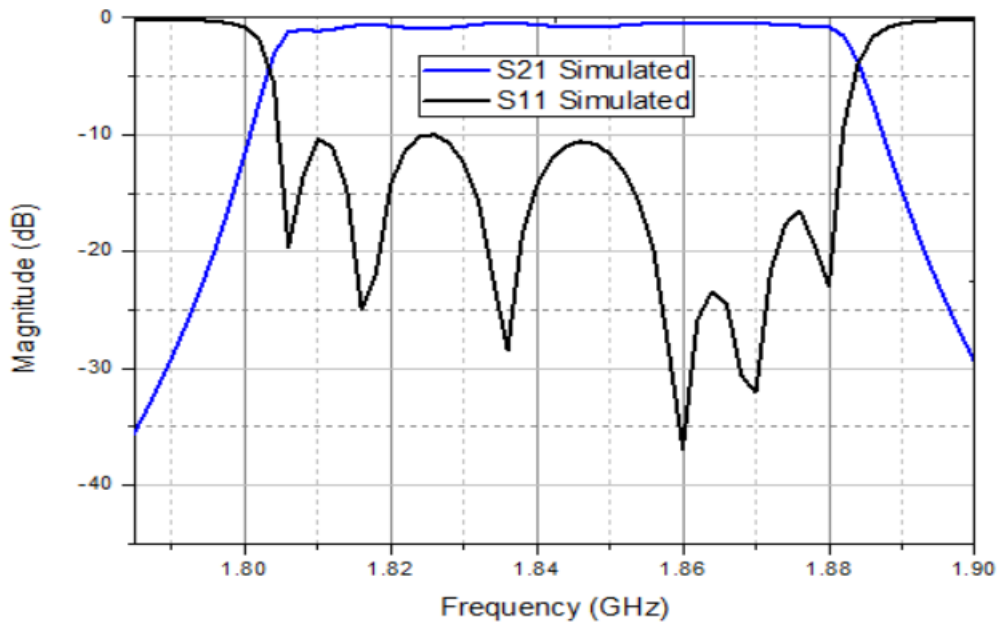


Figure 7.11: Simulated Passband response for a ceramic loaded filter with ridge and non-uniform width ceramic blocks

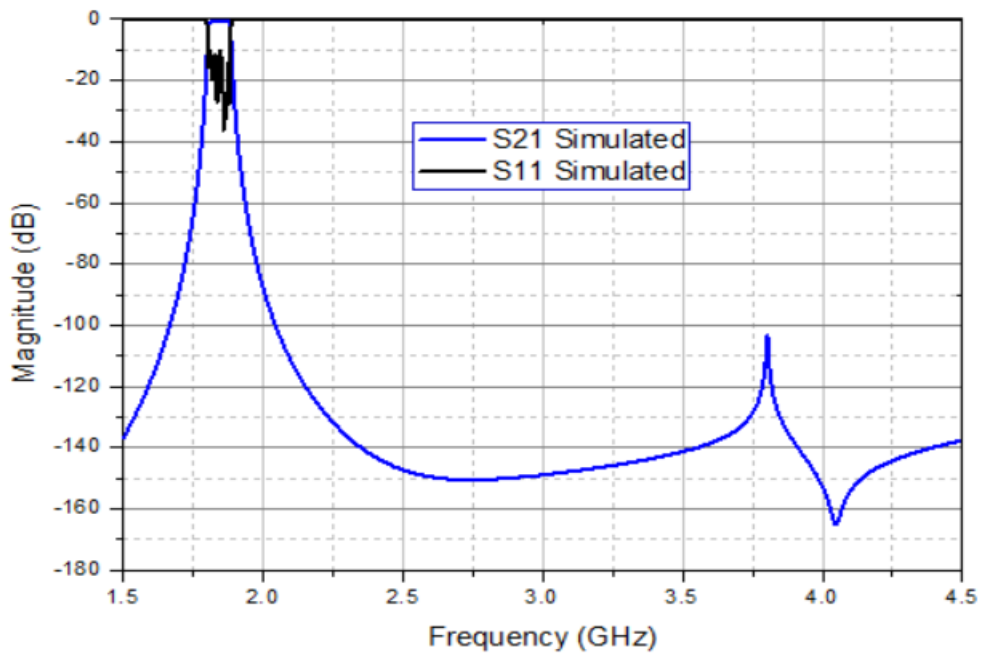


Figure 7.12: Simulated broadband response of a ceramic loaded filter with ridge and non-uniform width ceramic blocks

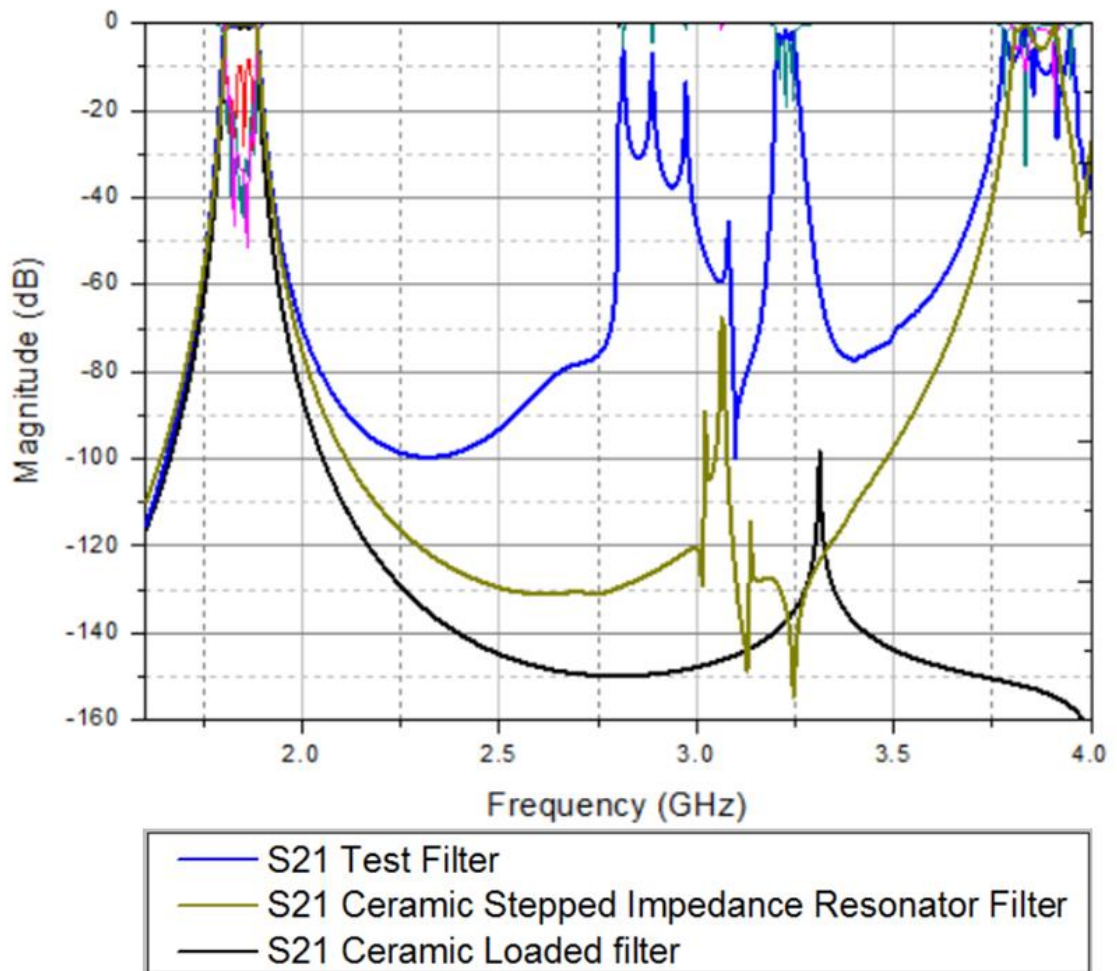


Figure 7.13: Comparison broad band response of Test filter with ceramic stepped impedance filter and ceramic loaded filter

7.3.1 Fabrication Details

The ceramic loaded filter is fabricated with ceramic blocks with ridge and different widths placed at the center of the cavity. Two different approaches have been tried to get proper metal to metal contact between cavity and top and bottom surfaces of ceramic blocks. In first approach, thin copper sheet were used as top and bottom lid. The ceramic blocks which are metallized from top and bottom, soldered from one end to these copper sheet using grooves on copper sheet shown in figure 7.14. The 'Robax' laser solder machine at radio

design is used to solder the ceramic block with copper sheet as shown in figure 7.15. This machine is set to provide the heating in temperature range from 250⁰ Celsius to 300⁰ Celsius. The 'Warton' lead free solder paste is used to solder the ceramic base with the thin copper sheet which has a melting point around 230⁰ Celsius to 240⁰ Celsius. The same thin copper sheet of 0.7 mm is used as a top lid and side walls are fabricated by aluminium with inductive iris as shown in figure 7.16 and 7.17. Tuning screws are used in a copper sheet with soldered inserts to hold the tuning screws for tuning. The purpose to use thin copper sheet is to apply pressure from top lid to remove the air gaps between metalized ceramic surface and top lid. Different clamp sizes are used for this purpose, but with small flat surface area and availability of tuning screws make it very difficult to clamp the filter at desired places shown in figure 7.18. This uneven clamping results in some air gap between the metalized ceramic top surface and top lid of filter, which makes the pass band of a filter shift down and introduces higher insertion loss. Some low quality silver paint which we used to metalized the ridge area also contributed in high insertion loss. But the out of band performance of a filter is still good and close to the simulated response. The in-band and out of band performance of a simulated and fabricated filter are shown in figure 7.19 and 7.20. Tuning screws were used to alleviate the effect of manufacturing tolerances and material discrepancies. It seems difficult to remove the air gap between the dielectric slab and external cavity through clamps, Therefore, another prototype is design with different approach by using copper plated aluminium cavity, where we soldered the ceramic from top and bottom with the cavity, as explained in [51]. Copper plating is used for the proper soldering of ceramics with the outer cavity. Same grooves are used to fix

the ceramics with base after applying the solder paste. Then top surface of the ceramics also filled with the solder paste, before applying top lid. This soldering provides a good mechanical contact between lids and ceramic blocks as shown in figure 7.21 and 7.22. The passband insertion loss is improved from -3.9dB (of previous design) to -1.99 dB shown in figure 7.23. Still with the chance of some air gaps and low quality metalized paint in ridge area contributed in high insertion loss. But with the improved insertion loss in comparison with the previous result the out of band performance is also improved and offer -52 dB attenuation upto 4.5 GHz shown in figure 7.24.

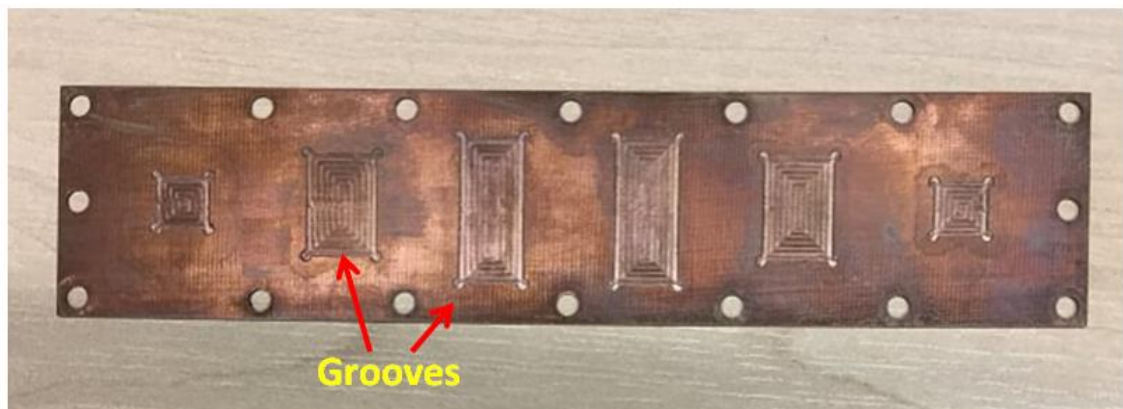


Figure 7.14: grooves on thin metal copper sheet

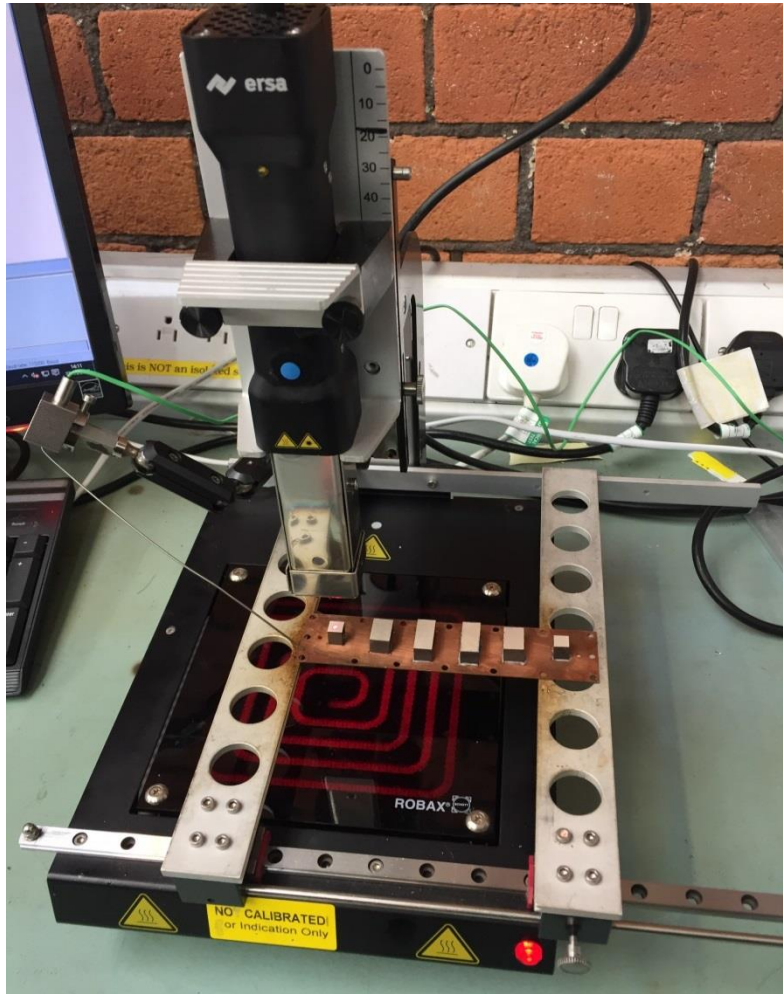


Figure 7.15: Soldering of Ceramic blocks with copper sheet from bottom

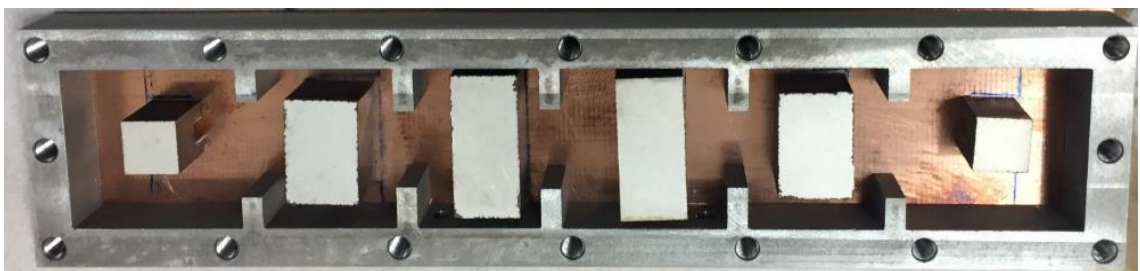


Figure 7.16: The aluminium side walls with the inductive irises without soldering.

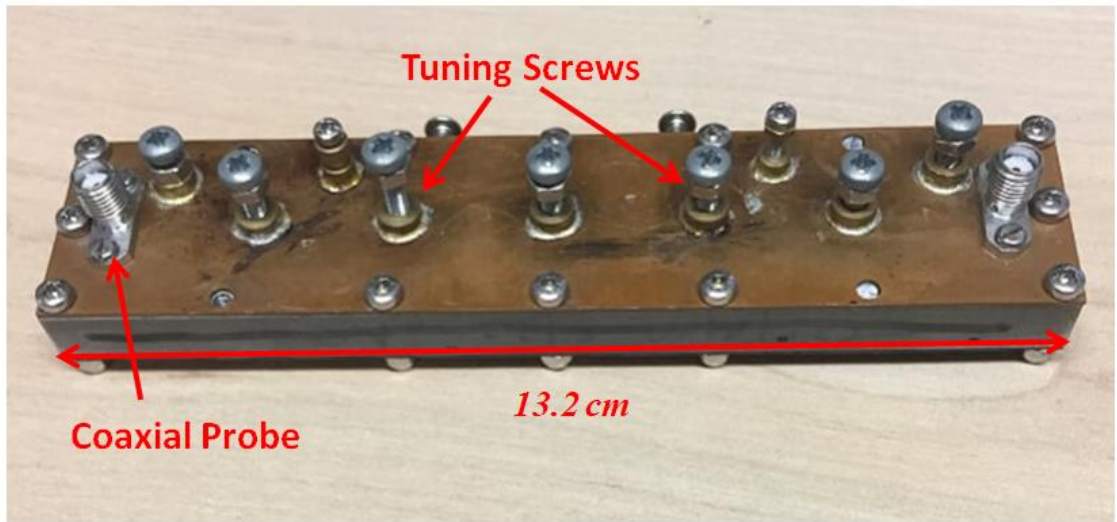


Figure 7.17: Fabricated filter with tuning screws

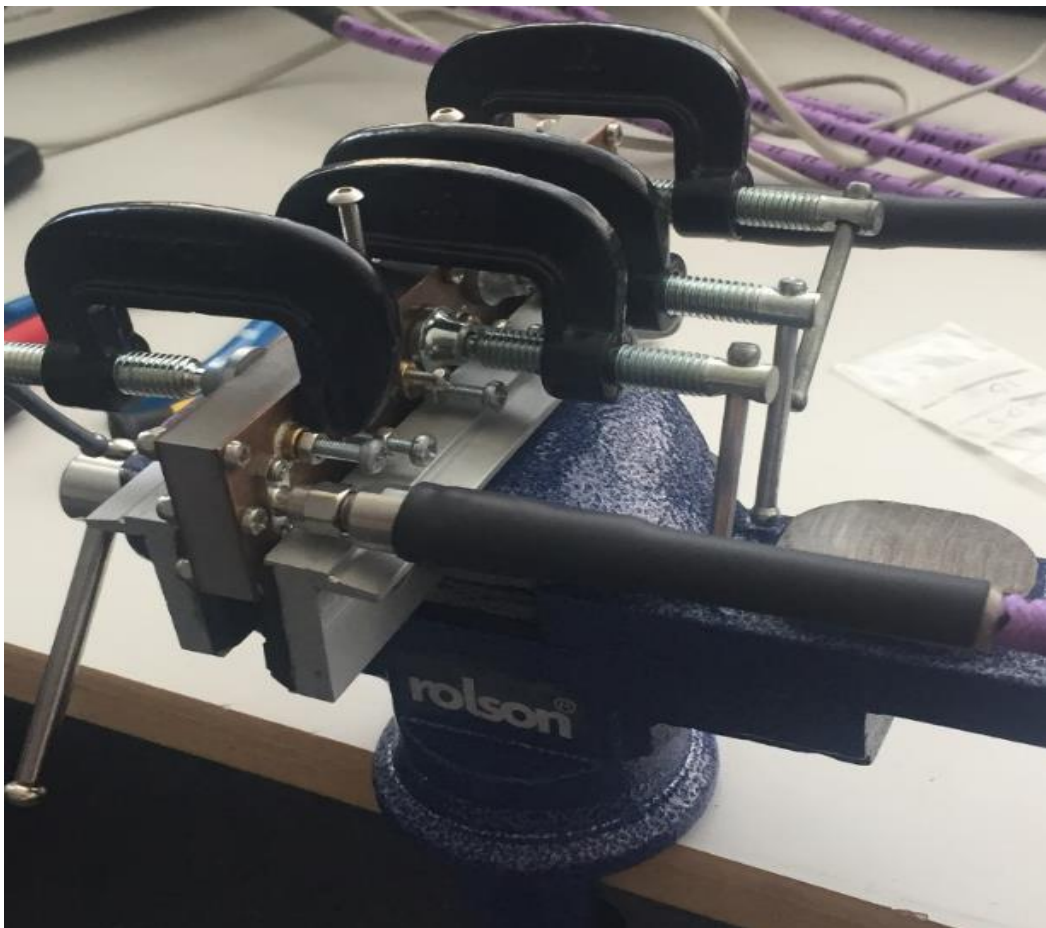


Figure 7.18: Clamping of a filter

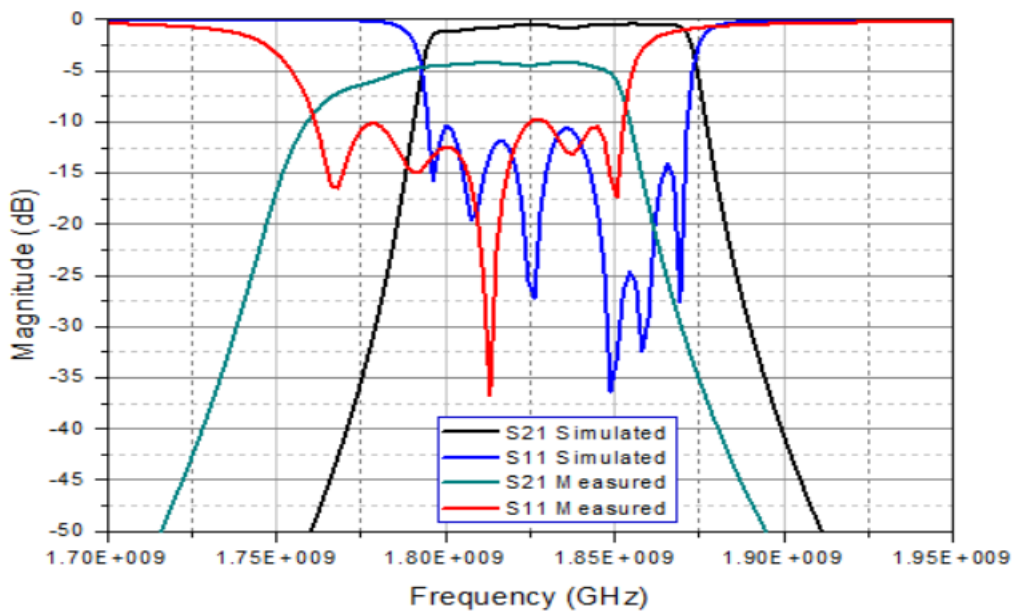


Figure 7.19: Pass band response of simulated and fabricated filter

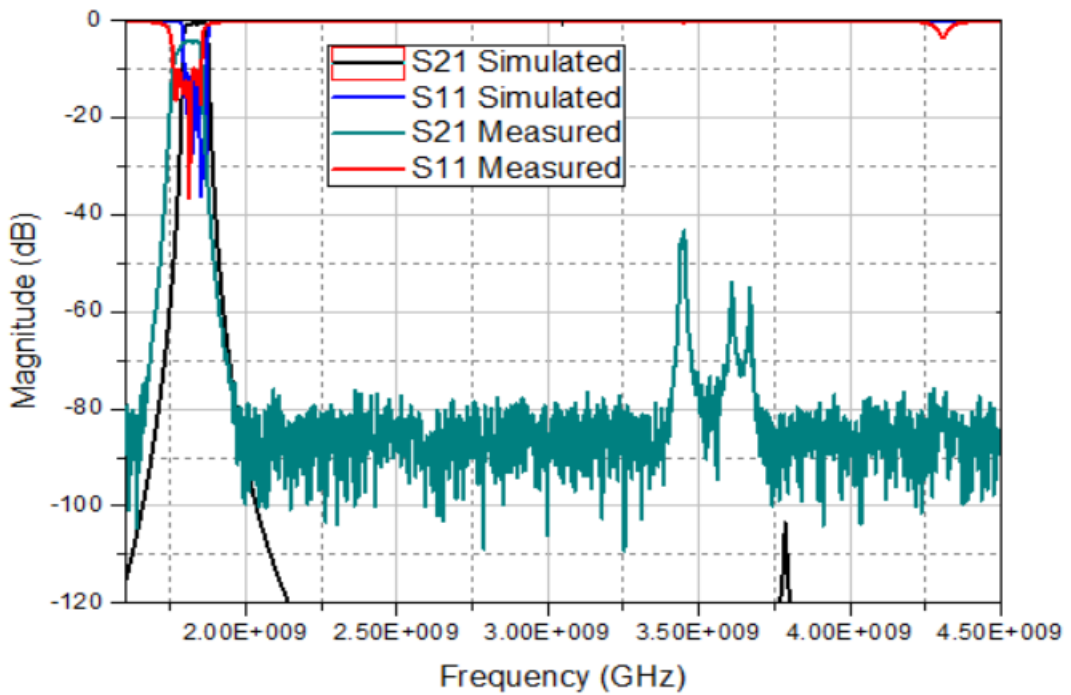


Figure 7.20: Broad band response of simulated and fabricated filter

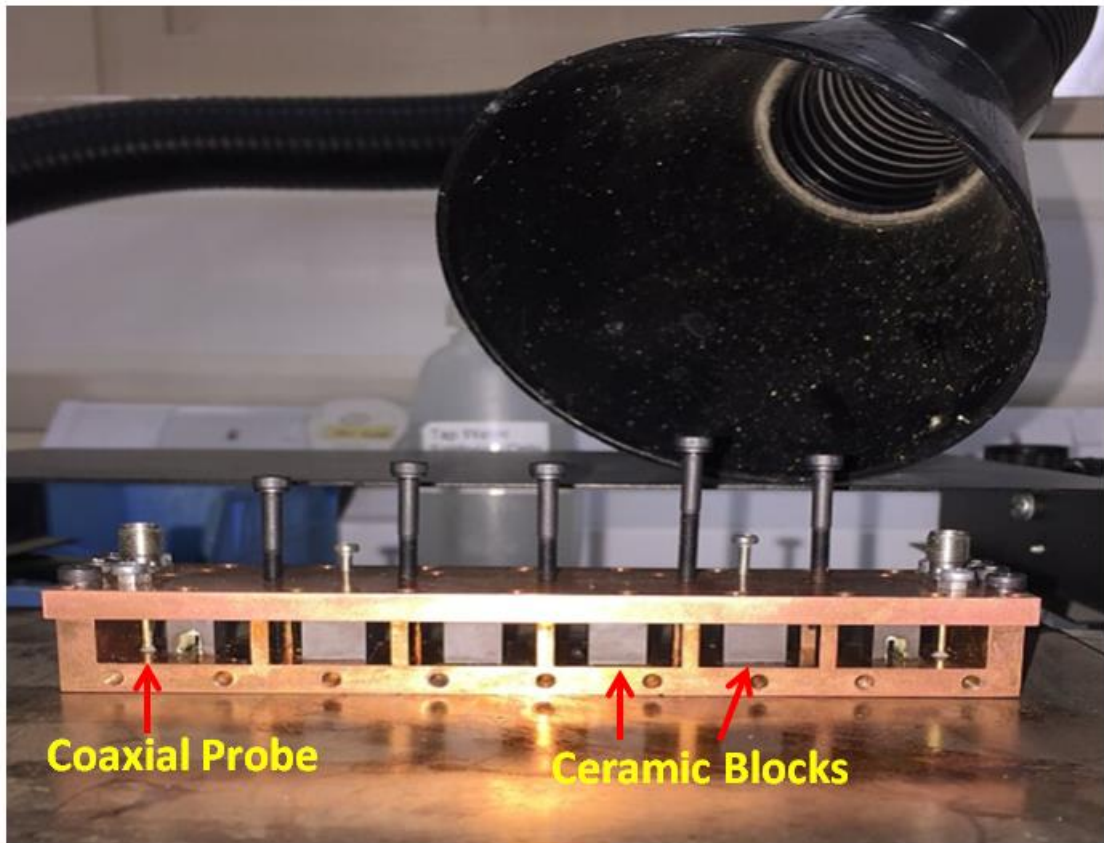


Figure 7.21: Ceramic top and bottom soldered with the cavity

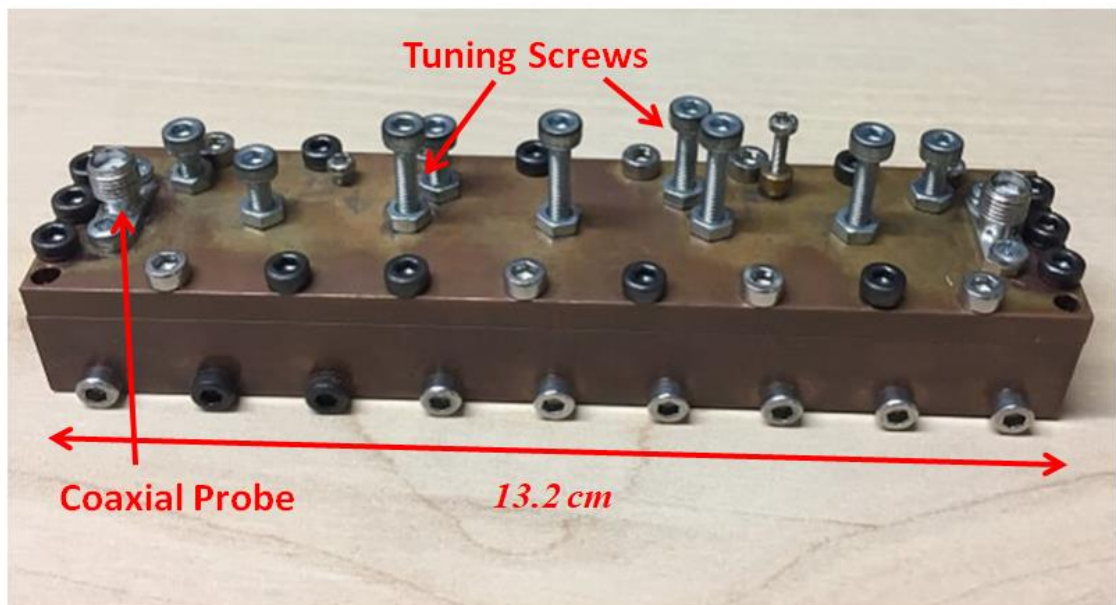


Figure 7.22: fabricated filter with copper plated aluminium cavity

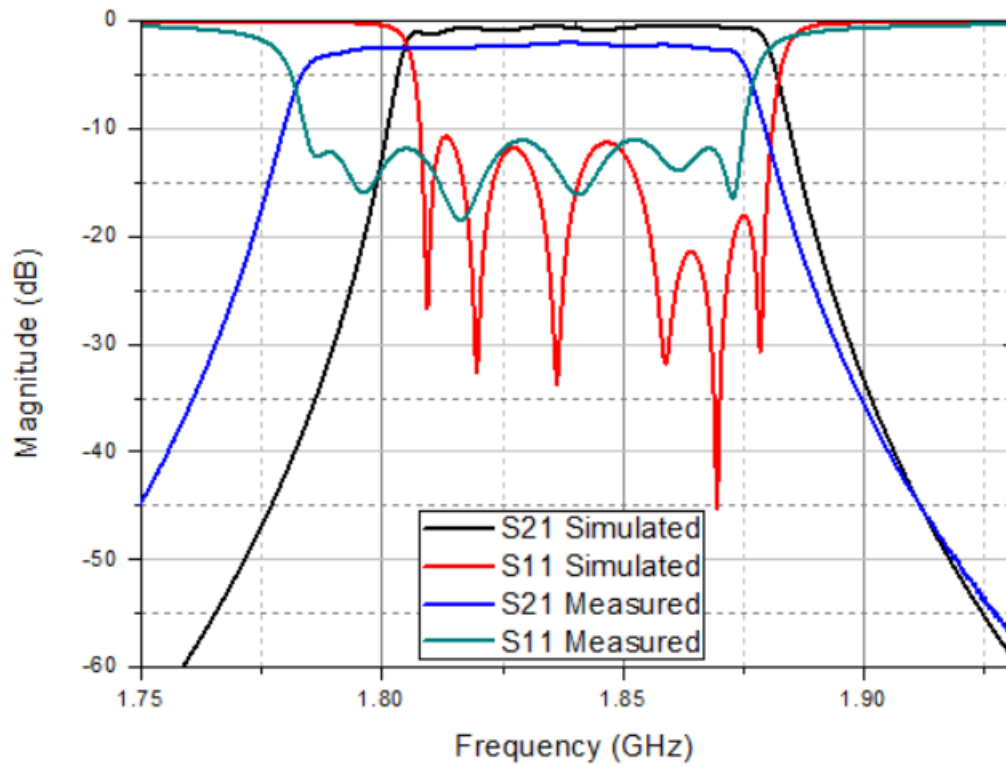


Figure 7.23: Passband response of simulated and fabricated filter

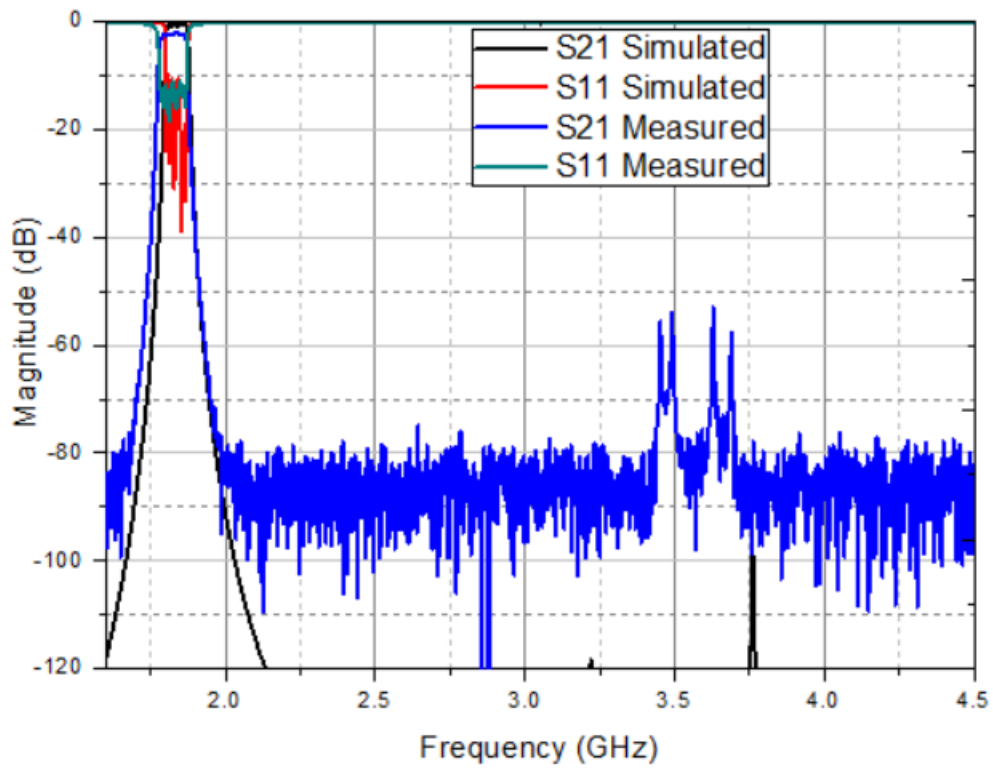


Figure 7.24: Broadband response of simulated and fabricated filter

7.4 Summary

Two different design are presented in this chapter to improve the spurious performance of ceramic filters. The monolithic six order chebyshev filter is designed with stepped impedance resonators which improves the spurious performance of a filter upto $2.02 * f_o$. The next filter design used the ceramic loaded resonator localised at the center of a cavity touching top and bottom. The resonators are designed with ridge and non-uniform ceramic blocks, to improve the spurious performance of chebyshev ceramic loaded filter. The filter is fabricated and measured to show the excellent out of band attenuation of upto $2.45 * f_o$. The filter is first fabricated with thin copper sheet to remove the air gaps between ceramic and top lid, and then again fabricated with all aluminium cavity soldered with ceramic blocks. The tuning screws are used to alleviate the effect of manufacturing tolerances and material discrepancies.

8

CONCLUSIONS AND FUTURE WORK

8.1 Introduction

The intention and motive behind this research is to improve the spurious performance of ceramic waveguide filters used in the RF front end of mobile base stations without degrading their electrical performance. Microwave filters represent the major portion in RF front end transceiver, used to select the desired portion of a spectrum and attenuating spurious signals presents in proximity of desired frequency ranges. The microwave filters, whose stop band performance are not good enough use low pass filters in cascade to get the required level of rejection.

In this thesis, miniaturized integrated ceramic resonators and ceramic loaded resonators are used to design chebyshev waveguide bandpass microwave filters with improved spurious performance. When the waveguide resonator is loaded with ceramic material having a permittivity ϵ_r , its physical volume is reduced by a factor of $\frac{1}{\epsilon_r}$. The Q factor of a resonator is also degraded with the same factor of $\frac{1}{\epsilon_r}$, but still an acceptable Q factor is maintained with the reduced volume in comparison with the coaxial resonator. The test filter with the permittivity of 43 is designed, whose fundamental frequency, Q factor and spurious resonances are calculated using classical waveguide equations and are verified through the High frequency structural simulator (HFSS). The outer

walls of the resonator are metallized by a silver paint having a conductivity of $4.4e7$, making it to act as a ceramic loaded resonator. The spurious performance of this test filter can be improved by applying different techniques like ceramic resonator with post, non-uniform width ceramic resonator and stepped impedance ceramic resonator.

A chebyshev ceramic waveguide filter is designed with two posts and all posts in this thesis. The insertion loss method of microwave filter design is used to realize these ceramic waveguide filters. All inductive coupling are achieved by placing the through metal plated through holes, which behaves as impedance inverters over a broad bandwidth of the filter. Their coupling is controlled by the holes diameter and their offset from the side walls of the filters.

The chebyshev ceramic non-uniform width resonator filters are designed with two and three non-uniform width ceramic resonators. The resonators with non-uniform width will spread the higher order resonances over a wider frequencies range; hence their level will be kept to a lower level as compared to standard filters. The filters are realized with inductive posts for inter-resonator coupling.

Other chebyshev ceramic waveguide filters are realized with the combination of posts and non-uniform width resonators. The advantage of good spurious free region for resonator with posts and good Q factor with spreading of higher order resonances for non-uniform width resonators is combined in these filters. The filter is also fabricated with posts and non-uniform width resonators in air filled structure. Tuning screws are also used to compensate any mechanical and tolerances.

Ceramic stepped impedance resonator is designed with stepped impedance and uniform impedance resonators. A different impedance ratio is used¹⁵⁹

improve the spurious performance of a ceramic waveguide filter. It provides the stop band attenuation of 60 dB upto 3.79 GHz which is $2.06 * f_o$. All monolithic ceramic bandpass filters improve the spurious performance upto different extent. But, there is an also a compromise between the Q factor and spurious performance of a filter. As some times for achieving a better spurious performance you have to allow a low Q factor of a filter.

The dielectric loaded resonator filter is designed with ridge and non-uniform width ceramic blocks. The ridge and non-uniform width ceramic block resonator improves the spurious performance of a filter upto $2.44 * f_o$. These blocks are placed at the center of a resonator and touch top and bottom of a cavity. The top and bottom surfaces are metallized with a silver paint having conductivity $4.4e7$. The inter-resonator coupling is realized through inductive irises and input/output coupling though coaxial probe. All other filters also used the coaxial probe at the center of a broad wall of the external resonators. The filter is fabricated with tuning screws to compensate the mechanical tolerances.

8.2 Future work

The goal of this research project has been successfully achieved as documented in previous chapters and briefly summarised above. The work presented in this thesis is limited to single mode ceramic waveguide filter. It can be extended in different aspects. The use of dual mode or triple mode resonators with metal posts can further reduce the volume of a filter.

The generalised chebyshev approach of all these filter design presented in this thesis would also be the further extension of this work.

The Stepped impedance ceramic waveguide resonator with two steps gives the further degree of freedom to control the spurious resonances.

The design of single ridge ceramic waveguide filter would also be the next design to improve the stop band performance of ceramic waveguide filters. The use of ridge instead of posts would give you the benefit of easy machining.

It could also be a one possible extension if we mixed the low Q SIR resonators with non-uniform width resonator which results in a good compromise between stop band performances and pass band insertion loss.

A generalised Chebyshev ceramic loaded resonator filter with better metal contact and conductivity could also be a good extension of this work. A 3rd order generalised chebyshev ceramic loaded filter with its broad band response is given in figure 8.1 and 8.2

Finally it seems reasonable to believe that the stop band performance of integrated ceramic circular waveguide filters could also benefit from the same proposed ideas.

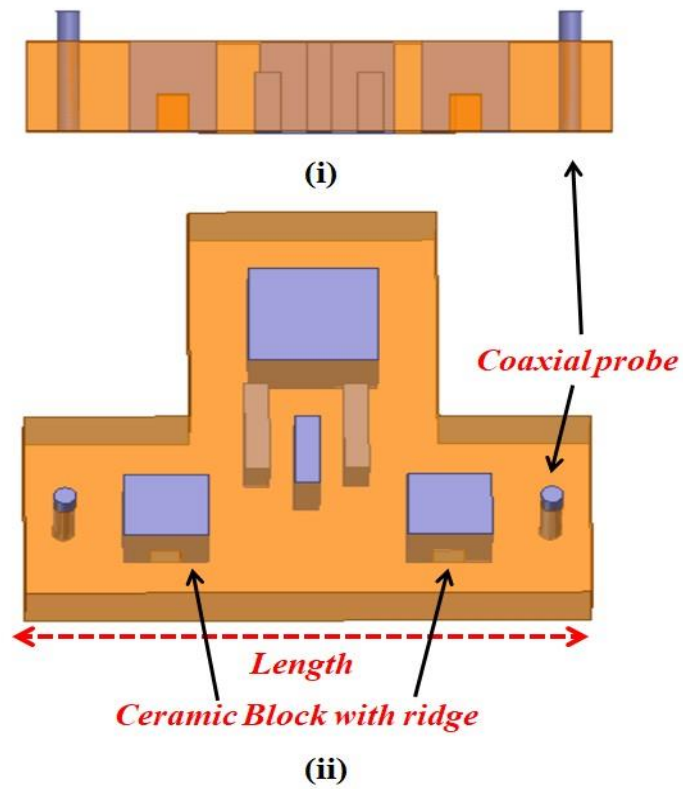


Figure 8.1: 3rd order generalised chebyshev ceramic loaded filter with ridge and non- ridge ceramic block (i) Side view (ii) Top view

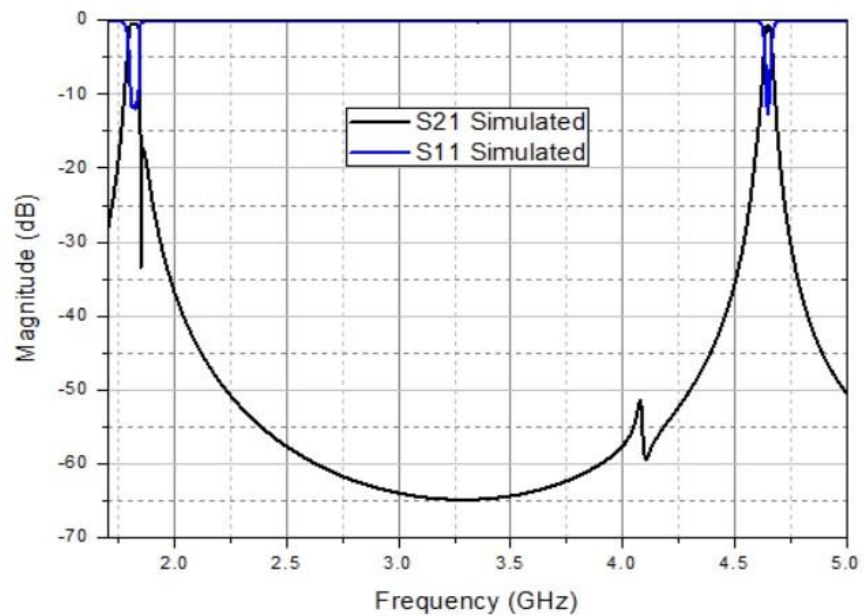


Figure 8.2: Broadband response of 3rd order generalised chebyshev ceramic loaded filter with ridge and non-ridge ceramic blocks

References

- [1] I. Hunter and I. o. E. Engineers, *Theory and Design of Microwave Filters*: Institution of Engineering and Technology, 2001.
- [2] G. L. Matthaei, L. Young, and E. M. T. Jones, *Microwave filters, impedance-matching networks, and coupling structures*: McGraw-Hill, 1964.
- [3] K. S. Packard, "The Origin of Waveguides: A Case of Multiple Rediscovery," *Microwave Theory and Techniques, IEEE Transactions on*, vol. 32, pp. 961-969, 1984.
- [4] R. Levy and S. B. Cohn, "A History of Microwave Filter Research, Design, and Development," *Microwave Theory and Techniques, IEEE Transactions on*, vol. 32, pp. 1055-1067, 1984.
- [5] R. M. F. A.W. Lawson, *"The Design of Microwave Filters"*. Available: G.L Ragan *Microwave Transmission Circuit*. New York: Dover Publication, INC., 1948.
- [6] S. B. Cohn, "Direct-Coupled-Resonator Filters," *Proceedings of the IRE*, vol. 45, pp. 187-196, 1957.
- [7] R. Levy, "Theory of Direct-Coupled-Cavity Filters," *Microwave Theory and Techniques, IEEE Transactions on*, vol. 15, pp. 340-348, 1967.
- [8] S. B. Cohn, "Parallel-Coupled Transmission-Line-Resonator Filters," *Microwave Theory and Techniques, IRE Transactions on*, vol. 6, pp. 223-231, 1958.
- [9] G. L. Matthaei, "Interdigital Band-Pass Filters," *Microwave Theory and Techniques, IRE Transactions on*, vol. 10, pp. 479-491, 1962.
- [10] G. Matthaei, "Comblin Bandpass Filter for Narrow and Moderate Bandwidth," *Microwave Journal*, vol. 6, pp. 82-91, August 1963.
- [11] B. F. Nicholson, "Equivalence between evanescent-mode and comblin filters," *Electronics Letters*, vol. 3, pp. 495-496, 1967.
- [12] D. G. Swanson and W. J. R. Hoefer, *Microwave Circuit Modeling Using Electromagnetic Field Simulation*: Artech House, Incorporated, 2003.
- [13] H. J. riblet, "waveguide filter having non identical section resonating at same fundamental frequency and different harmonic frequencies," US Patent 3153208, 1964.
- [14] R. Balasubramanian and P. Pramanick, "Computer aided design of H-plane tapered corrugated waveguide bandpass filters," *International Journal of RF and Microwave Computer-Aided Engineering*, vol. 9, pp. 14-21, 1999.
- [15] M. Morelli, I. Hunter, R. Parry, and V. Postoyalko, "Stop-band improvement of rectangular waveguide filters using different width resonators: selection of resonator widths," in *2001 IEEE MTT-S International Microwave Symposium Digest (Cat. No.01CH37157)*, 2001, pp. 1623-1626 vol.3.
- [16] M. Morelli, I. Hunter, R. Parry, and V. Postoyalko, "Stopband performance improvement of rectangular waveguide filters using stepped-impedance resonators," *IEEE Transactions on Microwave Theory and Techniques*, vol. 50, pp. 1657-1664, 2002.
- [17] R. Rezaiesarlak, P. Lohmannia, and M. Salehi, "Miniaturized waveguide filter with improved stop-band response," *Microwave and Optical Technology Letters*, vol. 56, pp. 512-515, 2014.
- [18] D. Budimir, "Optimized E-plane bandpass filters with improved stopband performance," *IEEE Transactions on Microwave Theory and Techniques*, vol. 45, pp. 212-220, 1997.
- [19] R. J. Cameron, "General coupling matrix synthesis methods for Chebyshev filtering functions," *IEEE Transactions on Microwave Theory and Techniques*, vol. 47, pp. 433-442, 1999.

- [20] A. Atia, A. Williams, and R. Newcomb, "Narrow-band multiple-coupled cavity synthesis," *IEEE Transactions on Circuits and Systems*, vol. 21, pp. 649-655, 1974.
- [21] J. D. Rhodes, *Theory of Electrical Filters*: Wiley, 1976.
- [22] D. M. Pozar, *Microwave Engineering*: Wiley, 2004.
- [23] R. J. Cameron, "Advanced coupling matrix synthesis techniques for microwave filters," *IEEE Transactions on Microwave Theory and Techniques*, vol. 51, pp. 1-10, 2003.
- [24] J. B. Thomas, "Cross-coupling in coaxial cavity filters - a tutorial overview," *IEEE Transactions on Microwave Theory and Techniques*, vol. 51, pp. 1368-1376, 2003.
- [25] S. Cogollos, P. Soto, M. Brumos, V. E. Boria, and M. Guglielmi, "Novel rectangular waveguide structures for advanced filter characteristics," in *2014 IEEE MTT-S International Microwave Symposium (IMS2014)*, 2014, pp. 1-4.
- [26] D. Sushrut, *Microwave Engineering*: Oxford University Press, 2014.
- [27] D. Swanson and G. Macchiarella, "Microwave filter design by synthesis and optimization," *IEEE Microwave Magazine*, vol. 8, pp. 55-69, 2007.
- [28] W. Chi, K. A. Zaki, A. E. Atia, and T. G. Dolan, "Dielectric combline resonators and filters," *IEEE Transactions on Microwave Theory and Techniques*, vol. 46, pp. 2501-2506, 1998.
- [29] G. L. Mitthaei, "Comblin bandpass filter for narrow and moderate bandwidth," *Microwave journal*, vol. 6, pp. 82-91, August 1963.
- [30] S. B. M. Hoft, "Q factor improvement of combline resonators," presented at the German Microwave Conference, University of ULM, ULM, Germany, 2005.
- [31] G. Shen and D. Budimir, "Novel Resonator Structures for Comblin Filter Applications," in *2002 32nd European Microwave Conference*, 2002, pp. 1-3.
- [32] R. Levy, R. V. Snyder, and G. Matthaei, "Design of microwave filters," *IEEE Transactions on Microwave Theory and Techniques*, vol. 50, pp. 783-793, 2002.
- [33] N. E. A. Rashid, M. T. Ali, and N. Hamzah, "Properties of dielectric combline resonator for base station filters," in *2004 RF and Microwave Conference (IEEE Cat. No.04EX924)*, 2004, pp. 76-79.
- [34] M. Golio, *The RF and Microwave Handbook*: CRC Press, 2000.
- [35] S. B. Cohn, "Microwave Filters, An Advancing Art," *IEEE Transactions on Microwave Theory and Techniques*, vol. 13, pp. 487-488, 1965.
- [36] P. Jarry and J. Beneat, *Advanced Design Techniques and Realizations of Microwave and RF Filters*: Wiley, 2008.
- [37] R. Wallace and K. Andreasson, *Introduction to RF and Microwave Passive Components*: Artech House Publishers, 2015.
- [38] W. G. Paul Wade, "Waveguides filter you can build-and Tune part 3. Evanescent Mode Waveguide Filters," *ARRL Periodicals Archive*, pp. 23-29, March 2010.
- [39] G. F. Craven and C. K. Mok, "The Design of Evanescent Mode Waveguide Bandpass Filters for a Prescribed Insertion Loss Characteristic," *IEEE Transactions on Microwave Theory and Techniques*, vol. 19, pp. 295-308, 1971.
- [40] N. P. Akers and P. D. Allan, "An Evanescent Mode Waveguide Bandpass Filter at Q Band (Short Papers)," *IEEE Transactions on Microwave Theory and Techniques*, vol. 32, pp. 1487-1489, 1984.
- [41] R. V. Snyder, S. Sanghoon, and K. Keck, "Bandstop filter design using evanescent mode resonators," in *IEEE MTT-S International Microwave Symposium Digest, 2003*, 2003, pp. 1073-1076 vol.2.
- [42] M. Makimoto and S. Yamashita, "Compact bandpass filters using stepped impedance resonators," *Proceedings of the IEEE*, vol. 67, pp. 16-19, 1979.
- [43] M. Makimoto and S. Yamashita, *Microwave Resonators and Filters for Wireless Communication: Theory, Design and Application*: Springer, 2001.
- [44] P. Z. Y. A. A. Apriyana, "A dual band BPF for concurrent dual band wireless Transciever," presented at the Electronics Packaging Technology, 2003 5th Conference (EPTC 2003), 2003.

- [45] R. D. Richtmyer, "Dielectric Resonators," *J. Applied Physics*, vol. 32, pp. 391-398, 1939.
- [46] S. B. Cohn, "Microwave Bandpass Filters Containing High-Q Dielectric Resonators," *IEEE Transactions on Microwave Theory and Techniques*, vol. 16, pp. 218-227, 1968.
- [47] W. H. Harrison, "A Miniature High-Q Bandpass Filter Employing Dielectric Resonators," *IEEE Transactions on Microwave Theory and Techniques*, vol. 16, pp. 210-218, 1968.
- [48] D. J. Masse, R. A. Pucel, D. W. Readey, E. A. Maguire, and C. P. Hartwig, "A new low-loss high-k temperature-compensated dielectric for microwave applications," *Proceedings of the IEEE*, vol. 59, pp. 1628-1629, 1971.
- [49] J. K. Plourde, D. F. Linn, H. M. O'Bryan, and J. Thomson, "Ba₂Ti₉O₂₀ as a Microwave Dielectric Resonator," *Journal of the American Ceramic Society*, vol. 58, pp. 418-420, 1975.
- [50] A. A. e. al., "Full-Wave design of spurious free DR TE mode bandpass filters," *IEEE Transaction on Microwave Theory and Techniques*, vol. 43, pp. 744-752, 1995.
- [51] V. Walker and I. C. Hunter, "Design of cross-coupled dielectric-loaded waveguide filters," *IEE Proceedings - Microwaves, Antennas and Propagation*, vol. 148, pp. 91-96, 2001.
- [52] M. T. Sebastian, *Dielectric Materials for Wireless Communication*: Elsevier Science, 2010.
- [53] M. Y. Sandhu and I. C. Hunter, "Miniaturized dielectric waveguide filters," *International Journal of Electronics*, vol. 103, pp. 1776-1787, 2016/10/02 2016.
- [54] I. C. Hunter and M. Y. Sandhu, "Monolithic integrated ceramic waveguide filters," in *2014 IEEE MTT-S International Microwave Symposium (IMS2014)*, 2014, pp. 1-3.
- [55] S. J. F. e. al, "Dielectric materials, devices, and circuits," *IEEE Transaction on Microwave Theory and Techniques*, vol. 50, pp. 706-720, 2002.
- [56] G.-C. L. L. Ji-Fuh, Marco Song, George HE, Tony An,, "Single Mode DR Filter for Wireless base Stations," *ZTE Communications*, 2011.
- [57] I. C. Hunter, L. Billonet, B. Jarry, and P. Guillon, "Microwave filters-applications and technology," *IEEE Transactions on Microwave Theory and Techniques*, vol. 50, pp. 794-805, 2002.
- [58] D. Kajfez and P. Guillon, *Dielectric Resonators*: Noble Publishing Corporation, 1998.
- [59] S. Ramo, J. R. Whinnery, and T. Van Duzer, *FIELDS AND WAVES IN COMMUNICATION ELECTRONICS, 3RD ED*: Wiley-India, 2008.
- [60] L. F. Chen, C. K. Ong, C. P. Neo, V. V. Varadan, and V. K. Varadan, *Microwave Electronics: Measurement and Materials Characterization*: Wiley, 2004.
- [61] C. Wang and K. A. Zaki, "Dielectric resonators and filters," *IEEE Microwave Magazine*, vol. 8, pp. 115-127, 2007.
- [62] G. Felix Hernandez and J. P. Martinez, "Analysis of Dielectric Resonators with Tuning Screw and Supporting Structure," *IEEE Transactions on Microwave Theory and Techniques*, vol. 33, pp. 1453-1457, 1985.
- [63] I. Hunter, S. Afridi, and M. Sandhu, "Integrated ceramic waveguide filters with improved spurious performance," in *2015 European Microwave Conference (EuMC)*, 2015, pp. 674-677.
- [64] W. Wersing, "Microwave ceramics for resonators and filters," *Current Opinion in Solid State and Materials Science*, vol. 1, pp. 715-731, 1996/10/01/ 1996.
- [65] T. Saad, *Microwave Engineers' Handbook*: Artech House, 1971.
- [66] J. F. Liang, H. C. Chang, and K. A. Zaki, "Coaxial probe modeling in waveguides and cavities," *IEEE Transactions on Microwave Theory and Techniques*, vol. 40, pp. 2172-2180, 1992.
- [67] S. Lucyszyn, D. Budimir, Q. H. Wang, and I. D. Robertson, "Design of compact monolithic dielectric-filled metal-pipe rectangular waveguides for millimetre-wave applications," *IEE Proceedings - Microwaves, Antennas and Propagation*, vol. 143, pp. 451-453, 1996.

- [68] H. L. K. Herbery Joseph Reich, Philip Franklin Ordnung, John Gordon Skalnik, *Microwave theory and techniques*, 1953.
- [69] P. M. Iglesias and I. C. Hunter, "Non-uniform Q-factor distribution in microwave filters," in *2012 42nd European Microwave Conference*, 2012, pp. 1182-1185.
- [70] P. P. Silvester and R. L. Ferrari, *Finite Elements for Electrical Engineers*: Cambridge University Press, 1996.
- [71] Ansys, "Ansys HFSS, Realize your Product promise," in <http://www.solidcad.co.za/WebsiteAssets/pdf/brochures/ansys-hfss-brochure-14.0.pdf>, I. ANSYS, Ed., ed, 2011.
- [72] (June 2005, 21-02-2007). ANSOFT: HFSS, A USER MANUAL. Available: <http://anlage.umd.edu/HFSSv10UserGuide.pdf>
- [73] S. Afridi, M. Sandhu, N. Somjit, and I. Hunter, "Monolithic ceramic waveguide filter with wide spurious free bandwidth," in *2016 46th European Microwave Conference (EuMC)*, 2016, pp. 241-244.
- [74] S. Afridi, M. Sandhu, and I. Hunter, "Mixed non-uniform width/evanescent mode ceramic resonator waveguide filter with wide spurious free bandwidth," in *2016 IEEE MTT-S International Conference on Numerical Electromagnetic and Multiphysics Modeling and Optimization (NEMO)*, 2016, pp. 1-3.
- [75] V. S. Bagad, *Microwave Engineering - I*: Technical Publications, 2009.
- [76] I. Robertson, N. Somjit, and M. Chongcheawchamnan, *Microwave and Millimetre-Wave Design for Wireless Communications*: Wiley, 2016.